Carbon molecular sieve materials for gas separations

Márcia Rafaela Silva de Andrade

Dissertation presented for the degree of

Doctor in Chemical and Biological Engineering

by the

University of Porto

Supervisor

Adélio Miguel Magalhães Mendes

LEPABE – Laboratory for Process Engineering, Environment, Biotechnology an Energy

Department of Chemical Engineering

Faculty of Engineering – University of Porto

Porto, 2019

Statement of originality

I certify that this work does not contain any material that has been used nor will be for the award of any other degree or diploma in my name or anyone, in any university or institution. In addition, I certify that, to the best of my knowledge, this work does not contain any material previously published or written by another person, expect where due reference has been made in the text.

_____

Márcia Rafaela Silva de Andrade

Statement

In order to fulfil the Rules of Ethics of the Doctoral Program of Chemical and Biological Engineering (PDEQB), we hereby declare that all the contents of the thesis presented by Márcia Rafaela Silva de Andrade, entitled 'Carbon molecular sieve materials for gas separations', is exclusively from the author with the collaborations mentioned in the thesis.

_____

Adélio Miguel Magalhães Mendes
Full Professor

This work was the result of the projects:

(i) UID/EQU/00511/2019 - Laboratory for Process Engineering, Environment, Biotechnology and Energy – LEPABE funded by national funds through FCT/MCTES (PIDDAC).

(ii) NORTE-01-0145-FEDER-000005 - LEPABE-2-ECO-INNOVATION, supported by North Portugal Regional Operational Programme (NORTE 2020), under the Portugal 2020 Partnership Agreement, through the European Regional Development Fund (ERDF).

(iii) SFRH/BD/93779/2013 – PhD grant, through Portuguese Foundation for Science and Technology (FCT) supported by funding POPH/ESF.

(iv) NORTE-08-5369-FSE-000028 - supported by North Portugal Regional Operational Programme (NORTE 2020), under the Portugal 2020 Partnership Agreement and the European Social Fund (ESF).

Acknowledgments

First of all, I would like to specially acknowledge my supervisor Prof. Adélio Mendes for the research theme and for providing the opportunity to work with him and in the Laboratory for Process Engineering, Environment, Biotechnology and Energy (LEPABE). My gratitude for all the enormous dedication, understanding, advices, support and enormous scientific inputs in all my PhD. work. Thank you!

I would like to acknowledge the financial support of project UID/EQU/00511/2019 - Laboratory for Process Engineering, Environment, Biotechnology and Energy – LEPABE funded by national funds through FCT/MCTES (PIDDAC); Project "LEPABE-2-ECO-INNOVATION" – NORTE-01-0145-FEDER-000005, funded by Norte Portugal Regional Operational Programme (NORTE 2020), under PORTUGAL 2020 Partnership Agreement, through the European Regional Development Fund (ERDFfor the fellowship grant. Also, I would like to acknowledge LEPABE, DEQ and FEUP for giving me all the excellent conditions to perform my work.

I would like to specially thank to Dr. Roger Whitley from Air Products and Chemicals for all the kindness, great discussions and various inputs during all work. Also, I want to thank Air Products for providing me a large quantity and variety of carbon molecular sieve raw materials. Its contribution was crucial to all the developed work, once again, my sincere gratitude!

I would like to kindly thank Prof. Margarida Bastos for all the fruitful discussions.

I want to thank Mr. Nelson Neves, from Neves&Neves company, for always being kind and always attend my requests in time. Also, a very special thanks to Mrs. Fátima Faustino for all the help, efficiency and kindness in most diverse administrative issues.

I want to thank my lab colleagues for all friendship and help, thanks for everything! I would like to very specially thank to Sandra Rodrigues for all the friendship, kindness, enormous support and affection, thank you for being always by my side all these years. Also, I would like to thank Frederico Relvas, Cátia Azenha and Tiago Araújo for all the kindness and help in the lab.

I would like to specially show my enormous gratitude to all my friends, for all the happy moments and support, to all of them thank you! Specially I would like to thank my dear friend Joana Roque, the so-called “Equipa”, for all the support, happiness and true friendship for all of these years.

I would like to specially acknowledge my family, without them I could not be able to be here and to finish my work. To my mother Elvira Silva, my father Eugénio Andrade, my brother Francisco Andrade, my sister-in-law Sandra Barbosa, my grandmother Maria Celeste Godinho, for my grandfather Francisco de Andrade Júnior, my grandmother Josefa Rodrigues, my aunts Maria Elisa Rodrigues and Maria das Dores Tinoco, thank you for all the love, support, patient, encouragement and for always being by my side. Thank you for being in my life!

My final words go to my dear boyfriend Rafael Rocha for all the restless support, comprehension, patient and above all, love. Thank you for always be by my side and for making me happy every day!

Abstract

Adsorption-based processes are considered efficient and low-cost for gas separations. The most used adsorption-based technology is the pressure swing adsorption (PSA), where adsorbents are the core of the process. Carbon molecular sieve (CMS) adsorbents are a particular class of activated carbons with specific properties such as narrow pore size distribution, ultramicropores < 0.7 nm, high resistance to harsh environmental conditions and low preparation costs. This type of adsorbents is widely used for kinetic-based PSA separations such as the production of nitrogen from air. After carbonization, these materials are often prone of oxygen chemisorption, which change the CMS pore size distribution and surface chemistry and then its ability to separate gases. The research on the preparation of aging-free tailor-made CMS adsorbents for achieving high adsorption performances is of critical importance to improve the performance of gas separations presently addressed by CMS and new gas separations.

The present thesis targets the preparation and characterization of new highly performing and oxygen-stable carbon molecular sieve adsorbents for O_2 / N_2 and C_3H_6 / C_3H_8 gas separations.

Oxygen and humidity aging-free carbon molecular sieve adsorbents were successfully prepared by the carbonization of a cellulosic precursor at 1200 ^oC, followed by milling to *ca*. 11 µm and post-treatment with propylene for 10 days. Comparing untreated and propylene treated samples, it was possible to identify structural and chemical differences. The treated sample was stable in contact with oxygen and humidity and then suitable for oxidant gas separations. The FTIR analyses allowed to propose a passivation mechanism for the propylene post-treatment and the oxygen chemisorption was identified as the main source of aging for non-passivated samples. The prepared samples were also characterized for the Dubinin-Astakhov analysis, O_2, N_2 and CO_2 adsorption isotherms and adsorption kinetics.

New high-performing carbon molecular sieve adsorbents for O_2 / N_2 gas separation and stable towards oxygen were prepared. The adsorbent materials were obtained by carbonizing a cellulosic precursor at 1000 ^oC followed by milling to *ca*. 1.6 µm and propylene post-treatment at 2 bar for passivation. The adsorbents were optimized and fully characterized. The carbon samples showed high adsorption kinetics

towards oxygen and high O_2 / N_2 kinetic selectivity – *ca*. 9×10^{-2} s^{-1} and 123 respectively. Compared with reported and commercial CMS, these parameters are outstanding permitting ultimately to develop more efficient PSA separation processes.

C_3H_6 / C_3H_8 gas separation is one of the most difficult gas separations because their physico-chemical properties are rather similar. The current separation of these species is accomplished by distillation, using very long distillation columns; cheaper processes are then urgently needed. Two types of carbon adsorbents were successfully prepared for separating C_3H_6 / C_3H_8. A carbon molecular sieve adsorbent was prepared displaying C_3H_6 / C_3H_8 disruptive equilibrium based selectivities – *ca*. 140 adsorbed concentration ratio at 25 ºC and 1 bar. This CMS was prepared by a single-carbonization step of a cellulosic precursor at 800 ºC. Mono- and multicomponent breakthrough experiments confirmed the performance of the adsorbent, previously characterised concerning adsorption equilibrium isotherms and adsorption kinetics. The adsorbent was also characterized using techniques such as thermogravimetric analysis, Fourier transform infrared spectroscopy and scanning electron microscopy; the pore size distribution was estimated from CO_2 adsorption isotherms at 0 ºC. A novel propane selective carbon molecular sieve adsorbent was prepared from a phenolic resin powder precursor. The precursor was pre-treated with phosphoric acid followed by a carbonization at 1100 ºC and post-treated at 2 bar of propylene. The obtained adsorbent showed remarkable performance for C_3H_8 / C_3H_6 gas separation, displaying inverse C_3H_8 / C_3H_6 adsorption selectivity – *ca*. 2 adsorbed concentration ratio at 25 ºC and 1 bar. This promising result opens the doors for the preparation of propane selective carbon molecular sieve adsorbents far more suitable for removing the propane from an enriched C_3H_6 / C_3H_8 feed stream.

Sumário

Os processos de adsorção para separações de gases são considerados eficientes e de baixo custo. A tecnologia de adsorção mais utilizada é a adsorção com modulação de pressão (PSA), onde os adsorventes são o núcleo do processo. Os adsorventes de peneiro molecular de carbono (CMS) são uma classe específica de carvões ativados com propriedades específicas, como distribuição de tamanho de poros estreita, ultramicroporos < 0.7 nm, alta resistência a condições ambientais adversas e baixos custos de preparação. Este tipo de adsorventes é amplamente utilizado para separações em PSA baseadas em diferenças cinéticas, como a produção de azoto do ar. Após carbonização, estes materiais são geralmente propensos à quimiorsorção de oxigénio, que altera a distribuição do tamanho de poros e a química da superfície do CMS, e, assim a sua capacidade para separar gases. Investigação baseada na preparação personalizada de CMS sem envelhecimento para alcançar altos desempenhos de adsorção é de crítica importância para melhorar o desempenho das separações gasosas atualmente abordadas pelos CMS assim como novas separações gasosas.

A presente tese visa a preparação e caracterização de novos adsorventes de peneiro molecular de carbono de alto desempenho e estáveis ao oxigénio para as separações gasosas O_2 / N_2 e C_3H_6 / C_3H_8.

Adsorventes de peneiro molecular de carbono sem envelhecimento ao oxigénio e humidade foram preparados com sucesso pela carbonização de um precursor celulósico a 1200 ºC, seguido de moagem para *ca.* 11 µm e pós-tratamento com propileno por 10 dias. Comparando amostras não tratadas e tratadas com propileno, foi possível identificar diferenças estruturais e químicas. A amostra tratada manteve-se estável em contato com oxigénio e humidade mostrando-se adequada para separações de gases oxidantes. As análises de FTIR permitiram propor um mecanismo de passivação para o pós-tratamento com propileno e a quimisorção de oxigénio foi identificada como a principal fonte de envelhecimento para amostras não passivadas. As amostras preparadas foram também caracterizadas pela análise de Dubinin-Astakhov, isotérmicas de adsorção de O_2, N_2 e CO_2 e cinética de adsorção.

Novos adsorventes de peneiro molecular de carbono de alto desempenho para a separação de gás O_2 / N_2 e estáveis em oxigénio foram preparados. Os materiais

adsorventes foram obtidos pela carbonização de um precursor celulósico a 1000 ºC, seguido de moagem até *ca.* 1.6 µm e pós-tratamento com propileno a 2 bar para passivação. Os adsorventes foram otimizados e totalmente caracterizados. As amostras de carbono apresentaram elevada cinética de adsorção para o oxigénio e alta seletividade cinética de O_2 / N_2 - *ca.* 9×10^{-2} s^{-1} e 123, respetivamente. Comparados com os CMS comerciais, estes resultados são excecionais, permitindo desenvolver processos de separação de PSA mais eficientes.

A separação de gás C_3H_6 / C_3H_8 é uma das separações gasosas mais difíceis devido às suas propriedades físico-químicas serem bastante semelhantes. A separação atual destas espécies é realizada por destilação, utilizando colunas de destilação muito longas; processos mais baratos são urgentemente necessários. Dois tipos de adsorventes de carbono foram preparados com sucesso para a separação de C_3H_6 / C_3H_8. Um adsorvente de peneiro molecular de carbono foi preparado exibindo seletividades de equilíbrio disruptivas para C_3H_6 / C_3H_8 - razão de concentração adsorvida *ca.* 140 a 25 ºC e 1 bar. Este CMS foi preparado por uma etapa de carbonização única de um precursor celulósico a 800 ºC. Experiências considerando curvas de rutura para mono e multicomponente confirmaram o desempenho do adsorvente, anteriormente caracterizado, relativamente a isotérmicas de equilíbrio de adsorção e cinética de adsorção. O adsorvente foi também caracterizado utilizando técnicas como análise termogravimétrica, espectroscopia de infravermelhos com transformada de Fourier e microscopia eletrónica de varredura; a distribuição do tamanho dos poros foi estimada a partir de isotérmicas de adsorção de CO_2 a 0 ºC. Um novo adsorvente de peneiro molecular de carbono seletivo ao propano foi preparado a partir de um precursor em pó de resina fenólica. O precursor foi pré-tratado com ácido fosfórico seguido de carbonização a 1100 ºC e pós-tratado com 2 bar de propileno. O adsorvente obtido apresentou um desempenho notável para a separação de gases C_3H_8 / C_3H_6, exibindo seletividade de adsorção inversa para a separação de gás C_3H_8 / C_3H_6 - razão de concentração adsorvida *ca.* 2 a 25 ºC e 1 bar. Este resultado promissor abre as portas para a preparação de adsorventes de peneiro molecular de carbono seletivos ao propano, muito mais adequados para remover o propano de uma corrente de alimentação enriquecida de C_3H_6 / C_3H_8.

Table of Contents

List of Figure Captions

Chapter I

Chapter II

Chapter III

Chapter IV

Chapter V

Appendix A

List of Table Captions

Chapter I

Chapter II

Chapter III

Chapter IV

Chapter V

Chapter I

Chapter 1 - Introduction

In the latest 60 years [1], carbon has been revolutionizing the materials science since it is an element that establishes bonds with almost any other element; displaying a wide spectrum of compounds and allotropic forms [2,3]. Its excellent properties allow its use in a large number of industrial applications [4–6] such as: i) carbon fibers for gas separations (carbon hollow fibers), ii) lubricants (graphite), iii) conductor materials (graphite electrodes), iv) structural materials for high temperature tribological applications (carbon–carbon composites), v) non-crystalline impermeable materials (vitreous carbon), vi) hardest materials (diamond) and also vii) porous gas adsorbent materials (activated carbons) [6,7].

Carbon materials have a porous structure with small amounts of different heteroatoms, such as oxygen and hydrogen. Some materials can also contain mineral matter (ash content) depending on the nature of the precursor material. The carbons pore structure is one of the main physical properties that characterizes this type of materials. Pore structure is formed by pores of different sizes, which in agreement with IUPAC [8–10], can be divided in three main groups:

i) Macropores, for pores larger than 50 nm;

ii) Mesopores, for pores ranging from 2 nm to 50 nm;

iii) Micropores, for pores smaller than 2 nm.

In agreement with IUPAC [8], these limits, determined by the adsorption-desorption of nitrogen at 77 K, are somewhat arbitrary, however they are useful and widely recognized. The nanopores class was also reported which includes the above three categories although with an upper limit of approximately 100 nm. Also, two types of narrow pores are described including ultramicropores, pores with width lower than 0.7 nm, and wide micropores, also called supermicropores [8].

Figure 1.1 shows a scheme of a typical carbon material pore network.

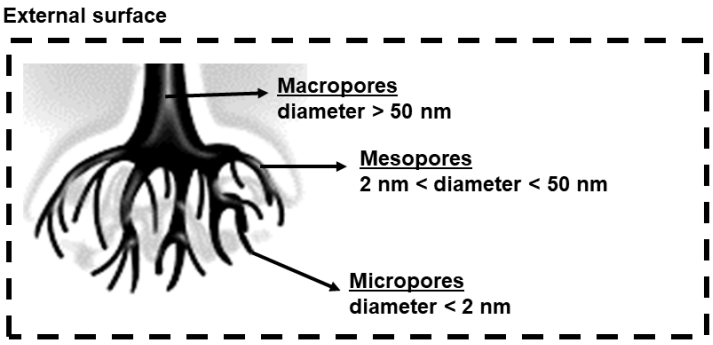

Figure 1.1. Schematic representation of a typical carbon material pore network (adapted from [10]).

Activated carbons (AC) are a special class of carbon materials. AC have been used in several applications for thousands of years constituting one of the most popular type of carbon materials in industrial field [6]. AC are porous materials with a large surface area and, for a long time, they were used extensively in water treatment and gas adsorption [3]. Their use in water purification started with ancient Egyptians that used charcoal to purify water for medicinal purposes. In the World War I occurred a big development on porous carbons uses [11]. Namely, the use of poisonous gases (such as chlorine, mustard gas and phosgene) triggered the large-scale production of gas masks incorporated with activated carbons for adsorbing these gases [7,12]. Also, and up to the period of 1940, a significant expansion of carbon black industry was observed derived from its extent use particularly in newspapers fabrication and printings in general. Furthermore, and also in this period, carbon fibers based on polyacrylonitrile (PAN) and pitch materials appeared for the first time. Some of these fibers were able to be oxidized for producing porous-activated fibers. Furthermore, fibers were impregnated in resins or in suitable pitch and then carbonized becoming tailor-made carbon-carbon composites with a wide range of structural applications [11]. Nowadays, the range of activated carbon types is intensively growing. Table 1.1 shows some types of industrial carbons [11].

Table 1.1. Types of industrial carbons.

Type of carbons
Activated carbons
Activated carbon fibers
Activated carbon cloth
Activated carbon felt
Carbon molecular sieves
Carbon black
Carbon films
Elastic carbon
Graphite/oxide refractories
Nanotubes with open and close ends
Carbon fiber/carbon composites
Carbon fiber/resin composites
Glassy carbon
Pyrolytic carbon

Generally, AC includes a group of materials with highly developed internal surface area and porosity, allowing a large capacity for adsorbing chemicals from gases and liquids [6]. As mentioned before, its large versatility converges in a high industrial significance being a class of materials used worldwide. One of the strongest market materials of AC are the so-called carbon molecular sieves. Carbon molecular sieves (CMS) are a particular class of activated carbons that display a microporous pore structure capable of discriminate molecules based on its size and shape [13]. Zeolites appear as another type of microporous materials that have similar applications of CMS, however, CMS have lower fabrication costs and high thermal and chemical resistance. Moreover, unlike zeolites, carbon molecular sieves display a broad micropore size distribution and shape making them more versatile materials.

More than 30 % of worldwide carbon research is related to the discovery of new precursor materials and optimization of pre- and post-carbonization treatments for producing adsorbents targeting a given application [6]. Table 1.2 shows examples of some commercial adsorption applications and used carbon adsorbents [14]. Bulk separations and processes are presented, being the term “bulk” defined by Keller [15] and related to the feed concentration of the adsorbed component above 10 wt. % [14,15].

Table 1.2. Some examples of commercial adsorption processes and respective adsorbents materials.

Type of separation		Material
Gas Bulk	Paraffins, isoparaffins, aromatics	Zeolites
	O_2 / N_2	CMS
	N_2 / O_2	Zeolites
	CO, CH_4, CO_2, N_2, Ar	AC followed by zeolites (layered beds)
	Hydrocarbons / vent streams	AC
	H_2O / ethanol	Zeolites (3A)
	Chromatographic analytical separations	A wide range of inorganic and polymer agents
Gas purification	CO_2 / C_2H_4, natural gas	Zeolites, CMS
	Hydrocarbons, halogenated organics	AC, silicates
	Natural gas, air, synthesis gas	Zeolite (3A), silicate, alumina
	Odors / air	Silicate, others
Liquid Bulk separations	Normal paraffins / isoparaffins, aromatics	Zeolites
	Detergent-range olefins / paraffins	Zeolites
	Chromatographic analytical separations	Wide range of inorganic, polymer and affinity agents
	p-xylene/o-xylene, m-xylene	Zeolites
Liquid purifications	H_2 / organics, oxygenated organics, halogenated organics, dehydration	Silica, alumina, zeolite, corn grits
	Organics, halogenated organics, oxygenated organics, water purification	AC, silicate, resins
	Drug detoxification in the body	AC

Adsorption processes can be crucial for the development of new technologies, such as fuel cells, water treatment, medical purposes, among others. A breakthrough in adsorbents conception is needed for solving critical problems, *e.g.*, hydrogen storage for hydrogen fuel cells. Hydrogen demand for fuel cell applications is increasing over the past decade; from 2015 to 2018 the number of fuel cell systems worldwide per year increased from 60 000 [16] to 225 000 units [17], which represents a very high number. Regarding fuel-grade hydrogen production by adsorption processes, the critical issue is the carbon monoxide removal to less than 1 ppm; being the main contaminant of fuel cell catalysts [18]. Since hydrogen fuel cells are considered a sustainable and competitive energy system, their development is of high interest [18] concerning the future needs together with a clean environment. However, nowadays, the high standards for decreasing air and water pollution demand adsorbents that are not commercially available yet [14]. In agreement with this, the development of commercial high-

performance adsorbent materials that can efficiently integrate industrial process with low energy consumption and being environmental-friendly is needed. For meeting the required challenges, tailoring the adsorbents based on fundamental principles could speed up the adsorbents design and consequently improve its performance on a given application [14]. Theoretical tools such as *ab initio* molecular orbital theory [19] and Monte Carlo simulations [20,21] can be useful for developing the adsorbents optimum design for a given application [14]. Some of the most challenging separation and purification applications, as well as respective promising adsorbents for those applications, are given on Table 1.3.

Table 1.3. Challenging separation and purification applications and promising adsorbents.

Application	Adsorbents
Sulfur removal from transportation fuels (gasoline, diesel and jet fuels)	π-complexation adsorbents [22,23], zeolites [24], among others [25]
CO removal from H_2 to < 1 ppm for fuel cells applications	π-complexation adsorbents [18], MOFs [26], AC + zeolites [27,28]
N_2 / CH_4 separation for natural gas upgrading	Zeolites [29], barium-exchanged ETS-4 dehydrated adsorbents [30,31]
C_3H_6 / C_3H_8 (+hydrocarbons) separation	π-complexation adsorbents [32,33], MOFs [34,35] , zeolites [36–39]
CH_4 storage for on-board vehicular storage	MOFs [40,41], AC [42,43], MOFs + AC [44]

1.1. Carbon molecular sieve adsorbents for gas separations

Carbon molecular sieves have a microporous structure capable to differentiate molecules on the basis of size, shape and pore surface area [45,46]. CMS display several advantages when compared with other AC such as narrower pore size distribution, higher hydrophobicity, higher resistance to both alkaline and acid media and thermal stability at higher temperatures under inert atmosphere [45,47]. The CMS performance is generally characterized by two major properties: i) kinetics and ii) capacity of adsorption [45,48]. Also, CMS adsorbents can present different configurations, but in general, the most used ones are powdered and granular. Its choice generally depends of its target application, *e.g.*, for cleaning a gas stream in a fixed bed, granular carbon

materials are preferable for avoiding significant pressure drops [10]. Figure 1.2 shows some of the possible configurations of carbon molecular sieve adsorbents.

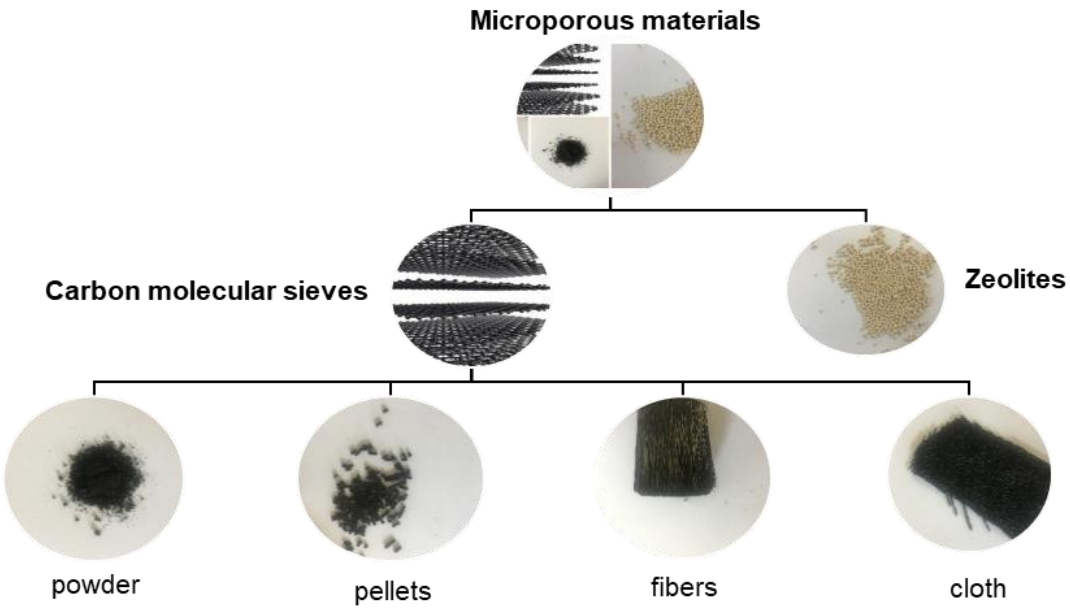

Figure 1.2. Typical configurations of CMS adsorbents.

Granular (pelletized) carbon molecular sieves typically present a mean particle size in the range of 1 mm-5 mm and are often used in fixed bed form for continuous processes and low pressure drops (in both liquid and gas phase applications). Gas phase applications, such as gas purification, air filtering and gas masks, solvent recovery, gas separation by PSA, catalysis, among others, typically use granular CMS. Furthermore, granular CMS are increasingly replacing powder CMS in some liquid phase applications such as gold extraction and drinking water treatment. Granular configuration, compared with powder, offers a lower pressure drop, and, also, they can be regenerated or reactivated more than once and therefore reused [10]. Powdered CMS display a typical particle size of less than 100 µm, most commonly, ranging between 15 µm – 25 µm. Almost 50 % of the produced CMS are in powder form, and, normally, its use is more incident in applications where the solute may display problems in diffusing from the transport pores. Here, since granular form would require a great amount of time to reach the equilibrium, powder configuration is preferable. Furthermore, in powder CMS, properties such as high density, hardness and abrasion index are not relevant as in other CMS forms [10].

CMS have been increasingly used for separation and purification of gases, which is of high interest for several industries [49]. In the latest years, a wide range of CMS have been prepared from a large diversity of precursor materials such as coal, coconut shell, polymers, biomass materials, among others [49–51]. One of the most used application for this type of materials in the industrial field is the separation of oxygen / nitrogen by using a pressure swing adsorption technology (PSA) – nitrogen production. Figure 1.3 illustrates a scheme of a PSA column for nitrogen production. Since oxygen and nitrogen have similar molecular diameters, 0.347 nm and 0.364 nm, respectively [52], separating these molecules by differences in the kinetics of adsorption would be highly preferable. As oxygen tends to adsorb faster than nitrogen on CMS it allows its kinetic separation, however, adsorption equilibrium capacity is generally similar for both gases [49]. These outstanding separation properties are mainly due to its very narrow pore size distribution (pore width usually ranging from 0.3 nm to 0.5 nm) [53–55]. Moreover, CMS pore size distribution can be controlled by varying the i) precursor material; ii) the carbonization conditions and iii) pre- and post-treatments, such as activation and carbon vapor deposition and passivation [49,54].

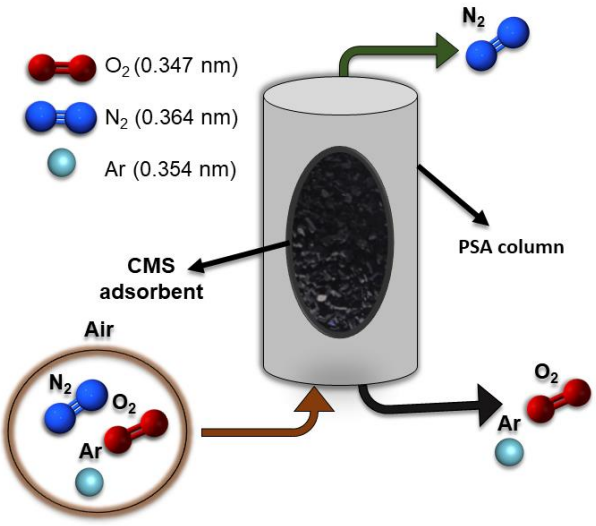

Figure 1.3. Scratch of a PSA column for nitrogen production.

1.1.1. Preparation of CMS adsorbents

Carbon molecular sieve adsorbents can be prepared from a wide diversity of precursor materials and through a variety of processes ranging from activation of precursors [56,57], controlled pyrolysis [58], modification of porous structure through

activation (*e.g.* oxygen, carbon dioxide) and/or carbon vapour deposition (CVD) (using organic agents such as benzene, toluene, methane, among others [56,57,59–61]). Generally, carbon molecular sieves preparation requires the following steps: i) precursor selection; ii) pre-treatments (optional); iii) pyrolysis reaction and iv) post-treatments (optional). Figure 1.4 shows the main preparation steps involved in carbon molecular sieve adsorbents preparation and characterization.

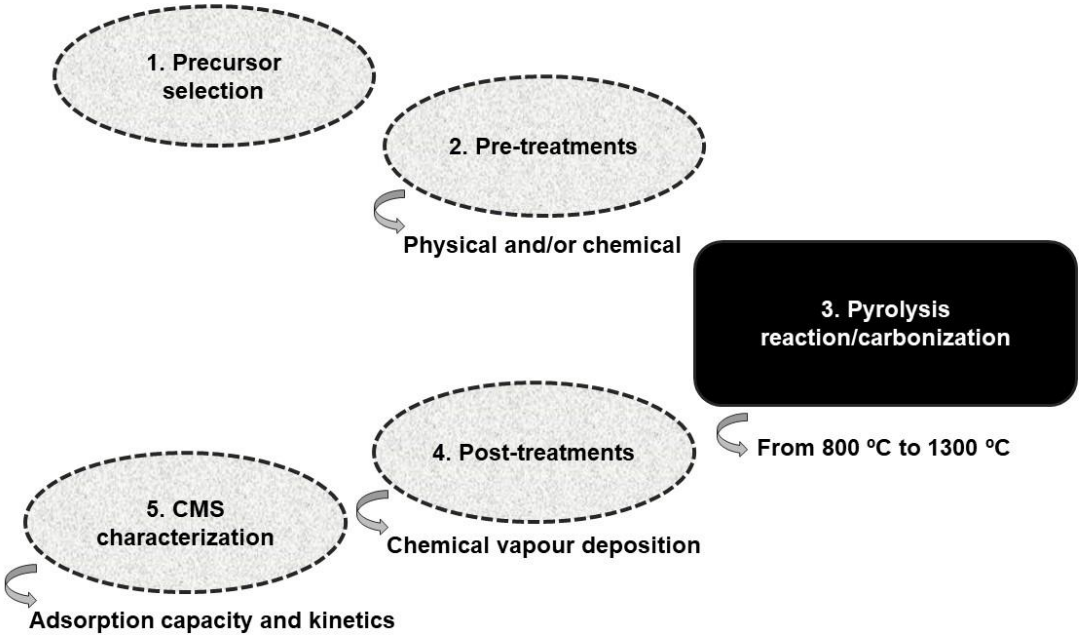

Figure 1.4. Main steps involved in CMS preparation and characterization.

Precursor selection

The selection of the precursor material accounts with several factors to considerer. Preferably, the precursor material should be cheap, easy to obtain and abundant. Also, it should originate adsorbents with high carbon content and low quantity of inorganic content, *i.e.*, low ash content. Furthermore, and not less important, the precursor material should not soften or melt when exposed to high temperatures, which is particularly important for pyrolysis reaction step (carbonization process). High density and considerable volatile content are important since the evolution/release of the volatiles during the pyrolysis results in a porous char, essential for making CMS. Further, density contributes to enhance the structural strength of the carbon material, crucial to withstand excessive particle crumble during extensive use [6]. The most used precursor materials for carbon molecular sieves fabrication include

wood, coal, lignite, coconut shell, peat, among others. Table 1.4 shows some examples of conventional precursor materials and its properties.

Table 1.4. Characteristics of conventional precursor materials used in CMS preparation.

Raw material	Carbon / %	Volatiles / %	Ash / %	Density / kg·m^{-3}	Texture of CMS
Softwood	40-45	55-60	0.3-1.1	0.3-1.1	Soft
Hardwood	40-42	55-60	0.3-1.2	0.3-1.2	Soft
Lignin	35-40	58-60	-	0.3-0.4	Soft
Nutshells	40-45	55-60	0.5-0.6	1.4	Hard
Soft coal	65-80	25-30	2.12	1.25-1.50	Medium hard
Petroleum coke	70-85	15-20	0.5-0.7	1.35	Medium hard
Semi hard coal	70-75	1-15	5-15	1.45	Medium hard
Hard coal	85-95	5-10	2.15	1.5-2.0	Hard

Nowadays, the use of biowastes and woods for CMS production is increasingly growing and appears to be very promising due to its "environmentally-friend" character. Moreover, in the last two decades, the research on new synthetic precursors has also emerged. This type of precursors includes viscose rayon, polyacrylonitrile, saran, phenolic resins, PFA, among others [62–64].

Pre-treatments

Precursor materials are often submitted to pre-treatments prior to carbonization process. On this step, the integrity of the material precursor can be ensured as well as the control of the uniformity of pores formation during pyrolysis reaction [65,66]. Generally, there are three types of pre-treatments: physical, chemical and physiochemical. Physical treatments, often called physical activation, are attributed to steam and/or carbon dioxide activation during carbonization process [67]. On the other hand, chemical treatments, called chemical activation, include treatments with chemical entities such as phosphoric acid, zinc chloride and metal compounds such as potassium hydroxide. Prior to carbonization, the use of phosphoric acid is preferable over zinc chloride, due to the environmental disadvantages of the later such as corrosion, among others. Also, zinc chloride functionalized carbons cannot be used in pharmaceutical and food industries due to its possible contamination of the products [67,68]. Potassium

hydroxide is an agent that allows the development of large microporosity; however, the yield of activated carbon impregnated is lower than when activated with phosphoric acid or zinc chloride. In addition, at temperatures > 650 ^{o}C the carbon content is lower. Thus, the most used activation agent is phosphoric acid. Most of the studies carried out with this agent explored the influence of the phosphoric acid solution concentration and carbonization end temperature on the porous structure of carbons. Due to the high polar character of phosphoric acid, and for controlling of physical and chemical interactions that occur in the bulk of the solution and in the substrate during impregnation, the most important factor to consider in this type of activation must be the concentration [67]. Finally, physiochemical treatments include the intersection of both chemical and physical treatments.

Table 1.5 shows some examples of chemical, physical and physiochemical activation pre-treatments applied on several precursor materials.

Table 1.5. Activation treatments applied on several precursor materials.

Activation method	Material	Activation agent	Reference
Chemical	Coconut shell, lignin	$ZnCl_2$	[69,70]
	Palm shell	H_2SO_4	[71]
	Walnut shell, macadamia nutshell	KOH	[72,73]
	Apricot stone, grain sorghum	H_3PO_4	[74,75]
Physical	Palm shell, coconut shell	Steam	[76,77]
	Macadamia nutshell, oil palm shell, coconut shell	CO_2	[78–80]
Physicochemical	Wood	H_3PO_4/Steam	[66]
	Peach stone	H_3PO_4/CO_2	[81]
	Peach stone	H_2SO_4/CO_2	[82]

Carbonization step

Carbonization step is the central point of the carbon molecular sieves preparation process. On this stage, the polymeric matrix is turned into carbon through a pyrolysis reaction [55]. The main operation parameters involved in the carbonization process are: i) pyrolytic end temperature, ii) heating rate, iii) soaking time and iv) inert flow (in case

of vacuum not be applied) [83]. During this step the precursor material is submitted to a specific heating protocol under a controlled inert atmosphere or vacuum [55].

The precursor material, generally with an organic macromolecular structure, during the heating/thermal treatment displays two distinct phases: i) formation of a gaseous fraction rich in hydrogen, light hydrocarbons and tar and ii) formation of a solid fraction rich in carbon-char. The gases and vapours derived from the solid are primary products since they derive from fragments of the carbonaceous structure. When this fraction is in the gas phase, the involved species react among themselves (influenced by treatment temperature and residence time), yielding secondary products (cracking). Not less important, the gas phase composition is also (highly) influenced for the precursor used in mild conditions. When the solid char formation begins, an enrichment of both relative carbon content and aromaticity occurs. Also, the decomposition of the polymeric matrix and solid char formation is accomplished by the release of gases such as H_2, CO, CO_2, H_2O and, also, residual CH_4; NH_3 and HCN can be formed depending on the precursor chemical nature [55,84]. At temperatures in the range of 450 ^oC – 500 ^oC there are few secondary reactions and the gas phase is mainly composed by stabilized primary products. On the other hand, with the temperature increase, secondary reactions become more significant, yielding at temperatures above 1000 ^oC gases such as methane, hydrogen and soot [10]. If high heating rates are applied during the heat treatment, cracking reactions can be very quick, and the soot may be deposited over char particles. Since a higher mass release is involved during the thermal treatment, the increase in aromaticity is followed by an increase in incipient microporosity due to the evolved high amount of functional groups and bridge chains, yielding void spaces [10]. After the carbonization, the char is composed by disordered graphitic crystals, and, among these crystals, there are small void spaces (micropores), which are often not accessible from the external surface since the meso/macropore network is blocked by soot deposition. This occurs specially when high temperatures and high heating rates are applied, being therefore very important for establishing the final textural properties of the char. High heating rates produce a very quick volatilization originating a solid with well-developed meso and macropore network and a low density, abrasion and hardness index. Unlike, slow heating rates generates a slower release of volatiles and does not favour the formation of large meso/macropore network, also, both density and

hardness are higher when compared with the ones obtained with high heating rates. Here, the incipient developed microporosity is higher than the one created at the high heating rates [10]. Further, carbonization atmosphere also influences the final carbon material since it controls/avoids undesired burn off and chemical damage of the precursor material. When carbonization is performed under vacuum it generally originates a material with a more narrower pore structure when compared with carbonization under inert gases (N_2, He, Ar). Accordingly, an inert atmosphere allows a more open porous network resultant from the removal of formed by-products and by avoiding the carbon deposition in the formed pores [85,86]. Also, the employed flowrate must be optimized since higher flowrates produce carbon materials with improved porosity but with minimal influence on the selectivities [85]. Considering this, the final carbonization product results in an amorphous carbon material with a specific pore network resultant from the heat treatment of a specific precursor by employing specific carbonization conditions (end temperature, soaking time, heating rate, gas atmosphere or vacuum, gas flow, if applicable).

Post-treatments

After the carbonization step, the carbon material is already formed presenting a specific pore network. For better tailoring the resultant carbon material and envisioning a high separation performance for a given application, a more precise pore tuning is needed [55]. Tuning the pores includes narrowing the pore size distribution or simply reduce or enlarge the pore widths. For assessing that, chemical vapour deposition (CVD), which generally consists in carbon deposition at the pores mouth narrowing them to match with the molecular size of the analyte, is often used. The most used carbon deposition agents include benzene [59,87–90], methylpentane [73] and methane [75,91]. Among these agents, benzene is the most used one since it does not generate intermediates during the cracking process, allowing then a more controlled deposition [91]. However, benzene has some drawbacks such as high toxicity and relatively high cost [92]. By contrast, methane appears to be a suitable alternative due its non-toxic character and low cost, however, it generates intermediates during the carbon deposition process. Namely, during the heating process methane can generate hydrocarbons such as ethane, ethylene and acetylene. Ethane has a short life time being

then converted to ethylene and then to acetylene [92]. Both ethylene and acetylene can generate carbon directly [91,92]. Considering this, the use of methane as a carbon deposition agent needs to be handled carefully for achieving an acceptable deposition [92]. Moreover, as well as the agent choice, the cracking operation conditions must be also optimized so that pore mouths be narrowed without causing significant loss in adsorption capacity of the material [80,87]. In addition, some homogeneity is preferable in the pore network of the carbon material. If the pore size distribution is too wide, the carbon deposition can cause just a continuous shrinkage of pores of all sizes shifting the pore size distribution to smaller average pore size without achieving the uniform pore size required for good selectivity [46,93]. Figure 1.5 shows a stretch of CVD process.

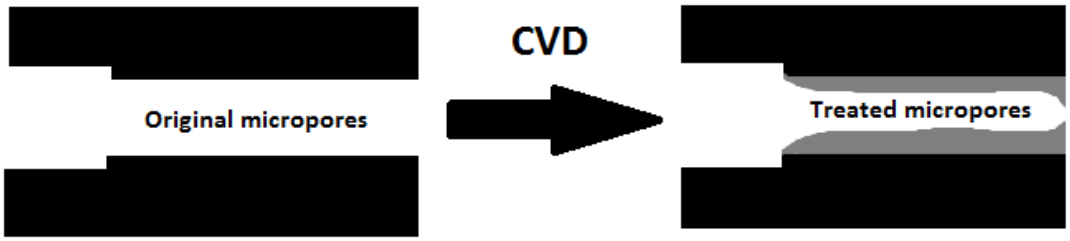

Figure 1.5. Representation of carbon vapour deposition process in carbon materials pore structure.

1.1.2. CMS surface chemistry

It is well known that properties such as pore size distribution and micropore surface area directly influence the carbon materials performance [10]. However, CMS with similar textural characteristics and properties can display a very different adsorption behaviour for the same adsorbate [10,94]. This happens since porous texture is not the only parameter that influences the carbon materials performance (adsorption capacity and kinetics) [10]. The nature and amount of surface functional groups must be also considered. The carbon atoms located at the edges of the basal atoms correspond to unsaturated carbons which contain unpaired electrons. When these sites are bonded to heteroatoms, they form surface groups. Among the existing surface groups, oxygen-bonded are the most frequent surface groups in carbons. Namely, CMS present a relatively large edge area resulting in a strong tendency for oxygen chemisorption. Accordingly, molecular oxygen can dissociate into atoms and react chemically with the surface containing-carbon atoms forming then oxygen compounds. This reaction/oxidation is particularly significant with the temperature increase; however,

this occurs even at room temperature on carbons previously treated at high temperatures but with highly reactive surface sites. Oxygen-bonded groups are not only formed by reaction with molecular oxygen, they can also result from reaction with other oxidizing gases such as ozone, nitrous oxide, carbon dioxide, among others, and, also by oxidizing solutions as nitric acid, hydrogen peroxide and others [10]. These reactions also allow tailoring the carbons surface by using oxidation agents for creating oxygen functionalities or by heat treatment envisioning its removal in a selective way or complete, depending on the applied temperatures [10,95]. Figure 1.6 shows some of the most important and common surface groups found on carbon materials.

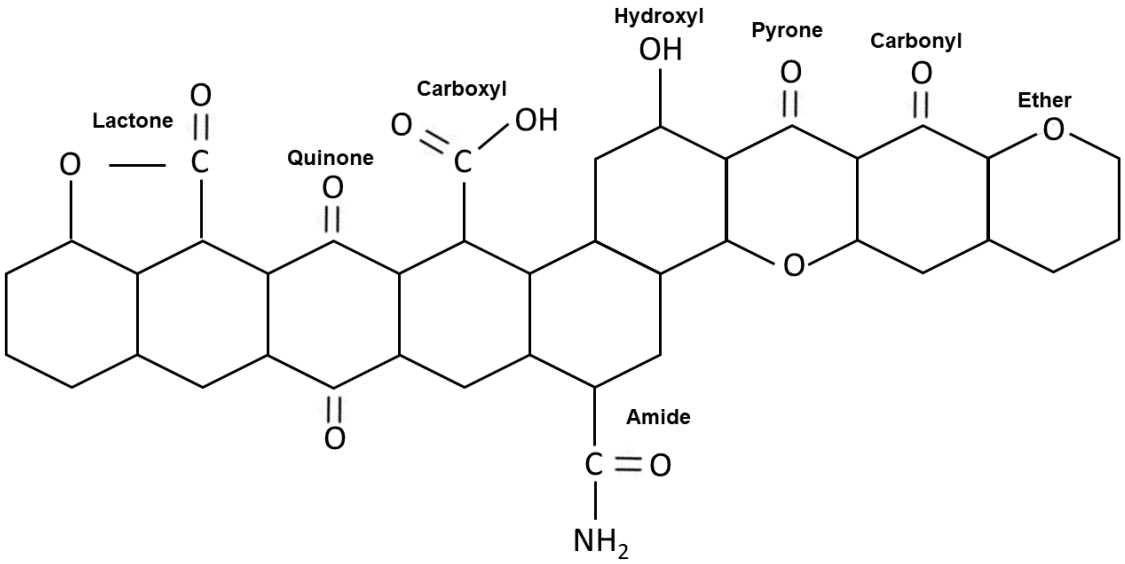

Figure 1.6. Most common surface functional groups present in carbon materials (adapted from [10]).

The surface-active sites associated with functional groups embody a small portion of the total surface area of carbon materials. Nevertheless, the introduction of small variations into chemical surface groups of a CMS may result in significant changes on its performance. This occurs since surface groups can strongly influence the interaction between the carbon material and the adsorbates [10]. In terms of carbon surface chemistry modifications, two principal effects must be taken into account: i) the modification of hydrophobic/hydrophilic character and ii) the modification of acid or basic character [96–98]. Generally, CMS display a hydrophobic character. However, when oxygen-containing surface groups are present, due its polar character, the surface becomes more hydrophilic since these groups can form hydrogen bonds with water molecules [10,98,99]. Figure 1.7 illustrates hydrogen bonds mechanism in carbon

oxygen-containing surface functional groups. Hydrogen bonds phenomenon is significantly relevant for example on the preparation of carbon-supported catalysts from aqueous solutions and for carbon materials adsorption compounds in a gas stream [10,94]. In the first one this is crucial since the wettability of the carbon-supported catalyst will control the degree of impregnation of the solution that contains the catalyst [10,94]; in the second one this effect is very important since the presence of oxygenated groups influence the adsorption of water molecules or even oxygen chemisorption present in the air, which can directly influence the carbon materials performance. Namely, oxygen chemisorption and/or water adsorption can block the access of the adsorbate into the micropores, influencing then the capacity and kinetics of adsorption [10,100].

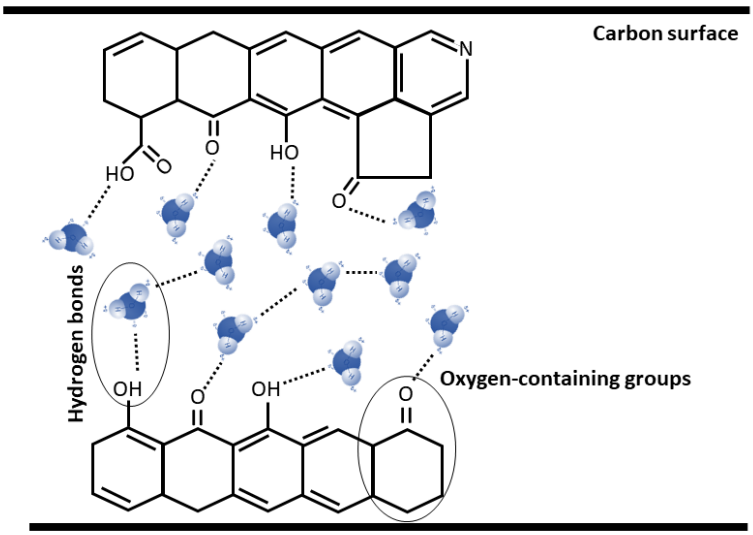

Figure 1.7. Illustration of water molecules interaction with oxygen-containing surface groups in CMS (adapted from [10]).

The basic or acid character of the surface functional groups can also strongly influence the carbons performance. CMS are amphoteric by nature, *i.e.*, they contain both acid and basic sites [10]. Functional groups such as carboxyl, hydroxyl, lactone, among others, act as acidic groups if the pH of the medium is higher than the pKa of these groups (basic medium) [10,101,102]. On the other hand, the discrimination of basic sites is not that simple [10]. There are reported two main features that contribute to the basicity of the carbons surface: i) delocalized π-electrons of fused aromatic structures and (ii) basic surface functional groups (*e.g.*, nitrogen-enriched

functionalities) [103]. Functional groups such as chromene, ketone and pyrone are known to contribute to the basicity of carbons [10,103–105]. Some studies searched for the basicity contribution of functional basic groups containing oxygen and resonating π-electrons in the carbon matrix [103]. Leon y Leon *et al.* [105] studied the basicity of the carbons surface considering two series of carbons and observed that oxygen-free carbon surfaces efficiently adsorbed protons from aqueous media [103]. The authors reported that this adsorption ability is attributed to the presence of π-electron rich areas located on the basal plane of carbon crystallites. Further, these regions are assumed to have a Lewis basic character [103,106]. Likewise, chemical modification of the surface by the introduction of nitrogen functionalities can also induce basicity. This modification can enhance the interactions between the carbon surface and acid species by dipole–dipole interactions, hydrogen bonding and covalent bonding [103,107]. In agreement with this, the overall acid or basic character of a CMS is related with the concentration and acid/basic strength of the surface functional groups. If the acid groups are in majority of number or their overall acidic strength is higher than the one for basic groups, the CMS acquires basic character and vice-versa [10]. Also, the pH of the medium in relation to the point of zero charge (pH_{PZC}) may be considered. Then, when the pH > pH_{PZC}, acid functionalities will dissociate and release protons into the medium leaving a negatively charged surface into the carbon [10,108]. By contrast, if the pH < pH_{PZC}, basic sites will combine with protons from the medium leaving a positively charged surface. Considering this, the performance and adsorbate interactions of the carbons can be adjusted by modifying the surface chemistry and/or the pH of the medium, when possible. In a simple approach, carbon materials with basic character are preferable for adsorbing acid molecules and acid character carbon for adsorbing basic molecules [10,108]. Furthermore, the adsorption of cations will be favoured in negative charged carbon surfaces and anions adsorption by positively charged carbon surfaces by electrostatic forces [109–111]. In agreement with this information, the carbon materials adsorption performance can be improved by modifying/tailoring its surface chemistry.

1.1.3. CMS pore size and geometry

Literature reports several studies for pores classification [112–116], however, giving a consistent porous classification in solid materials is difficult [117]. Kaneko [116]

reported an interesting classification of pores based on origin, structure, size and accessibility. Considering pores origin and structure two main categories can be defined:

i) intraparticle pores - pores allocated to individual particles, often designated as structurally intrinsic pores;

ii) injected intrinsic pores/extrinsic pores - pores formed by a reaction when a foreign substance is impregnated in the adsorbent material and subsequently removed by modification procedures.

Here, when the foreign substance does not contaminate the adsorbent material, *i.e.*, the substance is fully removed from the material, the formed pores are called pure extrinsic pores. Extrinsic pores could also be pillared, *i.e.*, can be produced by applying pillaring materials such as metal hydroxides. It is important to refer that some extrinsic intrapores could also be interparticle pores [116,117].

Other existent pores classification is based on their accessibility to surrounded adsorbates – Figure 1.8. Pores connected with the external surface and accessible to molecules and ions are called “open pores”; pores open only at one end are classified as “blind or dead-end pores”. Also, pores can be open at two ends being called “through pores” [117]. When porous solids/adsorbents are insufficiently heated, parts near the pores collapse inducing the formation of “closed pores” that do not communicate with adsorbate entities. Moreover, “closed pores” can also result from insufficient gas flowrate in adsorbate carbonization step [117]. Despite “closed pores” do not contribute for molecules adsorption, it influences the mechanical properties of the carbon adsorbent. Ruike *et al.* [113] designated “closed pores” by a type of pores that are not penetrated by helium at 303 K. There are other interpretations for “closed pores” such as pores whose width is smaller than the molecular size. Kaneko *et al.* [116] cited also classifications by IUPAC [9] and studies by Bindra *et al.* [118] based on pores geometry. In accordance to Kaneco [116] pores are divided by four geometrical shapes:

i) slite-shape pores;

ii) cylinder shape pores;

iii) cone-shape pores;

iv) ink-bottle pores.

This shape classification is very similar to the one proposed by IUPAC [9], the only difference is the funnel shape instead of cone-shape geometry proposed by Kaneko [116,117].

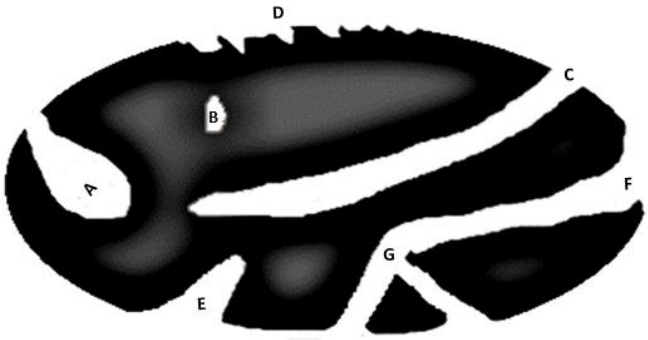

Figure 1.8. Pores classification scheme according with their accessibility to adsorbate molecules [9]. A, C, E – pores open only at one end; D, F – open pores; B – closed pores and G – pores open at two ends (adapted from [9]).

Literature also reports other types of pore shape such as rhomboid, elliptical and square shapes. However, for simplifying the irregularity in geometry, pores shape is regularly based on model systems. In agreement with this, pores modeled systems are preferable for describing different structures such as [9]:

i) cylinders (most likely the case of activated oxides like alumina);
ii) prisms (the case of some fibrous zeolites);
iii) cavities and windows (some zeolites);
iv) slits (may occur on clays and activate carbons);
v) spheres (often the pores are the voids resultant of solid spheres contact to each other; this is the case of gels such as silica gel, zirconia gel and others).

Pores description uses the combination of these forms and their modelling, depending still of its structural elements' arrangement [117]. Then, model development may include enough criteria for better describing pores system in terms of geometry, pore size, orientation, location and type of connectivity [117]. Since solid surface (adsorbent) chemistry and morphology influence the interactions with the adsorbate, its knowledge is needed for better access the materials performance for a given separation [14]. When an adsorbate molecule is placed into two flat surfaces, *i.e.*, in a

slit-shaped pore, it interacts with both surfaces and the potentials of the surfaces overlap. Also, the overlap extent depends on the surface pore size, decreasing with pore size increasing. When pores are cylindrical or spherical the potentials are even greater than in slit-like pores due to more atoms are interacting with the adsorbate molecule [14]. Table 1.6 shows the theoretical threshold pressure for nitrogen adsorption on carbons for different pore sizes and geometries [14]. The calculations were obtained by using Horvath–Kawazoe (HK) model [119] with a corrected version by Rege and Yang [120].The corrected model was based in pore dimensions from nitrogen isotherms that described well the pore dimensions for an extent number of materials, being included carbon and zeolites [119].

Table 1.6. N_2 theoretical threshold pressure for adsorption by varying pore size and pore shape.

Pore size (Å)	P/P_0 Slit-shaped pores	P/P_0 Cylindrical pores	P/P_0 Spherical pores
4	6.3×10^{-7}	1.3×10^{-12}	3.2×10^{-51}
5	9.1×10^{-6}	2.9×10^{-10}	1.1×10^{-42}
6	3.5×10^{-5}	8.3×10^{-9}	2.5×10^{-36}
7	1.2×10^{-4}	6.5×10^{-8}	6.2×10^{-32}
9	6.1×10^{-4}	3.5×10^{-6}	3.1×10^{-24}
12	2.6×10^{-3}	2.3×10^{-5}	1.2×10^{-20}

For N_2 at -196 ºC and P_0= 1 atm

1.2. Challenges in CMS preparation

1.2.1. CMS aging

Previous knowledge indicates that often, when carbon molecular sieves surface are exposed to air, even at room temperature, irreversible oxygen chemisorption can occur [121,122]. When oxygen chemically bonds the carbon surface its completely removal is possible by heating the material up to 700 ºC – 800 ºC under inert atmosphere or vacuum (CO and CO_2 release). However, when samples are again exposed to ambient air, oxygen-carbon interactions may occur, and, oxygenated surface groups can be formed. The formation of this oxygenated surface groups can favour the water adsorption into the carbon structure which is other type of critical aging in carbons. Therefore, the presence of oxygenated groups and, consequently, of water molecules linked to this groups, can result in a reduction of the effective pores diameter and can

directly change the CMS performance consequence of microporous properties modifications [121,123,124]. Verma and Walker [125] observed that when carbon molecular sieve materials were exposed to air at room temperature the kinetics of adsorption decreased significantly as well as the selectivity. For overcoming this carbon-oxygen interaction problem, Stoeckli and Kraehenbuehl [126] and Verma and Walker [125] applied a hydrogen surface treatment at high pressure and temperature for passivating carbon surface active sites where aging was occurring. However, this hydrogen passivation was not completely effective being necessary to search for other techniques [121]. Menendez *et al.* [98] observed that by heating activated carbons at high-temperatures and in an inert environment, oxygen-containing surface groups were effectively removed. However, the authors observed that some very reactive sites capable of re-adsorbing oxygen at room temperature still remained. For overcoming this, they performed a hydrogen passivation at high temperatures and observed that oxygen was removed as well as surface was free of active sites capable to adsorb oxygen at room temperature. Dastgheib *et al.* [127] submitted a series of activated carbons with different types of surface chemistry and microporosity to heat treatment under i) vacuum and ii) hydrogen. After the treatment, samples were submitted to oxygen adsorption, and, samples treated with hydrogen showed lower amounts of oxygen uptake than samples treatment under vacuum. The obtained results indicated that hydrogen treatment may have stabilized the surfaces of the carbons. Furthermore, Lagorsse *et al.* [128] suggested that despite hydrogen passivation stabilize a extend number of active sites they are not completely removed being necessary to apply other techniques to completely stabilize the samples. Jones and Koros [129] proposed the use of propylene as a cleaning agent of CMS membranes after exposure to contaminants. However, the authors could not find the reasons why propylene was so effective in removed the adsorbed contaminants. Years later, Menendez and Fuertes [121] observed that propylene could prevent oxygen chemisorption on carbon membranes without affect the material performance.

1.3. Potential industrial gas separations for CMS materials

The use of carbon molecular sieves is widespread, and, a specific application deals with a carbon material with specific characteristics. The applications can broadly be

divided into two general categories: i) liquid-phase applications and ii) gas-phase applications [12].

Liquid-phase applications differ from gas-phase applications mostly in CMS pore size distribution. Liquid-phase carbons present higher pore volume in the macropores range which allows a faster liquid diffusion into mesopores and micropores. Furthermore, larger pores allow higher adsorption of larger molecules, either impurities or products. CMS for liquid-phase separations can be used in powder, granular or shaped form. Powdered carbon particles are normally preferred for batch applications and, unlike, granular or shaped-carbon are more suitable for continuous flow systems [12]. Further, gas-phase applications are focused into separation processes, gas storage and catalysis. The use of CMS in chemical process industry, mainly for separating gases, has been known for several decades [12]. Most of carbon materials used in gas-phase applications are granular or shaped [12]. Also, gas separation processes comprehends the major gas-phase application of carbon molecular sieve materials [12]. The development on CMS research field allowed the fabrication of materials with suitable porosity for efficiently separate gases based in differences in adsorption capacity and/or differences in kinetics of adsorption [12,130].

Figure 1.9 shows some of the possible applications of carbon molecular sieve materials.

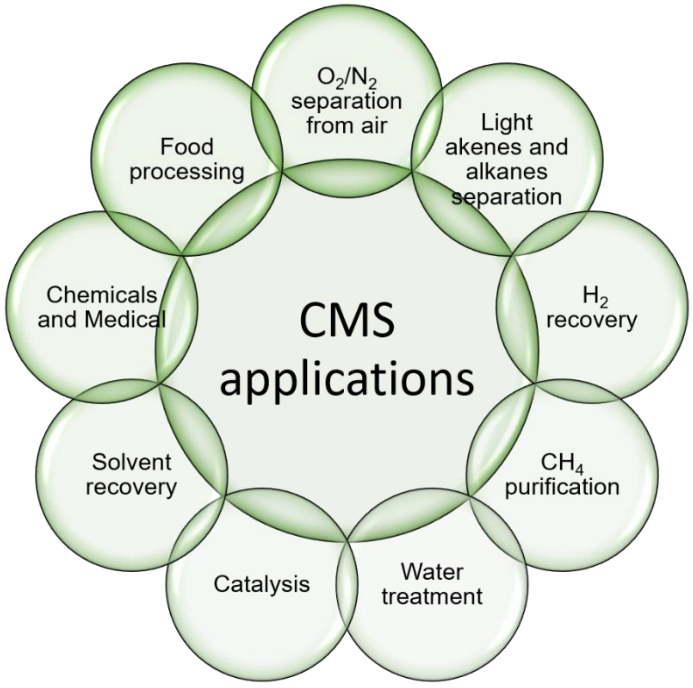

Figure 1.9. Possible applications of carbon molecular sieve materials.

1.3.1. Nitrogen and oxygen separation from air

One of the most important industrial applications of carbon molecular sieves is the air separation by nitrogen production [131]. The classical way for separating air is the cryogenic distillation. This process separates the main air gases (nitrogen 78 %, oxygen 21 %, argon 0.7 %) by differences in boiling points. However, this technology displays some drawbacks such as wasting energy by converting liquid into gas, wasting pure gas during storage due to evaporation, high-risk potential during gases transportation and storage and fixed high purity of the gases [132]. For overcoming these problems, technologies such as membrane systems and PSA become preferable. Membrane systems generally leads with N_2 purities of 95 % to 98 % and small gas flows (up to 200 $m^3 \cdot h^{-1}$). On the other hand, PSA systems allow for a higher range of applications as well as higher nitrogen purities (95 % to 99.999 %) and, also, higher flow rates can be used (up to 3000 $m^3 \cdot h^{-1}$) [132]. The development of PSA systems for air separation is closely followed by the development of adsorbent materials research, which are the core of the PSA technology [54,132]. PSA for air separation can be governed by both equilibrium and non-equilibrium sorption mechanisms. Specifically, air separation for nitrogen production is a non-equilibrium process since it is led by kinetics of adsorption [131]. Carbon molecular sieves appear as the adsorbent materials that display the necessary properties for kinetic separation since they discriminate molecules by differences in its kinetics of adsorption [133]. Namely, and for air separation processes, this occurs since ultramicropores (0.3 nm – 0.7 nm [134]) reduce the diffusion velocity of nitrogen and oxygen in distinct ways; oxygen molecules have faster diffusion into ultra- and micropores than nitrogen. This effect of “exclusion” by differences in kinetics is usually called “sieving effect” and it enriches the nitrogen concentration around the CMS particle. For making this effect industrially applicable, CMS pore distribution should mainly be located in ultra- and micropores range (0.3 nm – 2.0 nm [135]), which can be achieved by applying several chemical and physical treatments during the carbon material production [132].

A complete PSA system for air separation/nitrogen production consists in three main parts: i) air supply and purification; ii) adsorptive air separation and iii) nitrogen storage and supply [132]. Nitrogen, as well as argon, displays lower diffusivity when compared with oxygen, thus, nitrogen leaves the PSA column at high pressure during

the production step [54]. Unlike, oxygen is removed during depressurization and purge steps [54]. By optimizing the PSA operation conditions, the oxygen concentration can be easily less than 1 ppm [132]. Then, the developments in carbon molecular sieve adsorbents conception, embracing both equilibrium and kinetic gas separation, allows for new advances in PSA technology [18,29,54,136–140].

1.3.2. Propylene and propane separation

One of the most attractive separations in petrochemical industries are the olefin / paraffin mixtures [141]. Particularly, propylene / propane separation is one of the most difficult olefin / paraffin separations since they have similar volatilities and molecular size [142,143]. Propylene is often used in refinery operations and is the "construction-block" for several petrochemical products such as polypropylene, acrylonitrile, oxo-alcohols, propylene oxide, acrylic acid, isopropylalcohol, polygas chemicals, among others [38]. Propylene purity specifications depends on its finality: i) polymer-grade propylene (*ca.* 99.5 %), used for polypropylene and copolymers production; ii) chemical-grade propylene (*ca.* 95 %), used for several synthetic organic chemicals production and/or iii) refinery grade propylene (*ca.* 65 %) for producing alkylate [38,144].

Propylene consumption has been increasingly growing and it is expected to grow dramatically in the near future due to its high demand in several applications [38,145]. However, this increase in propylene consumption does not follows its production since it is limited by the production of side products, such as ethylene via steam cracking or gasoline from fluid catalytic cracking [38,145]. Regarding propane, its applications in motor fuel, when produced in refinery operations, often contains undesirable substantial amounts of propylene. Since propylene can cause deposition problems in the engine and injector, its removal when propane is used as a fuel is crucial. Furthermore, propylene can also polymerize in storage, fuel lines, or vaporizers, causing then, plugging by gum deposits. The expansion of propane use in motor fuel market opens new research areas since propylene removal becomes more important [144].

Propylene / propane separation is mainly accomplished by distillation-based technologies, which represent one of the most important and high cost processes in chemical industry [142,146]. Due to its high cost, alternative processes must be

considered for overcoming this problem. Adsorption-based separation processes appear as a versatile and cost-efficient separation processes. Here, the structure and properties of the employed adsorbent materials directly influence the separation performance. Hence, the adsorption separation can occur by two types of separation mechanisms: i) molecular sieving or steric size exclusion and/or ii) equilibrium or kinetics-based separation [142,147,148]. On most adsorbents studied for propylene / propane separations (zeolites or amorphous adsorbents), the separation mechanisms are based on adsorption capacity or size/molecular exclusion. Only a few materials can separate these adsorbates by differences in adsorption kinetics [142,147,148]. Materials such as microporous metal organic frameworks (MMOFs) showed a great potential for hydrocarbons separation [149–151]. Their capability in separating propylene / propane by equilibrium of adsorption and by differences in kinetics of adsorption is widely investigated. Also, adsorbents such as silica gel, zeolites 4A and 13X, chemical adsorbents with π-complexation metal (*e.g.* copper or silver ions), activated carbons and carbon molecular sieve materials have been studied for propylene / propane gas separations [36,38,148,152–155]. Membranes also appeared as a promising option for separating these entities [156–158].

The searching for new high-performance adsorbent materials derived from low-cost precursor materials is crucial for reaching more efficient and low-cost gas separation of these olefins / paraffins, specially propylene / propane, which is extremely important for several industrial applications.

1.4. Motivation and thesis outline

Carbon molecular sieve adsorbents are widely used in several industrial applications, especially in gas separation processes. This type of materials can be tailored depending on its target application, increasing then its specificity and performance on a given separation. However, depending on the applied treatments during its production, reactive sites can be formed and oxygen chemisorption can occur. This aging phenomenon can cause a loss of performance into carbon adsorbents being then necessary to stabilize them. The aim of this work concerns in the preparation of stabilized carbon molecular sieve materials targeting high performance materials for gas separations such as O_2 / N_2 and C_3H_6 / C_3H_8.

The present thesis is divided in six chapters as follows:

Chapter I presents an introduction of the work.

Chapter II studies the carbon molecular sieves aging by oxygen and humidity and its passivation by propylene post-treatment.

Chapter III reports the preparation and characterization of aging-free carbon molecular sieve adsorbents for O_2 / N_2 gas separation though kinetic selectivity.

Chapter IV reports the preparation and characterization of a stable and highly equilibrium C_3H_6 / C_3H_8 selective carbon molecular sieve adsorbent prepared from a single carbonization step of a low-cost cellulosic precursor.

Chapter V reports a novel carbon molecular sieve adsorbent with inverse C_3H_8 / C_3H_6 adsorption selectivity and prepared from a low-cost phenolic resin precursor.

Chapter VI presents the main conclusions of the thesis and exposes suggestions for future research.

Appendix A shows some of the set-ups used during the thesis work.

1.5. References

[1] M. Inagaki, F. Kang, Chapter 1- Introduction, in: Butterworth-Heinemann (Ed.), Mater. Sci. Eng. Carbon Fundam. (2nd Ed., Elsevier Inc., Waltham, 2014: p. 542. doi:10.1016/B978-0-12-800858-4.00001-2.

[2] C. Rolence, R.L. Machunda, K.N. Njau, Water hardness removal by coconut shell activated carbon, Int. J. Sci. Technol. Soc. 2 (2014) 97–102. doi:10.11648/j.ijsts.20140205.11.

[3] E. Gracia-Espino, F. López-Urías, H. Terrones, M. Terrones, Chapter 1 - Novel nanocarbons for adsorption, in: Nov. Carbon Adsorbents, 2012: pp. 3–34. doi:10.1016/B978-0-08-097744-7.00001-6.

[4] T.D. Burchell, Carbon materials for advanced technologies, 1999. doi:10.1016/B978-0-08-042683-9.X5000-6.

[5] H.O. Pierson, Handbook of carbon, graphite, diamonds and fullerenes, Noyes Publications, 1994.

[6] S.M. Manocha, Porous carbons, in: Sadhana, Springer India, 2003: pp. 335–348. doi:10.1007/BF02717142.

[7] F. Çeçen, Activated Carbon, in: Kirk-Othmer Encycl. Chem. Technol., 2014: pp. 1–34. doi:10.1002/0471238961.0103200902011105.a01.pub3.

[8] M. Thommes, K. Kaneko, A. V Neimark, J.P. Olivier, F. Rodriguez-Reinoso, J. Rouquerol, K.S.W. Sing, Physisorption of gases, with special reference to the evaluation of surface area and pore size distribution (IUPAC Technical Report), Pure Appl. Chem. 87 (2015) 1051–1069. doi:10.1515/pac-2014-1117.

[9] J. Rouquerol, D. Avnir, C.W. Fairbridge, D.H. Everett, J.M. Haynes, N. Pernicone, J.D.F. Ramsay, K.S.W. Sing, K.K. Unger, Recomendations for the characterization of porous solids, Pure Appl. Chem. 66 (1994) 1739–1758. doi:10.1351/pac199466081739.

[10] J.A. Menéndez-Diaz, I. Martín-Gullón, Types of carbon adsorbents and their production, Interface Sci. Technol. 7 (2006) 1–47. doi:10.1016/S1573-

4285(06)80010-4.

[11] H. Marsh, F. Rodríguez-Reinoso, Activated carbon, 1st Ed., Elsevier Ltd, Oxford, 2006.

[12] S.J. Allen, L. Whitten, G. Mckay, The production and characterisation of activated carbons: a review, Dev. Chem. Eng. Miner. Process. 6 (1998) 231–261. doi:10.1002/apj.5500060501.

[13] H.C. Foley, Carbogenic molecular sieves: synthesis, properties and applications, Microporous Mater. 4 (1995) 407–433. doi:10.1016/0927-6513(95)00014-Z.

[14] R.T. Yang, Adsorbents: fundamentals and applications, Jonh Wiley & Sons, Inc., 2003. doi:10.1038/nprot.2009.120.Multi-stage.

[15] G.E. Keller, Gas-adsorption process: state of the art, in: Ind. Gas Sep., 1983: pp. 145–169. doi:10.1021/bk-1983-0223.ch008.

[16] U.S. Department of Energy, Fuel cell technologies market report 2016, Washington D. C., 2016.

[17] R. Felseghi, E. Carcadea, M.S. Raboaca, C.N. Trufin, C. Filote, Hydrogen fuel cell technology for the sustainable future of stationary applications, Energies. 12 (2019) 1–28. doi:10.3390/en12234593.

[18] F. Relvas, R.D. Whitley, C. Silva, A. Mendes, Single-stage pressure swing adsorption for producing fuel cell grade hydrogen, Ind. Eng. Chem. Res. 57 (2018) 5106–5118. doi:10.1021/acs.iecr.7b05410.

[19] W.J. Hehre, Ab initio molecular orbital theory, Acc. Chem. Res. 9 (1976) 399–406. doi:10.1021/ar50107a003.

[20] G.P. Lithoxoos, L.D. Peristeras, G.C. Boulougouris, I.G. Economou, Monte Carlo simulation of carbon monoxide, carbon dioxide and methane adsorption on activated carbon, Mol. Phys. 110 (2012) 1153–1160. doi:10.1080/00268976.2012.659223.

[21] M. Jorge, C. Schumacher, N.A. Seaton, Simulation study of the effect of the chemical heterogeneity of activated carbon on water adsorption, Langmuir. 18

(2002) 9296–9306. doi:10.1021/la025846q.

[22] A.J. Hernández-Maldonado, G. Qi, R.T. Yang, Desulfurization of commercial fuels by π-complexation: monolayer CuCl/γ-Al_2O_3, Appl. Catal. B Environ. 61 (2005) 212–218. doi:10.1016/j.apcatb.2005.05.003.

[23] X. Ma, S. Velu, J.H. Kim, C. Song, Deep desulfurization of gasoline by selective adsorption over solid adsorbents and impact of analytical methods on ppm-level sulfur quantification for fuel cell applications, Appl. Catal. B Environ. 56 (2005) 137–147. doi:10.1016/j.apcatb.2004.08.013.

[24] J. Rui, F. Liu, R. Wang, Y. Lu, X. Yang, Adsorptive desulfurization of model gasoline by using different Zn sources exchanged NaY zeolites, Molecules. 22:305 (2017) 1–12. doi:10.3390/molecules22020305.

[25] V.C. Srivastava, An evaluation of desulfurization technologies for sulfur removal from liquid fuels, RSC Adv. 2 (2012) 759–783. doi:10.1039/c1ra00309g.

[26] V.I. Agueda, J.A. Delgado, M.A. Uguina, P. Brea, A.I. Spjelkavik, R. Blom, C. Grande, Adsorption and diffusion of H_2, N_2, CO, CH_4 and CO_2 in UTSA-16 metal-organic framework extrudates, Chem. Eng. Sci. 124 (2015) 159–169. doi:10.1016/j.ces.2014.08.039.

[27] J.A. Delgado, V.I. Águeda, M.A. Uguina, J.L. Sotelo, P. Brea, C.A. Grande, Adsorption and diffusion of H_2, CO, CH_4, and CO_2 in BPL activated carbon and 13X zeolite: evaluation of performance in pressure swing adsorption hydrogen purification by simulation, Ind. Eng. Chem. Res. 53 (2014) 15414–15426. doi:10.1021/ie403744u.

[28] A. Golmakani, S. Fatemi, J. Tamnanloo, Investigating PSA, VSA, and TSA methods in SMR unit of refineries for hydrogen production with fuel cell specification, Sep. Purif. Technol. 176 (2017) 73–91. doi:10.1021/ie070942d.

[29] S. Cavenati, C.A. Grande, A.E. Rodrigues, Layered pressure swing adsorption for methane recovery from $CH_4/CO_2/N_2$ streams, Adsorption. 11 (2005) 549–554. doi:10.1007/s10450-005-5983-7.

[30] S.J. Bhadra, S. Farooq, Separation of methane-nitrogen mixture by pressure swing adsorption for natural gas upgrading, Ind. Eng. Chem. Res. 50 (2011) 14030–14045. doi:10.1021/ie201237x.

[31] S. Kuznicki, V.A. Behl, I. Petrovic, P. Blosser, Barium exchanged ETS-4 and its use in a process for the separation of nitrogen from mixtures thereof with methane, WO 99/32222, 1999.

[32] S. Han, J. Park, J. Kim, S. Cho, Propylene recovery from propylene/propane/nitrogen mixture by PSA process, Adsorption. 11 (2005) 621–624. doi:10.1007/s10450-005-5995-3.

[33] C.A. Grande, D.P. Araujo, S. Cavenati, N. Firpo, E. Basaldella, A.E. Rodrigues, New π-complexation adsorbents for propane - propylene separation, Langmuir. 20 (2004) 5291–5297. doi:10.1021/la036400s.

[34] Y.S. Bae, C.Y. Lee, K.C. Kim, O.K. Farha, P. Nickias, J.T. Hupp, S.T. Nguyen, R.Q. Snurr, High propene/propane selectivity in isostructural metal-organic frameworks with high densities of open metal sites, Angew. Chemie - Int. Ed. 51 (2012) 1857–1860. doi:10.1002/anie.201107534.

[35] A. Cadiau, K. Adil, P.M. Bhatt, Y. Belmabkhout, M. Eddaoudi, A metal-organic framework – based splitter for separating propylene from propane, Science (80-.). 353 (2016) 137–140. doi:10.1126/science.aaf6323.

[36] F.A. Da Silva, A.E. Rodrigues, Adsorption equilibria and kinetics for propylene and propane over 13X and 4A zeolite pellets, Ind. Eng. Chem. Res. 38 (1999) 2051–2057. doi:10.1021/ie980640z.

[37] F.A. Da Silva, A.E. Rodrigues, Vacuum swing adsorption for propylene/propane separation with 4A zeolite, Ind. Eng. Chem. Res. 40 (2001) 5758–5774. doi:10.1021/ie0008732.

[38] M.C. Campo, A.M. Ribeiro, A. Ferreira, J.C. Santos, C. Lutz, J.M. Loureiro, A.E. Rodrigues, New 13X zeolite for propylene/propane separation by vacuum swing adsorption, Sep. Purif. Technol. 103 (2013) 60–70. doi:10.1016/j.seppur.2012.10.009.

[39] C.A. Grande, J. Gascon, F. Kapteijn, A.E. Rodrigues, Propane/propylene separation with Li-exchanged zeolite 13X, Chem. Eng. J. 160 (2010) 207–214. doi:10.1016/j.cej.2010.03.044.

[40] S. Kim, J.H. Kang, S.K. Kim, Y. Bae, Extraordinarily large and stable methane delivery of MIL-53 (Al) under LNG- ANG conditions, Chem. Eng. J. 365 (2019) 242–248. doi:10.1016/j.cej.2019.01.182.

[41] B. Li, H. Wen, W. Zhou, J.Q. Xu, B. Chen, Porous metal-organic frameworks: promising materials for methane storage, Chem. 1 (2016) 557–580. doi:10.1016/j.chempr.2016.09.009.

[42] J.E. Park, G.B. Lee, S.Y. Hwang, J.H. Kim, B.U. Hong, H. Kim, S. Kim, The effects of methane storage capacity using upgraded activated carbon by KOH, Appl. Sci. 8 (2018) 1–10. doi:10.3390/app8091596.

[43] M. Feroldi, A.C. Neves, C.E. Borba, H.J. Alves, Methane storage in activated carbon at low pressure under different temperatures and flow rates of charge, J. Clean. Prod. 172 (2018) 921–926. doi:10.1016/j.jclepro.2017.10.247.

[44] M. Beckner, A. Dailly, Adsorbed methane storage for vehicular applications, Appl. Energy. 149 (2015) 69–74. doi:10.1016/j.apenergy.2015.03.123.

[45] S. Sethupathi, M.J.K. Bashir, Z.A. Akbar, A.R. Mohamed, Biomass-based palm shell activated carbon and palm shell carbon molecular sieve as gas separation adsorbents, Waste Manag. Res. 33 (2015) 303–312. doi:10.1177/0734242X15576026.

[46] M.M.A. Freitas, J.L. Figueiredo, Preparation of carbon molecular sieves for gas separations by modification of the pore sizes of activated carbons, Fuel. 80 (2001) 1–6. doi:10.1016/S0016-2361(00)00066-1.

[47] T. Horikawa, J. Hayashi, K. Muroyama, Preparation of molecular sieving carbon from waste resin by chemical vapor deposition, Carbon N. Y. 40 (2002) 709–714. doi:10.1016/S0008-6223(01)00157-9.

[48] Y. Kawabuchi, H. Oka, S. Kawano, I. Mochida, N. Yoshizawa, The modification of

pore size in activated carbon fibers by chemical vapor deposition and its effects on molecular sieve selectivity, Carbon N. Y. 36 (1998) 377–382. doi:10.1016/S0008-6223(97)00186-3.

[49] C.R. Reid, I.P. O'Koy, K.M. Thomas, Adsorption of gases on carbon molecular sieves used for air separation. Spherical adsorptives as probes for kinetic selectivity, Langmuir. 14 (1998) 2415–2425. doi:10.1021/la9709296.

[50] J.E. Metcalfe, M. Kawahata, P.L. Walker, Molecular sieve properties of activated anthracite, Fuel. 42 (1963) 233–238.

[51] S. V Moore, D.L. Trimm, The preparation of carbon molecular sives by pore blocking, Carbon N. Y. 15 (1977) 177–180. doi:10.1016/0008-6223(77)90054-9.

[52] S. Sircar, Basic research needs for design of adsorptive gas separation processes, Ind. Eng. Chem. Res. 45 (2006) 5435–5448. doi:10.1021/ie051056a.

[53] D. Ruthven, Principles of adsorption and adsorption processes, Wiley-Interscience, New York, 1984.

[54] D.A.S.S. Ferreira, High-purity oxygen production by VPSA, University of Porto, 2015.

[55] M.M.C.C. Santos, Carbon molecular sieve membranes for gas separation: study, preparation and characterization, University of Porto, 2009.

[56] H.C. Joshi, R. Kumar, R.K. Singh, D. Lal, Preparation and characterization of molecular sieving carbon by methane and benzene cracking over activated carbon spheres, Carbon Scince. 8 (2007) 12–16. doi:10.5714/CL.2007.8.1.012.

[57] M. Jasieńko-Halat, K. Kedzior, Comparison of molecular sieve properties in microporous chars from low-rank bituminous coal activated by steam and carbon dioxide, Carbon N. Y. 43 (2005) 944–953. doi:10.1016/j.carbon.2004.11.024.

[58] R. Arriagada, G. Bello, R. García, F. Rodríguez-Reinoso, A. Sepúlveda-Escribano, Carbon molecular sieves from hardwood carbon pellets. The influence of carbonization temperature in gas separation properties, Microporous Mesoporous Mater. 81 (2005) 161–167. doi:10.1016/j.micromeso.2005.02.005.

[59] E. David, A. Talaie, V. Stanciu, A.C. Nicolae, Synthesis of carbon molecular sieves by benzene pyrolysis over microporous carbon materials, Mater. Process. Technol. 157–158 (2004) 290–296. doi:10.1016/j.jmatprotec.2004.09.046.

[60] S.N. Vyas, S.R. Patwarthan, H.B. Natraj, Synthesis and characterisation of carbon molecular sieves, J. Chem. Soc. 86 (1990) 3455–3460. doi:10.1039/FT9908603455.

[61] S.N. Vyas, S.R. Patwardhan, B. Gangadhar, Carbon molecular sieves from bituminous coal by controlled coke deposition, Carbon N. Y. 30 (1992) 605–612. doi:10.1016/0008-6223(92)90179-Z.

[62] M. Inagaki, New carbons - control of structure and functions, 1st Ed., Elsevier Science Ltd, Oxford, 2000. doi:10.1016/B978-0-08-043713-2.X5000-6.

[63] T.J. Mays, Chapter 3 - Active carbon fibers, in: Carbon Mater. Adv. Technol., Elsevier Science Ltd, 1999: pp. 95–118. doi:10.1016/B978-0-08-042683-9.X5000-6.

[64] J.M. Patrick, Porosity in carbons: characterization and applications, 1st ed., Edward Arnold, London, 1995.

[65] A.F. Ismail, D. Rana, T. Matsuura, H.C. Foley, Carbon-based membranes for separation processes, 2011. doi:10.1007/978-0-387-78991-0.

[66] T. Budinova, E. Ekinci, F. Yardim, A. Grimm, E. Björnbom, V. Minkova, M. Goranova, Characterization and application of activated carbon produced by H_3PO_4 and water vapor activation, Fuel Process. Technol. 87 (2006) 899–905. doi:10.1016/j.fuproc.2006.06.005.

[67] S.M. Yakout, G.S. El-Deen, Characterization of activated carbon prepared by phosphoric acid activation of olive stones, Arab. J. Chem. 9 (2016) S1155–S1162. doi:10.1016/j.arabjc.2011.12.002.

[68] D. Prahas, Y. Kartika, N. Indraswati, S. Ismadji, Activated carbon from jackfruit peel waste by H_3PO_4 chemical activation: pore structure and surface chemistry characterization, Chem. Eng. J. 140 (2008) 32–42. doi:10.1016/j.cej.2007.08.032.

[69] H.M. Mozammel, O. Masahiro, S. Bhattacharya, Activated charcoal from coconut shell using $ZnCl_2$ activation, Biomass and Bionergy. 22 (2002) 397–400. doi:10.1016/S0961-9534(02)00015-6.

[70] C. Pedrero, T. Cordero, J. Rodriguez-Mirasol, J.J. Rodriguez, Preparation of carbon molecular sieves by chemical vapor infiltration of lignin based microporous carbons, in: Proc. Am. Carbon Soc. Conf., 2001.

[71] J. Guo, W.S. Xu, Y.L. Chen, A.C. Lua, Adsorption of NH3 onto activated carbon prepared from palm shells impregnated with H_2SO_4, J. Colloid Interface Sci. 281 (2005) 285–290. doi:10.1016/j.jcis.2004.08.101.

[72] A. Ahmadpour, D.D. Do, The preparation of activated carbon from macadamia nutshell by chemical activation, Carbon N. Y. 35 (1997) 1723–1732. doi:10.1016/S0008-6223(97)00127-9.

[73] Z. Hu, E.F. Vansant, Carbon molecular sieves produced from walnut shell, Carbon N. Y. 33 (1995) 561–567. doi:10.1016/0008-6223(94)00141-L.

[74] A.M. Youssef, N.R.E. Radwan, I. Abdel-Gawad, G.A.A. Singer, Textural properties of activated carbons from apricot stones, Colloids Surfaces A. 252 (2005) 143–151. doi:10.1016/j.colsurfa.2004.09.008.

[75] T. Zhang, W.P. Walawender, L.T. Fan, Preparation of carbon molecular sieves by carbon deposition from methane, Bioresour. Technol. 96 (2005) 1929–1935. doi:10.1016/j.biortech.2005.01.026.

[76] M.A. Ahmad, Preparation of carbon molecular sieves from palm shell: effect of benzene deposition conditions, Adsorption. 15 (2009) 489–495. doi:10.1007/s10450-009-9199-0.

[77] T.S. Farris, C.G. Coe, O. Armor, J.M. Schork, High capacity coconut shell char for carbon molecular sieves, US5164355A, 1992.

[78] S. Guo, J. Peng, W. Li, K. Yang, L. Zhang, S. Zhang, H. Xia, Effects of CO_2 activation on porous structures of coconut shell-based activated carbons, Appl. Surf. Sci. 255 (2009) 8443–8449. doi:10.1016/j.apsusc.2009.05.150.

[79] J. Guo, A.C. Lua, Characterization of adsorbent prepared from oil-palm shell by CO_2 activation for removal of gaseous pollutants, Mater. Lett. 55 (2002) 334–339. doi:10.1016/S0167-577X(02)00388-9.

[80] C. Nguyen, D.D. Do, Preparation of carbon molecular sieves from macadamia nut shells, Carbon N. Y. 33 (1995) 1717–1725. doi:10.1016/0008-6223(96)00130-3.

[81] M. Molina-Sabio, F. Rodríguez-Reinoso, F. Caturla, M.J. Sellés, Developtment of porosity in combined phosphoric acid-carbon dioxide activation, Carbon N. Y. 34 (1996) 457–462. doi:10.1016/0008-6223(95)00209-X.

[82] C.G. Salazar, A. Sepúlveda-Escribano, F. Rodriguez-Reinoso, Preparation of carbon molecular sieves by pyrolytic carbon deposition, Adsorption. 11 (2005) 663–667. doi:10.1007/s10450-005-6003-7.

[83] A.R. Mohamed, M. Mohammadi, G.N. Darzi, Preparation of carbon molecular sieve from lignocellulosic biomass: a review, Renew. Sustain. Energy Rev. 14 (2010) 1591–1599. doi:10.1016/j.rser.2010.01.024.

[84] V.C. Geiszler, W.J. Koros, Effects of polyimide pyrolysis conditions on carbon molecular sieve membrane properties, Ind. Eng. Chem. Res. 35 (1996) 2999–3003. doi:10.1021/ie950746j.

[85] S.M. Saufi, A.F. Ismail, Fabrication of carbon membranes for gas separation - a review, Carbon N. Y. 42 (2004) 241–259. doi:10.1016/j.carbon.2003.10.022.

[86] P.J. Williams, W.J. Koros, Chapter 23 - Gas separation by carbon membranes, in: W.S.W.H. A.G. Fane (Ed.), Adv. Membr. Technol. Appl., John Wiley & Sons, New Jersey, 2008. doi:10.1002/9780470276280.ch23.

[87] S. Villar-Rodil, R. Denoyel, J. Rouquerol, A. Martínez-Alonso, J.M.D. Tascón, Fibrous carbon molecular sieves by chemical vapor deposition of benzene. Gas separation ability, Chem. Mater. 14 (2002) 4328–4333. doi:10.1021/cm021193n.

[88] M.A. Ahmad, W.M.A. Wan Daud, M.K. Aroua, Adsorption kinetics of various gases in carbon molecular sieves (CMS) produced from palm shell, Colloids Surfaces A. 312 (2008) 131–135. doi:10.1016/j.colsurfa.2007.06.040.

[89] M.A. Ahmad, W.M.A. Wan Daud, M.K. Aroua, Synthesis of carbon molecular sieves from palm shell by carbon vapor deposition, J. Porous Mater. 14 (2007) 393–399. doi:10.1007/s10934-006-9032-z.

[90] D. Adinata, W.M.A. Wan Daud, M.K. Aroua, Production of carbon molecular sieves from palm shell based activated carbon by pore sizes modification with benzene for methane selective separation, Fuel Process. Technol. 88 (2007) 599–605. doi:10.1016/j.fuproc.2007.01.009.

[91] S. Villar-Rodil, R. Navarrete, R. Denoyel, A. Albiniak, J.I. Paredes, A. Martínez-Alonso, J.M.D. Tascón, Carbon molecular sieve cloths prepared by chemical vapour deposition of methane for separation of gas mixtures, Microporous Mesoporous Mater. 77 (2005) 109–118. doi:10.1016/j.micromeso.2004.08.017.

[92] M. Mohammadi, G.D. Najafpour, A.R. Mohamed, Production of carbon molecular sives from palm shell through carbon deposition from methane, Chem. Ind. Chem. Eng. Q. 17 (2011) 525–533. doi:10.2298/CICEQ110506038M.

[93] M.A. Lillo-Ródenas, D. Cazorla-Amorós, A. Linares-Solano, Behaviour of activated carbons with different pore size distributions and surface oxygen groups for benzene and toluene adsorption at low concentrations, Carbon N. Y. 43 (2005) 1758–1767. doi:10.1016/j.carbon.2005.02.023.

[94] L.R. Radovic, F. Rodriguez-Reinoso, Carbon Materials in Catalysis, in: P.A. Thrower (Ed.), Chem. Phys. Carbon, 1996: pp. 243–358. doi:10.1201/9781482273199-10.

[95] C.A. Leon y Leon, L.R. Radovic, Interfacial chemistry and electrochemistry of carbon surfaces, in: P.A. Thrower (Ed.), Chem. Phys. Carbon, New York, 1994: pp. 213–310.

[96] S. Nouri, F. Haghseresht, M. Lu, Adsorption of aromatic compounds by activated carbon: effects of functional groups and molecular size, Adsorpt. Sci. Technol. 20 (2001) 1–15. doi:10.1260/026361702760120890.

[97] S. Nouri, Effect of functional groups and pH on the affinity and adsorption capacity of activated carbon: comparison of homogeneous and binary langmuir model parameters, Adsorpt. Sci. Technol. 21 (2003) 511–524.

doi:10.1260/026361703771953578.

[98] J.A. Menéndez, J. Phillips, B. Xia, L.R. Radovic, On the modification and characterization of chemical surface properties of activated carbon: in the search of carbons with stable basic properties, Langmuir. 12 (1996) 4404–4410. doi:10.1021/la9602022.

[99] A.J. Fletcher, Y. Uygur, K.M. Thomas, Role of surface functional groups in the adsorption kinetics of water vapor on microporous activated carbons, J. Phys. Chem. 111 (2007) 8349–8359. doi:10.1021/jp070815v.

[100] L. Xu, M. Rungta, J. Hessler, W. Qiu, M. Brayden, M. Martinez, G. Barbay, W.J. Koros, Physical aging in carbon molecular sieve membranes, Carbon N. Y. 80 (2014) 155–166. doi:10.1016/j.carbon.2014.08.051.

[101] T.M. Ward, F.W. Getzen, Influence of pH on the adsorption of aromatic acids on activated carbon, Environ. Sci. Technol. 4 (1970) 64–67. doi:10.1021/es60036a006.

[102] J.E. Kilduff, C.J. King, Effect of carbon adsorbent surface properties on the uptake and solvent regeneration of phenol, Ind. Eng. Chem. Res. 36 (1997) 1603–1613. doi:10.1021/ie960545v.

[103] A. Rehman, M. Park, S. Park, Current progress on the surface chemical modification of carbonaceous materials, Coatings. 9 (2019) 1–21. doi:10.3390/coatings9020103.

[104] M. V. Lopez-Ramon, F. Stoeckli, C. Moreno-Castilla, F. Carrasco-Marin, On the characterization of acidic and basic surface sites on carbons by various techniques, Carbon N. Y. 37 (1999) 1215–1221. doi:10.1016/S0008-6223(98)00317-0.

[105] C.A. Leon y Leon, J.M. Solar, V. Calemma, L.R. Radovic, Evidence for the protonation of basal plane sites on carbon, Carbon N. Y. 30 (1992) 797–811. doi:10.1016/0008-6223(92)90164-R.

[106] H.P. Boehm, Some aspects of the surface chemistry of carbon blacks and other

carbons, Carbon N. Y. 32 (1994) 759–769. doi:10.1016/0008-6223(94)90031-0.

[107] M.S. Shafeeyan, W.M.A.W. Daud, A. Houshmand, A. Shamiri, A review on surface modification of activated carbon for carbon dioxide adsorption, J. Anal. Appl. Pyrolysis. 89 (2010) 143–151. doi:10.1016/j.jaap.2010.07.006.

[108] L.R. Radovic, I.F. Silva, J.I. Ume, J.A. Menéndez, C.A. Leon y Leon, A.W. Scaroni, An experimental and theoretical study of the adsorption of aromatics possessing electron-withdrawing and electron-donating fucntional groups by chemically modified activated carbons, Carbon N. Y. 35 (1997) 1339–1348. doi:10.1016/S0008-6223(97)00072-9.

[109] K.M. Doke, E.M. Khan, Equilibrium, kinetic and diffusion mechanism of Cr (VI) adsorption onto activated carbon derived from wood apple shell, Arab. J. Chem. 10 (2017) S252–S260. doi:10.1016/j.arabjc.2012.07.031.

[110] D. Graham, Characterization of physical adsorption systems. III. The separate effects of pore size and surface acidity upon the adsorbent capacities of activated carbons, J. Phys. Chem. 59 (1955) 896–900. doi:10.1021/j150531a022.

[111] M.A. Montes-Morán, D. Suárez, J.A. Menéndez, E. Fuente, On the nature of basic sites on carbon surfaces: an overview, Carbon N. Y. 42 (2004) 1219–1225. doi:10.1016/j.carbon.2004.01.023.

[112] E.A. Boucher, Porous materials: structure, properties and capillary phenomena, J. Mater. Sci. 11 (1976) 1734–1750. doi:10.1007/BF00737529.

[113] M. Ruike, T. Kasu, N. Setoyama, T. Suzuki, K. Kaneko, Inaccessible pore characterization of less-crystalline microporous solids, J. Phys. Chem. 98 (1994) 9594–9600. doi:10.1021/j100089a038.

[114] M.M. Dubinin, Micropore structures of charcoal adsorbents. 1. A general characterization of micro- and supermicropores in the fissure model, Russ. Chem. Bull. 28 (1979) 1560–1564. doi:10.1007/BF00950967.

[115] D.H. Everett, IUPAC, Definitions, terminology and symbols in colloid and surface chemistry, in: Int. Union Pure Appl. Chem. Div. Phys. Chem., 1972: pp. 579–638.

[116] K. Kaneko, Determination of pore size and pore size distribution: 1. Adsorbents and catalysts, J. Memb. Sci. 96 (1994) 59–89. doi:10.1016/0376-7388(94)00126-X.

[117] B.D. Zdravkov, J.J. Cermák, M. Ŝefara, J. Janků, Pore classification in the characterization of porous materials: a perspective, Cent. Eur. Geol. 5 (2007) 385–395. doi:10.2478/s11532-007-0017-9.

[118] B. Bindra, O.P. Jasuja, A.K. Singla, Poroscopy: a method of personal identification revisited, Anil Aggrawal's Internet J. Forensic Med. Toxicol. 1 (2000).

[119] G. Horváth, K. Kawazoe, Method for the calculation of effective pore size distribution in molecular sieve carbon, J. Chem. Eng. Japan. 16 (1983) 470–475. doi:10.1252/jcej.16.470.

[120] S.U. Rege, R.T. Yang, Corrected Horvath-Kawazoe equations for pore-size distribution, AlChE J. 46 (2000) 734–750. doi:10.1002/aic.690460408.

[121] I. Menendez, A.B. Fuertes, Aging of carbon membranes under different environments, Carbon N. Y. 39 (2001) 733–740. doi:10.1016/S0008-6223(00)00188-3.

[122] J.S. Mattson, H.B. Mark, Activated carbon: surface chemistry and adsorption from solution, Marcel Dekker, New York, 1971.

[123] S.C. Rodrigues, M. Andrade, J. Moffat, F.D. Magalhães, A. Mendes, Preparation of carbon molecular sieve membranes from an optimized ionic liquid-regenerated cellulose precursor, J. Memb. Sci. 572 (2019) 390–400. doi:10.1016/j.memsci.2018.11.027.

[124] M.C. Campo, T. Visser, K. Nijmeijer, M. Wessling, F.D. Magalhães, A.M. Mendes, Influence of pyrolysis parameters on the performance of CMSM, Int. J. Chem. Eng. 2009 (2009) 1–6. doi:10.1155/2009/147879.

[125] S.K. Verma, P.L. Walker, Carbon molecular sieves with stable hydrophobic surfaces, Carbon N. Y. 30 (1992) 837–844. doi:10.1016/0008-6223(92)90004-G.

[126] H.F. Stoecklii, F. Kraehenbuehl, The enthalpies of immersion of active carbons, in

relation of the dubinin theory for the volume filling of micropores, Carbon N. Y. 19 (1981) 353–356. doi:10.1016/0008-6223(81)90059-2.

[127] S.A. Dastgheib, T. Karanfil, Adsorption of oxygen by heat-treated granular and fibrous activated carbons, J. Colloid Interface Sci. 274 (2004) 1–8. doi:10.1016/j.jcis.2004.01.047.

[128] S. Lagorsse, F.D. Magalhães, A. Mendes, Aging study of carbon molecular sieve membranes, J. Memb. Sci. 310 (2008) 494–502. doi:10.1016/j.memsci.2007.11.025.

[129] C.W. Jones, W.J. Koros, Carbon molecular sieve gas separation membranes-II. Regeneration following organic exposure, Carbon N. Y. 32 (1994) 1427–1432. doi:10.1016/0008-6223(94)90136-8.

[130] I.P.P. Cansado, P.A.M. Mourão, M.L.R. Carrot, P.J.M. Carrott, Activated carbons prepared from natural and synthetic raw materials with potential applications in gas separations, Adv. Mater. Res. 107 (2010) 1–7. doi:10.4028/www.scientific.net/AMR.107.1.

[131] D. Shen, M. Bülow, N.O. Lemcoff, Mechanisms of molecular mobility of oxygen and nitrogen in carbon molecular sieves, Adsorption. 9 (2003) 295–302. doi:10.1023/A:1026239829164.

[132] A. Schulte-Schulze-Berndt, K. Krabiell, Nitrogen generation by pressure swing adsorption based on carbon molecular sieves, Gas Sep. Purif. 7 (1993) 253–257. doi:10.1016/0950-4214(93)80026-S.

[133] H. Qinglin, S.M. Sundaram, S. Farooq, Revisiting transport of gases in the micropores of carbon molecular sieves, Langmuir. 19 (2003) 393–405. doi:10.1021/la026451+.

[134] K.M. Steel, W.J. Koros, Investigation of porosity of carbon materials and related effects on gas separation properties, Carbon N. Y. 41 (2003) 253–266. doi:10.1016/S0008-6223(02)00309-3.

[135] S. Lowell, J.E. Shields, M.A. Thomas, M. Thommes, Chapter 4 - Adsorption

mechanism, Charact. Porous Solids Powders Surf. Area, Pore Size Density. 16 (2004) 15–57. doi:10.1007/978-1-4020-2303-3_4.

[136] S. Cavenati, C.A. Grande, A.E. Rodrigues, Separation of $CH_4/CO_2/N_2$ mixtures by layered pressure swing adsorption for upgrade of natural gas, Chem. Eng. Sci. 61 (2006) 3893–3906. doi:10.1016/j.ces.2006.01.023.

[137] S. Cavenati, C.A. Grande, A.E. Rodrigues, Upgrade of methane from landfill gas by pressure swing adsorption, Energy & Fuels. 19 (2005) 2545–2555. doi:10.1021/ef050072h.

[138] S. Sircar, Pressure swing adsorption, Ind. Eng. Chem. Res. 41 (2002) 1389–1392. doi:10.1021/ie0109758.

[139] C.A. Grande, A.E. Rodrigues, Layered vacuum pressure-swing adsorption for biogas upgrading, Ind. Eng. Chem. Res. 46 (2007) 7844–7848. doi:10.1021/ie070942d.

[140] C. Grande, S. Cavenati, A.E. Rodrigues, Separation column and pessure swing adsorption process for gas purification, WO 2008/072215 A3, 2008.

[141] M. Kanezashi, S. Miyauchi, S. Hayakawa, H. Nagasawa, T. Yoshioka, T. Tsuru, Propylene/propane permeation properties of metal-doped organosilica membranes with controlled network sizes and adsorptive properties, J. Japan Pet. Inst. 59 (2016) 140–148. doi:10.1627/jpi.59.140.

[142] J. Li, D.H. Olson, J. Seidel, T.J. Emge, H. Gong, H. Zeng, J. Li, Zeolitic imidazolate frameworks capable for kinetic separation of propane and propylene, J. Am. Chem. Soc. 131 (2009) 10368–10369. doi:10.1021/ja9039983.

[143] A.M. Umo, E.N. Bassey, Simulation and performance analysis of propylene-propane splitter in petroleum refinery case study, Int. J. Chem. Eng. Appl. 8 (2017) 1–4. doi:10.18178/ijcea.2017.8.1.621.

[144] P.F. Bryan, Removal of propylene from fuel-grade propane, Sep. Purif. Rev. 33 (2004) 157–182. doi:10.1081/SPM-200042095.

[145] A.M. Aitani, Propylene production, in: T.& Francis (Ed.), Encycl. Chem. Process.,

New York, 2006: pp. 2461–2466. doi:10.1081/E-ECHP-120037901.

[146] R.B. Eldridge, Olefin/paraffin separation technology: a review, Ind. Eng. Chem. Res. 32 (1993) 2208–2212. doi:10.1021/ie00022a002.

[147] R.T. Yang, Gas Separation by Adsorption Processes, 1987. doi:10.1016/C2013-0-04269-7.

[148] J. Padin, S.U. Rege, R.T. Yang, L.S. Cheng, Molecular sieve sorbents for kinetic separation of propane/propylene, Chem. Eng. Sci. 55 (2000) 4525–4535. doi:10.1016/S0009-2509(00)00099-3.

[149] J.W. Yoon, I.T. Jang, K. Lee, Y.K. Hwang, J. Chang, Adsorptive separation of propylene and propane on a porous metal-organic framework, copper trimesate, Bull. Korean Chem. Soc. 31 (2010) 220–223. doi:10.5012/bkcs.2010.31.01.220.

[150] K. Li, D.H. Olson, J. Seidel, T.J. Emge, H. Gong, H. Zeng, J. Li, Zeolitic imidazolate frameworks for kinetic separation of propane and propene, J. Am. Chem. Soc. 131 (2009) 10368–10369. doi:10.1021/ja9039983.

[151] U. Böhme, B. Barth, C. Paula, A. Kuhnt, W. Schwieger, A. Mundstock, J. Caro, M. Hartmann, Ethene/ethane and propene/propane separation via the olefin and paraffin selective metal − organic framework adsorbents CPO-27 and ZIF-8, Langmuir. 29 (2013) 8592–8600. doi:10.1021/la401471g.

[152] J.P. Chen, R.T. Yang, A molecular orbital study of the selective adsorption of simple hydrocarbon molecules on Ag^+- and Cu^+-exchanged resins and cuprous halides, Langmuir. 11 (1995) 3450–3456. doi:10.1021/la00009a030.

[153] C.A. Grande, S. Cavenati, F.A. Da Silva, A.E. Rodrigues, Carbon molecular sieves for hydrocarbon separations by adsorption, Ind. Eng. Chem. Res. 44 (2005) 7218–7227. doi:10.1021/ie050376r.

[154] W. Zhu, F. Kapteijn, J.A. Moulijn, Shape selectivity in the adsorption of propane/propene on the all-silica DD3R, Chem. Commun. (1999) 2453–2454. doi:10.1039/A906465F.

[155] S.U. Rege, J. Padin, R.T. Yang, Olefin/paraffin separations by adsorption: π-

complexation vs. kinetic separation, AlChE J. 44 (1998) 799–809. doi:10.1002/aic.690440405.

[156] M. Teixeira, M. Campo, D.A. Tanaka, M.A. Tanco, C. Magen, A. Mendes, Carbon – Al_2O_3 – Ag composite molecular sieve membranes for gas separation, Chem. Eng. Res. Des. 90 (2012) 2338–2345. doi:10.1016/j.cherd.2012.05.016.

[157] K.M. Steel, W.J. Koros, An investigation of the effects of pyrolysis parameters on gas separation properties of carbon materials, Carbon N. Y. 43 (2005) 1843–1856. doi:10.1016/j.carbon.2005.02.028.

[158] X. Ma, S. Williams, X. Wei, J. Kniep, Y.S. Lin, Propylene/propane mixture separation characteristics and stability of carbon molecular sieve membranes, Ind. Eng. Chem. Res. 54 (2015) 9824–9831. doi:10.1021/acs.iecr.5b02721.

Chapter II

Chapter 2 - Preparation of oxygen and humidity-stable carbon molecular sieves by propylene post-treatment[1]

Graphical abstract

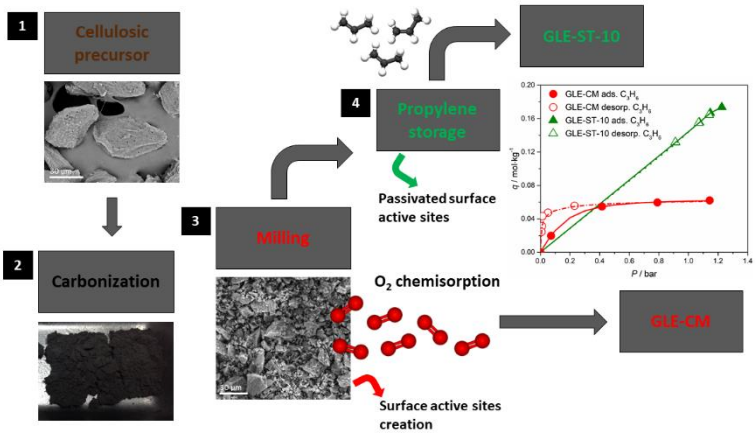

2.1. Abstract

Carbon molecular sieve adsorbents were prepared from a cellulosic precursor carbonized at 1200 ºC end temperature and milled to *ca*. 11 µm particle diameter. The samples were then post-treated in a 2 bar propylene atmosphere for 0, 5, 10 and 12 days; a sample aged for 3 years in contact with air was also considered. Samples were characterized by thermogravimetric analysis, Fourier transform infrared spectroscopy, Raman and micropores volume by Dubinin-Astakhov analysis. O_2 and N_2 adsorption isotherms and adsorption kinetics were also obtained. It was observed that the propylene post-treatment passivates the adsorbent preventing the oxygen chemisorption. The Fourier transform infrared spectroscopy analysis allowed to propose a passivation mechanism. The characterization performed permitted to conclude that it is the oxygen chemisorption that blocks the pores, especially at the constrictions, making the untreated samples slower and displaying a smaller adsorption capacity.

[1]M. Andrade, A. Mendes, Preparation of oxygen and humidity-stable carbon molecular sieves by propylene post-treatment, submitted, (2019).

2.2. Introduction

The research on carbon adsorbents has been focused on the development of new approaches for producing materials with improved properties for obtaining high gas separation performances [1,2]; authors generally include a basic characterization of these materials, quite often missing to include stability studies.

Despite carbon materials being known for displaying a high chemical and physical stability, they appear to be vulnerable in terms of stability towards some species such as humidity and oxygen [1,3]. Among carbon materials, carbon molecular sieve membranes (CMSM) seem to be the most sensitive in terms of oxidation and pore blockage, when compared with carbon molecular sieve (CMS) adsorbents [1,4,5]. However, both are susceptible to drastic performance changes when in contact with these species. Particularly for CMS adsorbents, a small change in the effective size of the pores constrictions (ultramicropores) can highly affect the kinetics and capacity of adsorption of a given gas molecule [1]. When chemisorption occurs, it can create constrictions on pore network, commonly resulting in a significant decrease on the adsorption capacity and kinetics [1]. Besides, despite carbon materials have low affinity to water, the presence of hydrophilic groups on the surface allow to seed the formation of water clusters for relative humidities higher than *ca*. 40 % that when detach block the pores [1]. However, Rodrigues *et al.* [6] reported carbon molecular sieve membranes that do not exhibit pore blockage even at relative humidities higher than 80 %; these authors found that hydrophilic groups homogenously distributed on the carbon materials surface allow water molecules to hop continuously between sites avoiding the formation of water clusters that could block the pores [6,7]. Oxygenated surface complexes have been the most widely studied functional groups in carbons surface area [8–10]; most carbons oxidize at room temperature and, when heated at 900-1000 ^{o}C under vacuum or under an inert gas, release the formed oxygenated surface groups leaving, however, very reactive sites. These reactive sites enhance the chemical adsorption even at room temperature [11]. This reaction is often quite fast at the beginning slowing down gradually [11,12]. As slower is the reaction with moist air, much oxygen is bound to carbons surface. This phenomenon, referred to as “aging”, was firstly described by Puri [13]. Afterwards, some authors suggested that oxygen chemisorption phenomenon is similar to high temperature oxygen doping [14]. Menendez and Fuertes

[15] examined the aging of carbonized resin films on porous alumina tubes exposed to different environments such as air, nitrogen and propylene. After exposure they concluded that oxygen was the major cause of aging. Lagorsse *et al.* [1] found that, in dry conditions, oxygen chemisorption was the main aging agent of carbon molecular sieve membranes. Xu *et al*. [16] proposed that, depending on the nature of the precursor material, the post-carbonization exposure conditions to oxygen allow its chemisorption at the "edges" in the surface of the ultramicropores. These "edges" correspond to defects in carbon structure and are sensitive to the oxygen chemisorption [15,16]. Several authors reported different techniques for stabilizing carbon materials, targeting these active "edges". Jones and Koros [17] showed that propylene acts as organics cleaning agent, originating the carbon samples regeneration. Lagorsse *et al.* [1], after treating CMSM at 620 ^{o}C under pure hydrogen observed a 22 % decrease on the O / C ratio and consequently the removal of a substantial amount of oxygen surface groups. However, these authors observed that despite this treatment seemed to increase the surface stability it still left reactive sites to oxygen chemisorption. Menendez and Fuertes [15] investigated the use of propylene as a chemical agent for preventing oxygen chemisorption. These authors observed that propylene prevented the aging and the carbon materials performance was not significantly affected by the treatment [15,16]. The propylene should chemisorb at these active sites through the double bound, passivating them. Jones and Koros [17] assessed also the passivation effect of ethylene but curiously they observed no passivation effects.

This work reports the preparation of two carbon molecular sieve adsorbents, one not passivated (GLE-CM) and the other passivated (GLE-ST-10). Both samples were prepared in the same conditions but only GLE-ST-10 was exposed to propylene for 10 days. Moreover, an aliquot of sample GLE-CM was allowed to contact with atmospheric air for 3 years, originating sample GLE-CMA. All samples were fully characterized for determining the differences and then better understand the passivation process. FTIR spectra showed remarkable differences; oxygenated functional groups of sample GLE-ST-10 were removed after propylene storage and a new oxygenated functional group was formed – R-O-R'. Samples display substantial differences in adsorption capacity and kinetics for O_2 and N_2. Moreover, Dubinin-

Astakhov analysis showed also large differences in the micropore volume of, GLE-CM, GLE-CMA and GLE-ST-10 samples.

2.3. Experimental

2.3.1. Materials

GLE-AP cellulosic precursor was provided by Air Products and Chemicals Inc.; mean particle size of *ca.* 58 µm. Oxygen (99.995 % pure), nitrogen (99.999 % pure), carbon dioxide (99.9 % pure) and helium (99.999 % pure) were supplied by Linde. Propylene (99.5 % pure) and sulfur hexafluoride (99.9 % pure) were from Praxair.

2.3.2. Carbon molecular sieve adsorbents preparation

The carbon molecular sieve adsorbents preparation comprehended three steps: i) carbonization, ii) milling and iii) propylene storage.

2.3.3. Carbonization step

The carbonization of the samples was conducted in an alumina tube (5049 cm^3 of volume and 7.1 cm of inner diameter) inside a tubular Termolab TH furnace. The temperature of the oven was controlled using three thermocouples, placed in contact with the alumina tube, as indicated in Figure 2.1. The carbonized end temperature was set to 1200 ^oC with 120 minutes of soaking time, with a heating rate of 0.5 $^oC \cdot min^{-1}$ and a nitrogen flow of 510 $mL \cdot min^{-1}$. After carbonization the samples were naturally cooled until room temperature.

2.3.4. Milling step

After carbonization samples were milled in a Retsch PM 100 planetary ball mill at 160 min^{-1} wheel speed.

2.3.5. Propylene post-treatment

After the milling step, sample GLE-ST-10 was placed in a stain-steel tank, evacuated and filled up with propylene at 2 bar (at ambient temperature). Figure 2.1 summarizes the preparation steps for obtaining the carbon adsorbents.

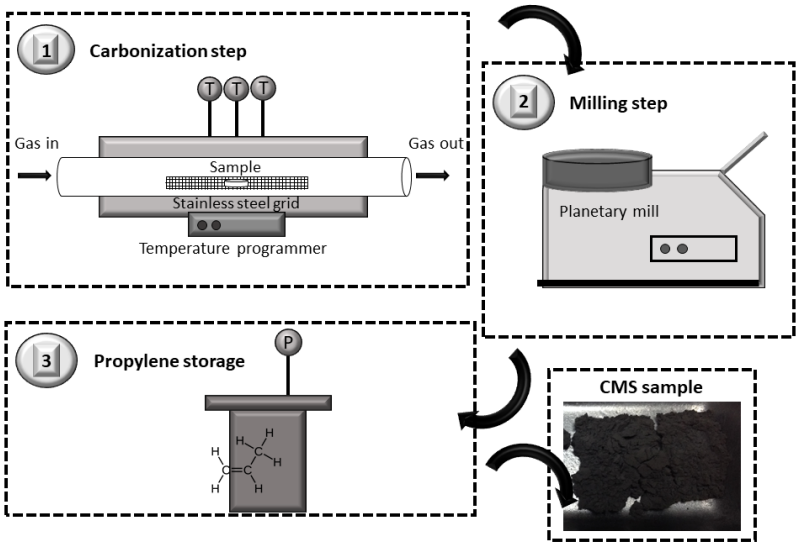

Figure 2.1. Preparation steps for producing the carbon adsorbents; step 3 was only applied to GLE-ST-10.

Also, other samples were prepared varying the propylene time exposure. Table 2.1 shows the preparation conditions for samples GLE-CM, GLE-CMA and GLE-ST-*x*, where *x* indicates the sample contact time, in days, with propylene.

Table 2.1. Preparation conditions of all prepared CMS samples.

Samples	Description
GLE-CM	Carbonized and milled at 160 rpm – fresh sample
GLE-CMA	Carbonized and milled at 160 rpm – oxygen exposure by 3 years
GLE-ST-5	Carbonized, milled at 160 rpm and post-treated with C_3H_6 by 5 days
GLE-ST-10	Carbonized, milled at 160 rpm and post-treated with C_3H_6 by 10 days
GLE-ST-12	Carbonized, milled at 160 rpm and post-treated with C_3H_6 by 12 days

2.3.6. Thermogravimetric analysis (TGA)

Thermogravimetric analysis was conducted in a Netzsch STA 449 F3 Jupiter thermogravimetric balance; a sample with 16.8 mg was used. The proximate analysis protocol was performed using a protocol described elsewhere [18]. Figure 2.2 pictures the proximate analysis program.

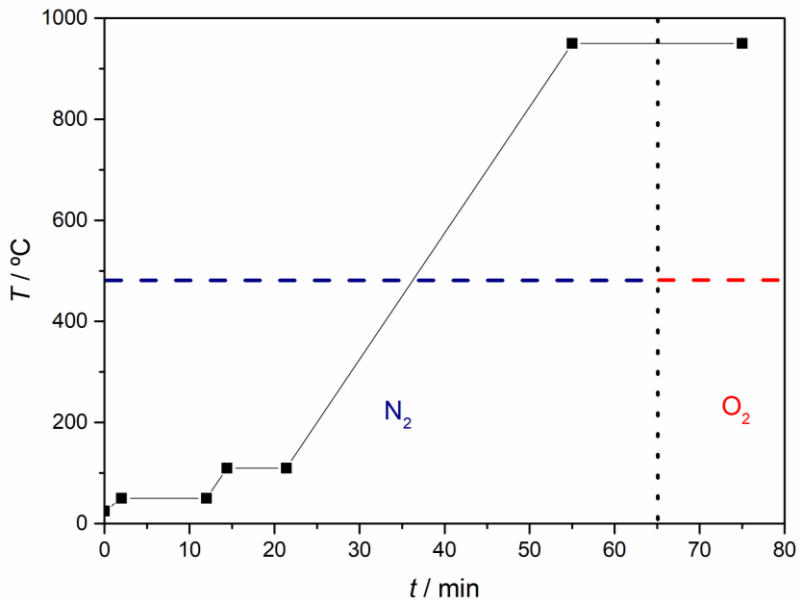

Figure 2.2. Proximate analysis program steps.

2.3.7. Scanning electron microscopy (SEM)

Micrographs of the carbon adsorbents were obtained using a Phenom XL Scanning Electron Microscope. The Phenom XL was equipped with two detectors, an elemental analysis detector (EDS) and a secondary electron detector (SED).

2.3.8. Fourier transform infrared spectroscopy (FTIR)

The infrared spectra were recorded using a VERTEX 70 FTIR spectrometer (BRUKER) in transmittance mode with a high sensitivity DLaTGS detector at room temperature. Samples were analysed in transmission mode, using pellets of potassium bromide (KBr) containing 1 % of mass fraction of the carbon sample. The spectra were recorded from 4000 cm^{-1} to 400 cm^{-1} with a resolution of 4 cm^{-1}.

2.3.9. Confocal Raman imaging (CRI)

CRI analysis was performed in a WITec alpha300 RA equipment. Confocal Raman microscopy results from the combination of confocal microscopy and Raman microscopy techniques. Table 2.2 shows the used CRI scan parameters for analysing the samples.

Table 2.2. CRI scan parameters used for GLE-CM and GLE-ST-10 analysis.

Parameter	GLE-CM	GLE-ST-10
Points per line	30	50
Lines per image	40	70
Scan width /µm	3	5
Scan weight / µm	4	7
Integration time /ms	100	150
Excitation wavelength / nm	532	532
Laser power	1	1

2.3.10. Micropores characterization

The Dubinin-Astakhov (DA) equation (Eq. 2.1) was used to fit the experimental data obtaining then the micropore volume (W_0) and the characteristic energy of adsorption (E_0) [19,20]:

$$\frac{W}{W_0} = \exp\left[-\left(\frac{RT \ln(P_0 / P)}{E_0} \right)^n \right] \quad (2.1)$$

where W is the micropore volume, P is the pressure, W_0 is the total micropore volume, E_0 is the characteristic energy for adsorption, P_0 is the vapor pressure of the free liquid, R is the gas constant, T is the absolute temperature and n is an adjustable parameter.

2.3.11. Adsorption equilibrium isotherms and gas uptake experiments

Adsorption equilibrium isotherms and experimental uptake curves were obtained by volumetric method [21,22]. The used volumetric set-up is described elsewhere [21]. Two pressure sensors of 2 bar and 7 bar (Drück ref. PMP 4010) were used (reading error of 0.1 % of full scale). Also, for guaranteeing isothermal conditions, a Huber K12-cc-NR thermostatic bath was used. Prior to adsorption tests, samples were regenerated at 70 ºC for 4 hours under vacuum (pressure < 0.002 bar), using an Alcatel 1004A rotary vacuum pump.

Langmuir (Eq. 2.2), Toth (Eq. 2.3) and Langmuir-Freudlich (SIPS) (Eq. 2.4) are the most used adsorption equilibrium isotherms equations. Langmuir and Toth are thermodynamically consistent; however, Toth has one more fitting parameter [23]. SIPS equation (Eq. 2.4) has also three parameters, however, is not applicable for low pressures since it does not converges to Henry Law [23,24].

$$q = q_s \frac{bP}{1+bP} \tag{2.2}$$

$$q = q_s \frac{bP}{\left(1+\left(bP\right)^t\right)^{1/t}} \tag{2.3}$$

$$q = q_s \frac{\left(bP\right)^{1/n}}{1+\left(bP\right)^{1/n}} \tag{2.4}$$

where q is the adsorbed solute concentration at pressure P, q_s is the adsorbed saturation capacity, b is the adsorption affinity constant and t and n are parameters used to characterize the heterogeneity of the adsorbent surface. Normally, t is less than the unity; for t = 1, Toth equation reduces to the Langmuir equation [23].

The inverse of the apparent diffusion time constant ($D \cdot r^{-2}$) was obtained fitting the experimental uptake curves to the so-called non-isothermal model for constant-volume and variable-pressure conditions [25]; the fractional uptake by this model is:

$$F = 1 - \sum_{n=1}^{\infty} \frac{9\left(1+\alpha^*\right)\left[\frac{Y_n}{-q_n^2}\right]^2 \exp\left(-q_n^2 \tau\right)}{\frac{1}{\beta_n^*} + \frac{3}{2}\frac{\beta}{\beta_n^*}\left[q_n \cot q_n \left(\frac{Y_n}{q_n^2}\right)+1\right] + \frac{3}{2}\frac{\alpha^* B_n}{q_n^4 \beta_n^*}} \tag{2.5}$$

where $B_n = Y_n\left[(q_n^2 - \alpha)\, q_n \cot q_n - 2\alpha\right] + q_n^2(q_n^2 - \alpha)$, $Y_n = q_n \cot q_n - 1$ and $\alpha^* = KV$. Considering that $V = V_s / V_g$ and V_s and V_g correspond to the structural volume of the adsorbent sample and the total gas phase volume (in both tanks), respectively.

2.4. Results and discussion

2.4.1. Thermogravimetric analysis

A proximate analysis was performed for determining the humidity, volatile matter, fixed carbon and ashes of the samples – Figure 2.3.

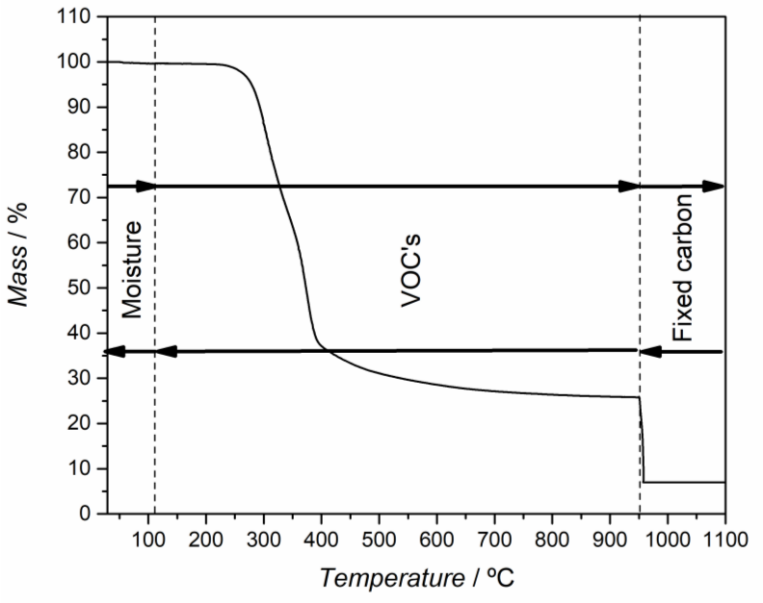

Figure 2.3. Proximate analysis of GLE-AP precursor by thermogravimetric method. The removed species are identified in the respective intervals.

Table 2.3 shows the summary of proximate analysis results for GLE-AP precursor.

Table 2.3. Proximate analysis results by thermogravimetry of GLE-AP precursor.

	GLE-AP precursor
Humidity / %	0.5
Volatile matter / %	73.7
Fixed carbon / %	18.4
Ashes / %	7.4

From Figure 2.3 and Table 2.3 it can be concluded that GLE-AP cellulosic precursor displays *ca.* 7 % of ashes, which is in the range for similar materials [26–28]. Also, it presents *ca.* 74 % of volatile matter and *ca.* 18 % of yield of fixed carbon, which is within values reported for similar cellulosic materials [29–31].

2.4.2. Scanning electron microscopy

The samples surface morphology was analysed through SEM. Micrographs of the GLE-AP precursor and samples GLE-CM and GLE-ST-10 are shown in Figures 2.4 and 2.5, respectively.

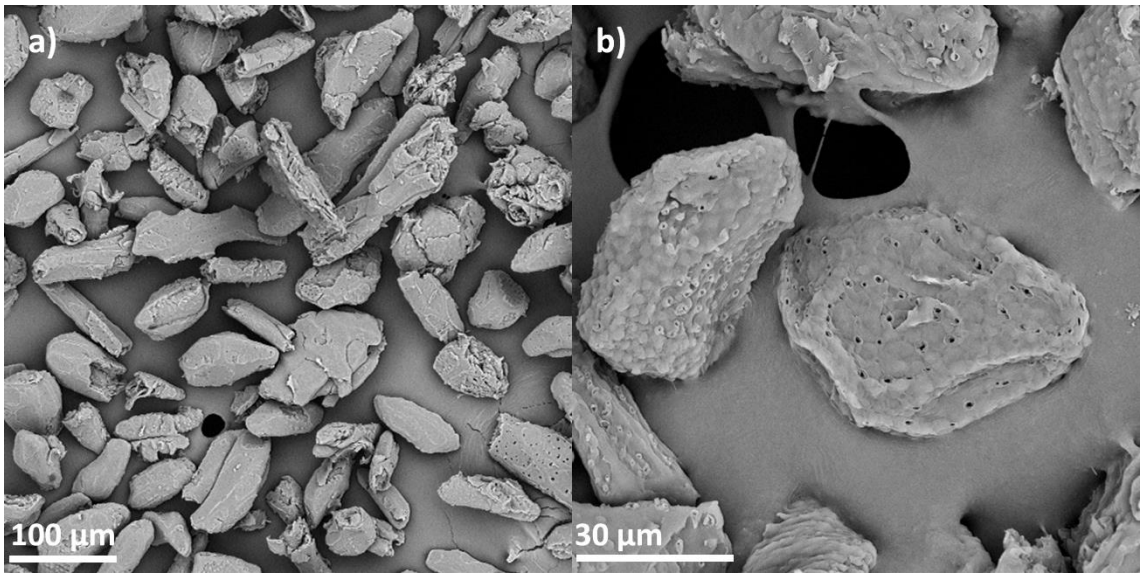

Figure 2.4. SEM micrographs of GLE-AP precursor with magnification of: a) 500× and b) 2500×.

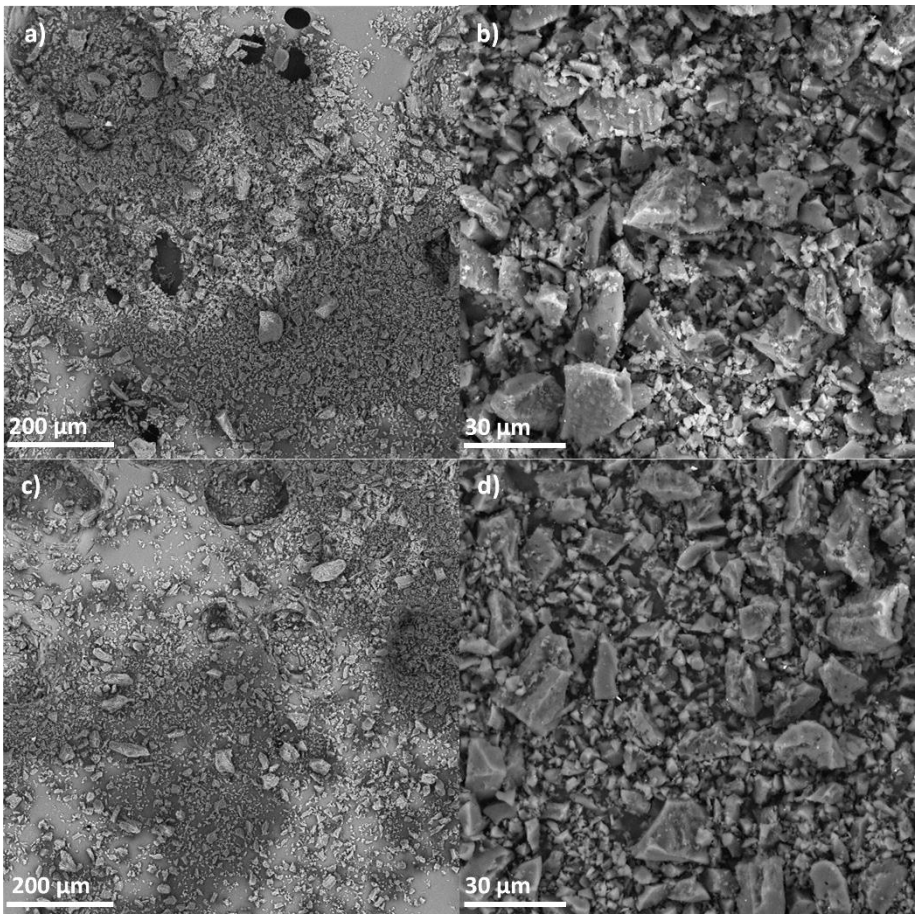

Figure 2.5. SEM micrographs of GLE-CM: a) and b); and GLE-ST-10: c) and d) carbon samples. The magnification of a) and c) was 310× and for b) and d) was 2000×.

SEM micrographs show morphological changes between the precursor material and the derived carbon molecular sieve adsorbents. The precursor micrograph, GLE-AP,

indicates particles with an average diameter of *ca.* 40-60 µm and some stomas, pores responsible for gaseous changes is vegetal organisms [32]. On the other hand, GLE-CM and GLE-ST-10 SEM micrographs are similar. Further, since after carbonization the samples were milled and, also, considering the shrinkage occurred in the carbonization process, both samples presented a smaller particle size when compared with the respective precursor.

2.4.3. Fourier transform infrared spectroscopy

FTIR analysis was performed for the precursor material and derived carbon adsorbents. The GLE-CM sample, aged for 3 years in lab conditions – named GLE-CMA, was also characterized, besides the other samples – GLE-CM and GLE-ST-10. Figure 2.6 shows the obtained FTIR spectra of GLE-AP precursor material and GLE-CM, GLE-CMA and GLE-ST-10 carbon samples.

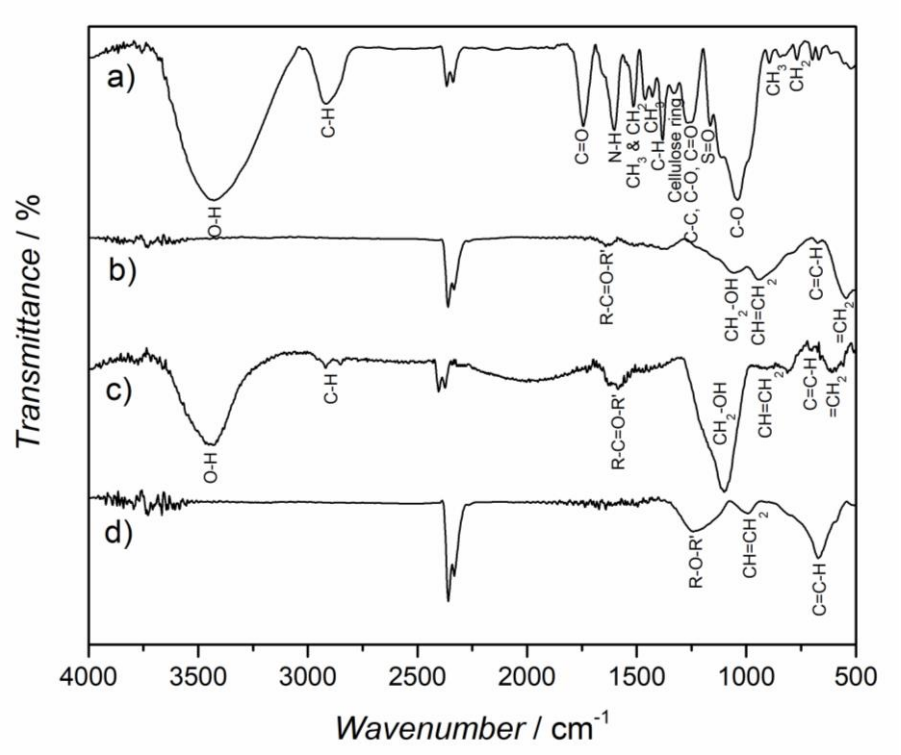

Figure 2.6. FTIR spectra of: a) GLE-AP and derived carbon adsorbents, b) GLE-CM, c) GLE-CMA and d) GLE-ST-10.

GLE-AP FTIR spectrum shows the presence of a O-H stretch vibration at 3429 cm^{-1} attributed to water physically adsorbed on sample surface. Also, a C-H stretching vibration band is detected at 2914 cm^{-1}, and, the twin bands that appear at 2366 cm^{-1}

and 2336 cm^{-1} are related to CO_2 present in the ambient air. A C=O stretching vibration band ascribed to esters appears at 1740 cm^{-1}, and, a C=C stretching vibration band is detected at 1604 cm^{-1}. At 1520 cm^{-1} a CH_3 and CH_2 sp^3 band is identified and at 1379 cm^{-1} is observed a C-H rocking vibration band assigned to alkanes or to C-H in methyl and phenolic alcohols. At 1330 cm^{-1} is observed a band ascribed to the vibration of the cellulose ring. At 1250 cm^{-1} appears a band attributed to C-C, C-O and C=O stretching vibration and at 1167 cm^{-1} is observed a band assigned to S=O stretching vibration. Finally, a C-O stretching vibration band ascribed to alkoxy groups appears at 1035 cm^{-1} and at 895 cm^{-1} and 771 cm^{-1} is detected a band attributed to CH_3 and CH_2 groups, respectively [33–37].

Since samples GLE-CM and GLE-ST-10 display a distinct behaviour for oxygen interactions, it may be expectable having differences in its surface chemistry. GLE-CM FTIR spectrum shows a R-C=O-R' carbonyl band at 1641 cm^{-1} and a CH_2-OH stretch vibration band assigned to primary alcohols at 1062 cm^{-1} was also detected. At 997 cm^{-1} a C=CH_2 out-of-plane wagging vibration band was observed. And at 673 cm^{-1} appears a C=C-H bending vibration band. Finally, at 547 cm^{-1} a =CH_2 twisting vibration band is observed. On the other hand, in GLE-ST-10 spectrum are present much less and distinct functional groups compared with GLE-CM. Namely, a R-O-R' group vibration band at 1247 cm^{-1} is formed. The CH=CH_2 out-of-plane vibration band at 991 cm^{-1} and the C=C-H band located at 671 cm^{-1} are present in both spectra; however, C=C-H band is more intense on this sample [33–37]. Also, FTIR spectra of GLE-CM and GLE-CMA reveal significant differences; namely, the appearance of a O-H stretching vibration band at 3437 cm^{-1} and the more intense CH_2-OH stretching vibration band at 1101 cm^{-1}, indicating possible aging by humidity exposure. Also, the R-C=O-R' band observed at 1589 cm^{-1} appears to increase with oxygen and humidity exposure; unlike, group CH=CH_2 decreases with the aging time.

Literature reports that propylene can act as a "cleaning agent" of the oxygenated-surface groups [6,15]. In agreement, FTIR spectra indicate that after propylene exposure oxygenated groups R-C=O-R' and CH_2-OH are removed. Also, the peak corresponding to CH=CH_2 group decreases significantly with oxygen and humidity time exposure. Figure 2.7 illustrates possible deletion mechanisms; Reaction 1 [38] occurs in presence of water, which can be easily adsorbed from moment the sample is

removed from the oven and placed under the propylene atmosphere, and attacks the carbonyl groups producing namely the function group C=C-H. The presence of this group increases significantly after the propylene treatment, supporting the proposed mechanism. Reaction 2 refers to the removal of the hydroxymethylene group (a primary alcohol) to form also group R-O-R'. The appearance of group R-O-R' signal is also observed in the FTIR spectra supporting the proposed mechanism. Reaction 3 refers to the partial deletion of vinyl group after reaction with adsorbed water to form also group R-O-R'.

Finally, when untreated CMS is allowed to contact with atmospheric air – sample GLE-CMA, Reactions 3 and 4 should take place where functional groups O-H and CH_2-OH increase substantially – Reaction 3 – and CH_2-OH group reacts with oxygen to produce R-C=O-R' and water – Reaction 4.

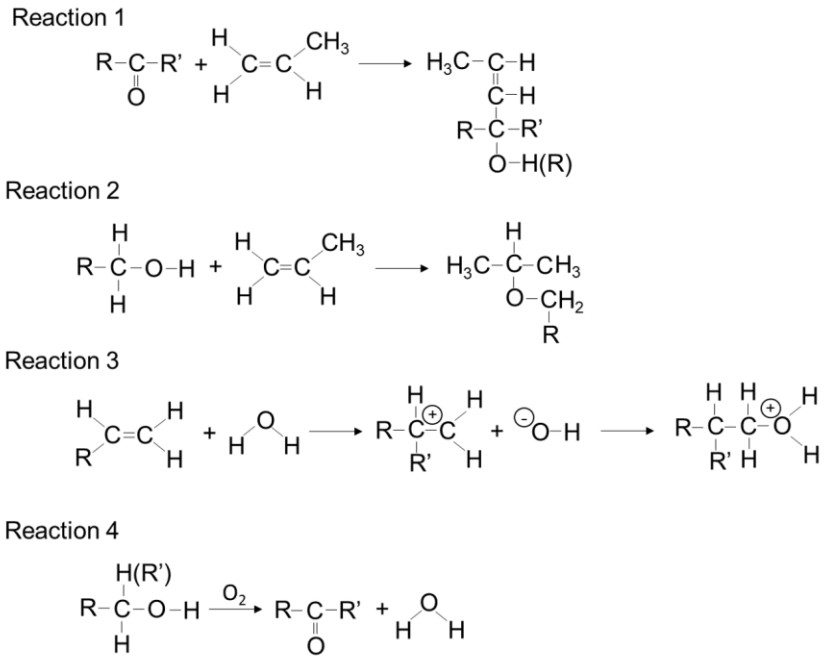

Figure 2.7. Proposed deletion mechanism of oxygenated functional groups carbonyl, hydroxymethylene (primary alcohol) and partial deletion of vinyl groups.

2.4.4. Confocal Raman Imaging

Figure 2.8 shows the obtained average Raman spectra of GLE-CM and GLE-ST-10. Generally, in carbonaceous materials, the most important bands are: G band (graphitic band), situated at approximately 1575 cm^{-1}, and the D band (disorder band), situated at approximately 1355 cm^{-1} [39]. Namely, G band is ascribed to in-plane carbon stretching

vibrations of perfect graphene sheets and the D band is assigned to hybridized mode vibrations associated to graphene edges indicating the presence and/or degree of disorder in the carbon structure [40].

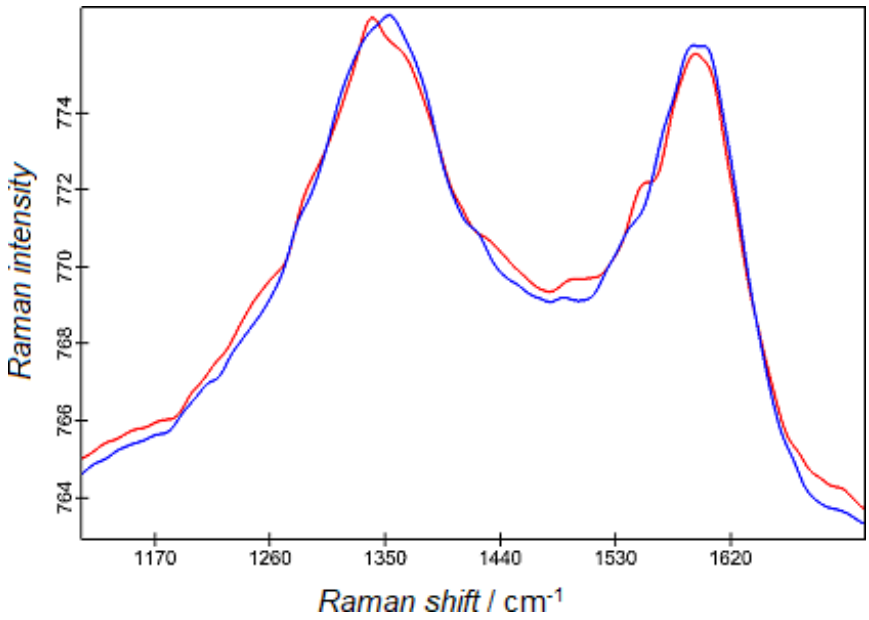

Figure 2.8. Raman spectra for GLE-CM (blue) and GLE-ST-10 (red) samples.

Figure 2.8 shows that Raman spectra, which are similar to other spectra reported in literature [41,42], reveals minor differences between the two samples. Generally, the Raman intensity of G and D bands increase with the carbonization end temperature. This indicates that the carbon framework becomes more graphitized, but also, that more imperfections are introduced in the graphene structures corresponding to an increase in amorphous carbon, respectively [43]. As reported elsewhere [43,44], beyond the carbonization end temperature of 800 ºC, D and G bands become very similar. Though, since GLE-CM and GLE-ST-10 CMS adsorbents were carbonized at the same temperature of 1200 ºC, the Raman spectra were expected to be similar.

2.4.5. Micropores characterization

CO_2 adsorption equilibrium isotherms at 0 ºC were obtained for GLE-CM, GLE-CMA and GLE-ST-10 samples. Figure 2.9 plots the obtained CO_2 adsorption equilibrium isotherms.

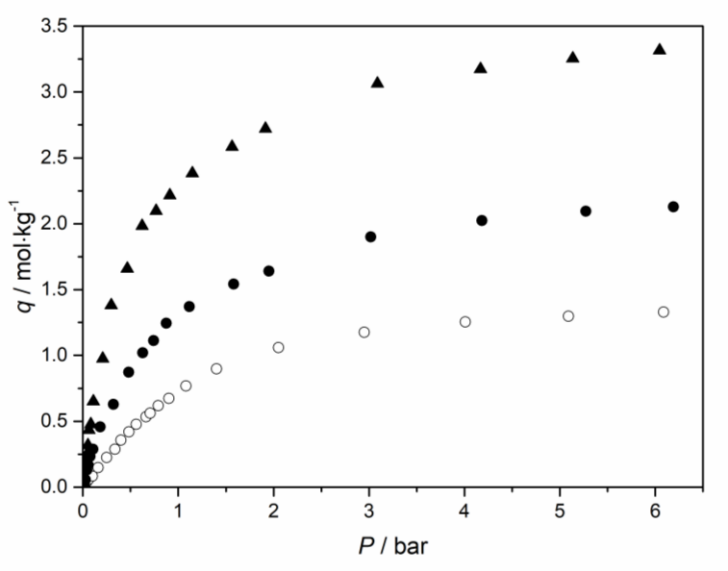

Figure 2.9. CO_2 adsorption equilibrium isotherms at 0 ºC for GLE-CM (●), GLE-CMA (○) and GLE-ST-10 (▲).

Figure 2.9 indicates that the aged samples display significant less pore volume, while the passivated sample is the one displaying the highest pore volume. Oxygen aging often results in pore blockage [1,45], which may justify these differences.

Figure 2.10 shows sulfur hexafluoride adsorption equilibrium isotherms at 25 ºC for samples GLE-CM and GLE-ST-10. Sulfur hexafluoride is a spherical molecule with a large diameter – 0.55 nm [46], which can be used to probe the volume of the larger micropores.

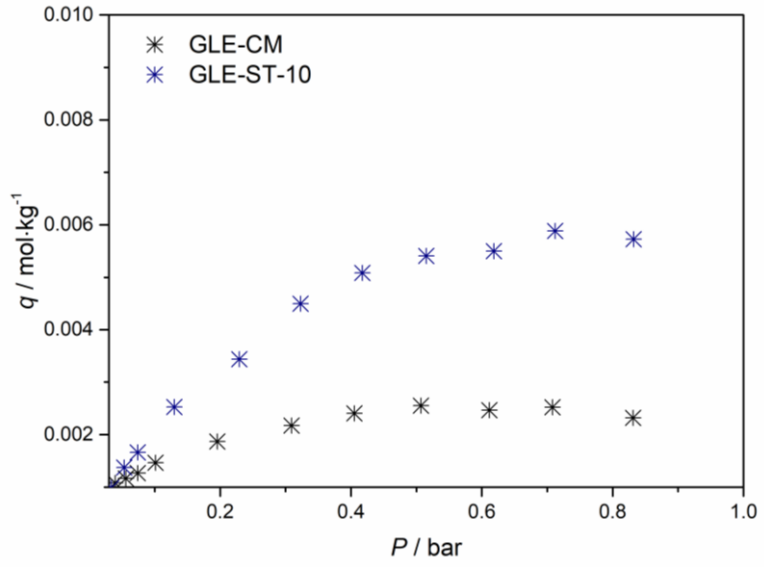

Figure 2.10. SF_6 adsorption equilibrium isotherm at 25 ºC of GLE-CM and GLE-ST-10 samples.

Sample GLE-CM displays a much smaller SF_6 adsorption capacity when compared to the passivated sample. This is a strong evidence that the oxygen chemisorption also blocks larger micropores.

Figure 2.11 plots the CO_2 characteristic curves for samples GLE-CM, GLE-CMA, GLE-ST-10. From the DA fitting, E_0 was obtained from the slop of the plot and the W_0 from the interception.

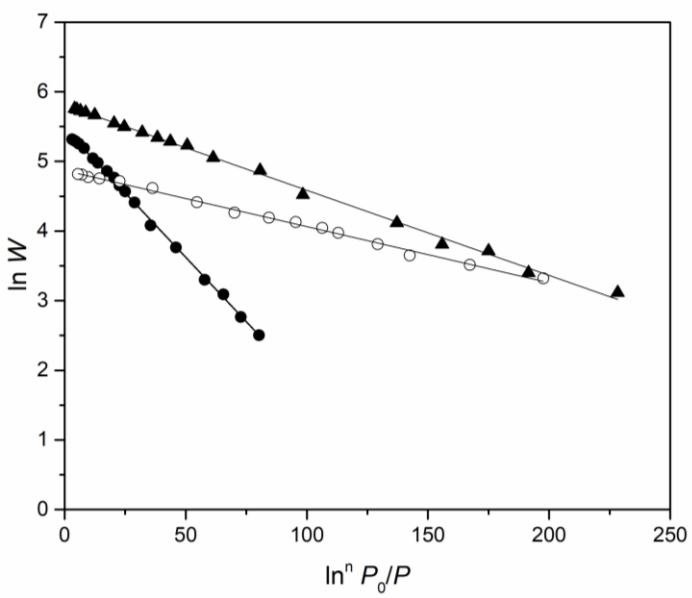

Figure 2.11. CO_2 characteristic curves for GLE-CM (●), GLE-CMA (○) and GLE-ST-10 (▲). The solid lines correspond to the DA fitting.

As it can be observed by Figure 2.11 very distinct characteristic curves were obtained. The corresponding DA fitting parameters are given in Table 2.4. Since Stoeckli equation is not applicable ($n \neq 2$), the mean pore width (l) was obtained by a weighted average [20].

Table 2.4. Structural parameters for GLE-CM, GLE-CMA and GLE-ST-10 samples.

Parameter	GLE-CM	GLE-CMA	GLE-ST-10
n	2.3	3.4	2.8
W_0 / $cm^3 \cdot kg^{-1}$	282.24	68.99	287.88
E_0 / $kJ \cdot mol^{-1}$	8.97	10.81	11.60
l / nm	0.81	0.74	0.76

Table 2.4 indicates that GLE-CMA has the lowest micropore volume, which agrees with the previous results. GLE-CM and GLE-ST-10 have approximately the same

micropore volume, indicating that the oxygen chemisorption blocks mostly the smallest micropores; effectively, also the mean pore width of GLE-ST-10 is smaller than for sample GLE-CM indicating that for this average the smaller micropores are weighting more. Finally, the characteristic energy is also higher for sample GLE-ST-10 than for sample GLE-CM indicating the weight of the smaller micropores and a surface chemistry change; sample GLE-ST-10 has smaller pores justifying then a higher average characteristic energy.

2.4.6. Adsorption equilibrium isotherms and uptake rate measurements

The adsorption equilibrium isotherms of oxygen and nitrogen on GLE-CM, GLE-CMA and GLE-ST-10 were determined at 25 ºC – Figure 2.12.

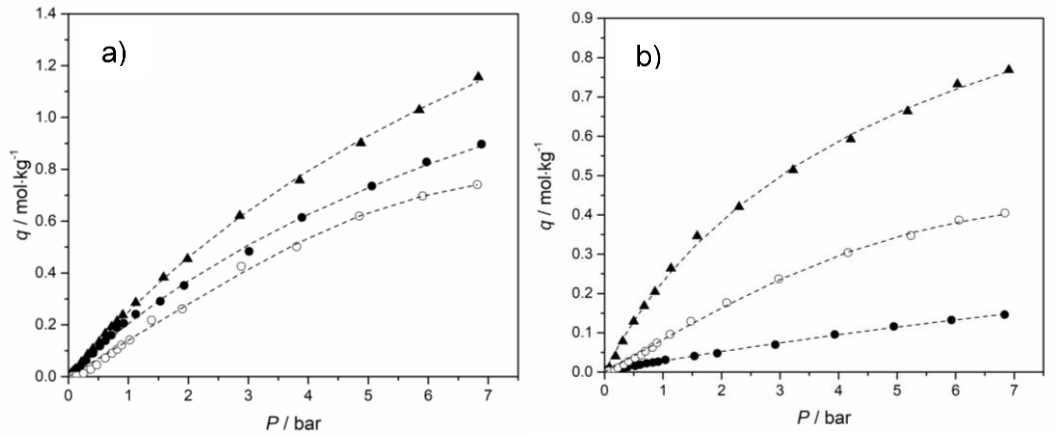

Figure 2.12. GLE-CM (●), GLE-CMA (○) and GLE-ST-10 (▲): a) O_2 and b) N_2 adsorption equilibrium isotherms at 25 ºC. The dashed lines correspond to Toth equation fitting.

Table 2.5 shows the obtained Toth equation parameters for oxygen and nitrogen on GLE-CM, GLE-CM and GLE-ST-10 CMS adsorbents.

Table 2.5. Toth equation parameters for O_2 and N_2 on GLE-CM, GLE-CMA and GLE-ST-10 CMS samples.

		Toth equation			
		q_s / mol·kg^{-1}	b / bar^{-1}	t	$\sum\left(q-q^*\right)^2$
GLE-CM	O_2	2.424	0.096	0.893	2.27×10^{-3}
	N_2	2.151	0.015	0.587	4.32×10^{-5}
GLE-CMA	O_2	0.828	0.170	3.994	3.72×10^{-3}
	N_2	0.478	0.174	2.787	6.79×10^{-4}
GLE-ST-10	O_2	2.979	0.090	0.980	1.08×10^{-3}
	N_2	1.457	0.207	0.856	1.55×10^{-3}

From Figure 2.12 and Table 2.5 it can be concluded that the samples display quite different adsorption isotherms for O_2 and N_2; generally, the adsorption saturation capacity for oxygen is larger than for nitrogen and the adsorption capacity for both gases follow GLE-ST-10 > GLE-CM > GLE-CMA. However, it should be emphasized that adsorbents GLE-CM and GLE-CMA display a quite different surface chemistry where GLE-CMA shows the highest *t* values (surface heterogeneity). This is responsible for, at 7 bar, the adsorption concentration of nitrogen on GLE-CM being lower than on GLE-CMA.

Table 2.6 shows the obtained inverse of apparent diffusion time constant, kinetic selectivity and adsorption capacity of samples GLE-CM, GLE-CMA, GLE-ST-5, GLE-ST-10 and GLE-ST-12, at *ca.* 1 bar and 25 ºC.

Table 2.6. Inverse of apparent diffusion time constant ($D\cdot r^{-2}$), kinetic selectivity and adsorption capacity of all prepared samples, at 25 ºC and *ca.* 1 bar.

Sample	Gas specie	q / mol·kg^{-1}	$D\cdot r^{-2}$ / s^{-1}	S_{O_2/N_2}
GLE-CM	O_2	0.21	1.18×10^{-1}	VL.[1]
	N_2	0.03	n.d.	
GLE-CMA	O_2	0.14	8.64×10^{-5}	VL.
	N_2	0.07	n.d.	
GLE-ST-5	O_2	0.19	8.10×10^{-2}	VL.
	N_2	0.02	n.d.	
GLE-ST-10	O_2	0.24	2.58×10^{-4}	30
	N_2	0.23	8.67×10^{-6}	
GLE-ST-12	O_2	0.34	1.06×10^{-4}	15
	N_2	0.19	6.89×10^{-6}	

[1] Very large

Table 2.6 shows that the $D \cdot r^{-2}$ for sample GLE-CMA, compared with sample GLE-CM, decreases significantly with the oxygen contacting time – aging time. Further, nitrogen uptakes were too slow for being measurable. Regarding GLE-ST-5, GLE-ST-10, and GLE-ST-12, only samples post-treated with propylene during 10 and 12 days displayed stability towards oxygen. Also, both oxygen and nitrogen adsorption kinetics decreased with the propylene contact time. The obtained results indicate that propylene exposure not only passivated the surface but also changes the surface properties. Sample GLE-CM displays the highest O_2 adsorption kinetics and negligible N_2 adsorption kinetics; it should be emphasized that the CMS sample was divided in two and the O_2 and N_2 uptake curves were obtained with a fresh sample. The fast O_2 adsorption kinetics was assigned to the oxygen chemisorption, which produces an abnormal adsorption kinetic read. On the other hand, the negligible N_2 adsorption kinetics may indicate pore blockage due to O_2 chemisorption – the samples were milled under air conditions before being characterized.

Table 2.6 shows also that the O_2 capacity increases with propylene contact time indicating that more pores are accessible for adsorbing O_2. On the other hand, N_2 adsorption behaviour displays a more complex behaviour; sample GLE-ST-10 displays the highest adsorption capacity, although very close to the one obtained on GLE-ST-12. On the other hand, GLE-ST-5 exhibited the lowest adsorption capacity, which indicate a poor passivation with consequent oxygen chemisorption; actually, sample GLE-ST-5 displays a similar behaviour as sample GLE-CM.

Figure 2.13 shows the adsorption and desorption isotherms of propylene on samples GLE-CM and GLE-ST-10 at 25 ºC.

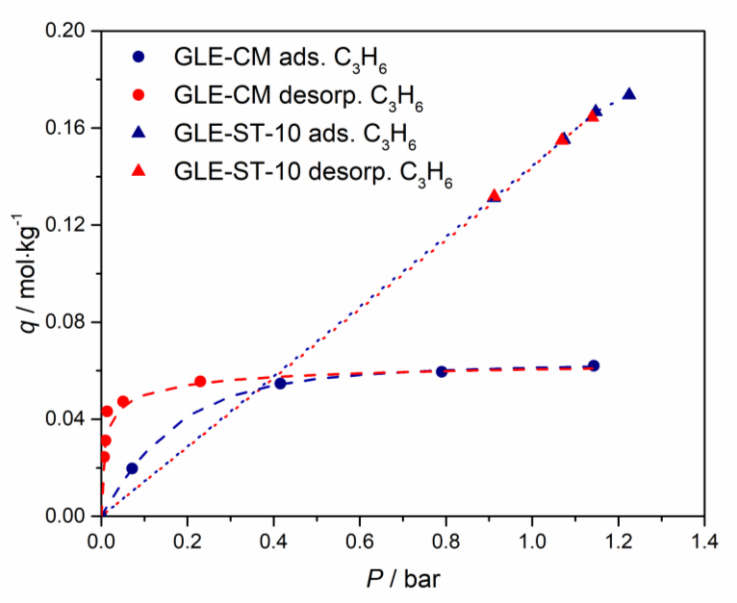

Figure 2.13. Propylene adsorption and desorption isotherms on samples GLE-CM and GLE-ST-10. Dotted-lines correspond to Langmuir fitting and dashed-lines to Toth fitting.

Figure 2.13 evidences that propylene adsorption behaviour on both samples is quite different. On sample GLE-CM, propylene displays significant chemisorption; unlike, on sample GLE-ST-10 propylene adsorption is linear and fully reversible.

2.5. Conclusions

Several CMS adsorbents were prepared from a cellulosic precursor for assessing the propylene passivation to the oxygen chemisorption. Samples were carbonized at 1200 ^{o}C end temperature and milled at 160 rpm after carbonization. Sample GLE-ST-10 was post-treated with propylene during 10 days at 2 bar and exhibited no oxygen chemisorption. FTIR spectra showed remarkable differences between propylene post-treated sample (GLE-ST-10) and a not-treated sample (GLE-CM); a passivation reaction mechanism was proposed. Briefly, groups carbonyl and hydroxymethylene react with propylene producing C=C-H and R-O-R' and vinyl groups to produce R-O-R', which are less reactive groups. On the other hand, after contacting with the atmospheric air for a long period of time, sample GLE-CMA displays a substantial increase in functional groups O-H and CH_2-OH assigned to the reaction of water with functional group $CH=CH_2$. Oxygen and nitrogen adsorption isotherms and kinetics were also quite different. GLE-ST-10 showed superior stability, high O_2 / N_2 kinetic selectivity and high adsorption capacity compared with the other samples; sample GLE-ST-5 displayed some O_2 chemisorption and sample GLE-ST-12 displayed smaller adsorption capacity and adsorption kinetics. GLE-CMA sample, a GLE-CM sample aged for 3 years, was also assessed; both adsorption capacity and kinetics decreased substantially but also the surface chemistry changed becoming more heterogeneous.

2.6. Acknowledgments

This work was financially supported by: project UID/EQU/00511/2019 - Laboratory for Process Engineering, Environment, Biotechnology and Energy – LEPABE funded by national funds through FCT/MCTES (PIDDAC); Project "LEPABE-2-ECO-INNOVATION" – NORTE-01-0145-FEDER-000005, funded by North Portugal Regional Operational Programme (NORTE 2020), under PORTUGAL 2020 Partnership Agreement, through the European Regional Development Fund (ERDF). The authors want to acknowledge Prof. M. Bastos for the fruitful discussions. The authors are thankful to Air Products and Chemicals, Inc. for generously providing the precursor material.

2.7. References

[1] S. Lagorsse, F.D. Magalhães, A. Mendes, Aging study of carbon molecular sieve membranes, J. Memb. Sci. 310 (2008) 494–502. doi:10.1016/j.memsci.2007.11.025.

[2] S. Lagorsse, F.D. Magalhães, A. Mendes, Carbon molecular sieve membranes: sorption, kinetic and structural characterization, J. Memb. Sci. 241 (2004) 275–287. doi:10.1016/j.memsci.2004.04.038.

[3] J.A. Lie, M.B. Hägg, Carbon membranes from cellulose: synthesis, performance and regeneration, J. Memb. Sci. 284 (2006) 79–86. doi:10.1016/j.memsci.2006.07.002.

[4] B. McEnaney, E. Alain, Y.-F. Yin, T.J. Mays, Porous carbons for gas storage and separation, in: Des. Control Struct. Adv. Carbon Mater., Nato Science Series, 2001: pp. 295–318. doi:10.1007/978-94-010-1013-9_17.

[5] S.M. Saufi, A.F. Ismail, Fabrication of carbon membranes for gas separation - a review, Carbon N. Y. 42 (2004) 241–259. doi:10.1016/j.carbon.2003.10.022.

[6] S.C. Rodrigues, M. Andrade, J. Moffat, F.D. Magalhães, A. Mendes, Carbon membranes with extremely high separation factors and stability, Energy Technol. 7 (2019). doi:10.1002/ente.201801089.

[7] A.M.M. Mendes, M.R.S. de Andrade, M.F. da S. Boaventura, S.C.V. Rodrigues, A carbon molecular sieve membrane, method of preparation and uses thereof, WO2017/068517 A1, 2017.

[8] N. Petrov, T. Boudinova, Oxidized carbon from polyolefin wax, Chem. Ing. Tech. 64 (1992) 64–66. doi:10.1002/cite.330640112.

[9] N. Petrov, T. Budinova, M. Razvigorova, E. Ekinci, F. Yardim, V. Minkova, Preparation and characterization of carbon adsorbents from furfural, Carbon N. Y. 38 (2000) 2069–2075. doi:10.1016/S0008-6223(00)00063-4.

[10] H.P. Boehm, Some aspects of the surface chemistry of carbon blacks and other carbons, Carbon N. Y. 32 (1994) 759–769. doi:10.1016/0008-6223(94)90031-0.

[11] H. Boehm, Surface chemical characterization of carbons from adsorption studies, in: Elsevier (Ed.), Adsorpt. by Carbons, 2008: pp. 301–327. doi:10.1016/B978-008044464-2.50017-1.

[12] M. Voll, H.P. Boehm, Basic surface oxides on carbon - II. Stoichiometry and kinetics of the formation reaction, thermal decomposition, Carbon N. Y. 8 (1970) 741–752. doi:10.1016/0008-6223(70)90099-0.

[13] B.R. Puri, Surface oxidation of charcoals at ordinary temperatures, in: Proc. Fifth Bienn. Conf. Carbon, Pennsylvania, 1961: pp. 165–170. doi:10.1016/b978-0-08-009707-7.50027-3.

[14] M. Kiyono, P.J. Williams, W.J. Koros, Effect of pyrolysis atmosphere on separation performance of carbon molecular sieve membranes, J. Memb. Sci. 359 (2010) 2–10. doi:10.1016/j.memsci.2009.10.019.

[15] I. Menendez, A.B. Fuertes, Aging of carbon membranes under different environments, Carbon N. Y. 39 (2001) 733–740. doi:10.1016/S0008-6223(00)00188-3.

[16] L. Xu, M. Rungta, J. Hessler, W. Qiu, M. Brayden, M. Martinez, G. Barbay, W.J. Koros, Physical aging in carbon molecular sieve membranes, Carbon N. Y. 80 (2014) 155–166. doi:10.1016/j.carbon.2014.08.051.

[17] C.W. Jones, W.J. Koros, Carbon molecular sieve gas separation membranes-II. Regeneration following organic exposure, Carbon N. Y. 32 (1994) 1427–1432. doi:10.1016/0008-6223(94)90136-8.

[18] M. Ottaway, Use of thermogravimetry for proximate analysis of coals and cokes, Fuel. 61 (1982) 713–716. doi:10.1016/0016-2361(82)90244-7.

[19] N.D. Hutson, R.T. Yang, Theoretical basis for the Dubinin-Radushkevitch (D-R) adsorption isotherm equation, Adsorption. 3 (1997) 189–195. doi:10.1007/BF01650130.

[20] S.C. Rodrigues, R. Whitley, A. Mendes, Preparation and characterization of carbon molecular sieve membranes based on resorcinol–formaldehyde resin, J. Memb.

Sci. 459 (2014) 207–216. doi:10.1016/j.memsci.2014.02.013.

[21] J.C. Santos, F.D. Magalhães, A. Mendes, Contamination of zeolites used in oxygen production by PSA: effects of water and carbon dioxide, Ind. Eng. Chem. Res. 47 (2008) 6197–6203. doi:10.1021/ie800024c.

[22] D. Ferreira, R. Magalhães, P. Taveira, A. Mendes, Effective adsorption equilibrium isotherms and breakthroughs of water vapor and carbon dioxide on different adsorbents, Ind. Eng. Chem. Res. 50 (2011) 10201–10210. doi:10.1021/ie2005302.

[23] D.D. Do, Adsorption analysis: equilibria and kinetics, Queensland, 1998. doi:10.1142/p111.

[24] M.M.C.C. Santos, Carbon molecular sieve membranes for gas separation: study, preparation and characterization, University of Porto, 2009.

[25] M. Kočiřík, P. Struve, M. Bülow, Analytical solution of simultaneous mass and heat transfer in zeolite crystals under constant-volume/variable-pressure conditions, J. Chem. Soc. Faraday Trans. 1. 80 (1984) 2167–2174. doi:10.1039/F19848002167.

[26] C.J. Ewansiha, J.E. Ebhoaye, I.O. Asia, L.O. Ekebafe, C. Ehigie, Proximate and mineral composition of coconut (Cocos Nucifera) shell, Int. J. Pure Appl. Sci. Technol. 13 (2012) 57–60.

[27] M.N.M. Iqbaldin, I. Khudzir, M.I.M. Azlan, A.G. Zaidi, B. Surani, Z. Zubri, Properties of coconut shell activated carbon, J. Trop. For. Sci. 25 (2013) 497–503. doi:97591071.

[28] R. Mamat, M.R. Hainin, N.A. Hassan, N.A.A. Rahman, M.N.M. Warid, M.K. Idham, A review of performance asphalt mixtures using bio-binder as alternative binder, J. Teknol. 77 (2015) 17–20. doi:10.11113/jt.v77.6681.

[29] W. Li, J. Peng, L. Zhang, K. Yang, H. Xia, S. Zhang, S. Guo, Preparation of activated carbon from coconut shell chars in pilot-scale microwave heating equipment at 60 kW, Waste Manag. 29 (2009) 756–760. doi:10.1016/j.wasman.2008.03.004.

[30] K. Promdee, J. Chanvidhwatanakit, S. Satitkune, C. Boonmee, T. Kawichai, S. Jarernprasert, T. Vitidsant, Characterization of carbon materials and differences from activated carbon particle (ACP) and coal briquettes product (CBP) derived from coconut shell via rotary kiln, Renew. Sustain. Energy Rev. 75 (2017) 1175–1186. doi:10.1016/j.rser.2016.11.099.

[31] S. Ouyang, S. Xu, N. Song, S. Jiao, Coconut shell-based carbon adsorbents for ventilation air methane enrichment, Fuel. 113 (2013) 420–425. doi:10.1016/j.fuel.2013.06.004.

[32] A. Daszkowska-Golec, I. Szarejko, Open or close the gate – stomata action under the control of phytohormones in drought stress conditions, Front. Plant Sci. 4 (2013) 1–16. doi:10.3389/fpls.2013.00138.

[33] R.M. Silverstein, G.C. Bassler, T.C. Morrill, Spectrometric identification of organic compounds, in: Wiley, New York, 1981.

[34] H.F. Shurvell, Spectra-structure correlations in the mid- and far-infrared, Handb. Vib. Spectrosc. (2006). doi:10.1002/0470027320.s4101.

[35] A. Sartape, A. Mandhare, P. Salvi, D. Pawar, P. Raut, M. Anuse, S. Kolekar, Removal of Bi (III) with adsorption technique using coconut shell activated carbon, Chinese J. Chem. Eng. 20 (2012) 768–775. doi:10.1016/S1004-9541(11)60247-4.

[36] C. Rolence, R.L. Machunda, K.N. Njau, Water hardness removal by coconut shell activated carbon, Int. J. Sci. Technol. Soc. 2 (2014) 97–102. doi:10.11648/j.ijsts.20140205.11.

[37] R. Boopathy, S. Karthikeyan, A.B. Mandal, G. Sekaran, Adsorption of ammonium ion by coconut shell-activated carbon from aqueous solution: kinetic, isotherm, and thermodynamic studies, Environ. Sci. Pollut. Res. 20 (2013) 533–542. doi:10.1007/s11356-012-0911-3.

[38] M.B. Smith, J. March, March's Advanced Organic Chemistry: Reactions, Mechanisms, and Structure, 5th ed., Wiley-Interscience, 2001.

[39] A.C. Ferrari, J. Robertson, Interpretation of Raman spectra of disordered and

amorphous carbon, Phys. Rev. B. 61 (2000) 14095–14107. doi:10.1103/PhysRevB.61.14095.

[40] M. Šupová, J. Svítilová, Z. Chlup, M. Černý, Z. Weishauptová, T. Suchý, V. Machovič, Z. Sucharda, M. Žaloudková, Relation between mechanical properties and pyrolysis temperature of phenol formaldehyde resin for gas separation membranes, Ceram. – Silikáty. 56 (2012) 40–49.

[41] A. Ganesan, R. Mukherjee, J. Raj, M.M. Shaijumon, Nanoporous rice husk derived carbon for gas storage and high performance electrochemical energy storage, J. Porous Mater. 21 (2014) 839–847. doi:10.1007/s10934-014-9833-4.

[42] T.S. Blankenship II, N. Balahmar, R. Mokaya, Oxygen-rich microporous carbons with exceptional hydrogen storage capacity, Nat. Commun. 1545 (2017) 12. doi:10.1038/s41467-017-01633-x.

[43] S. Tanaka, T. Yasuda, Y. Katayama, Y. Miyake, Pervaporation dehydration performance of microporous carbon membranes prepared from resorcinol/formaldehyde polymer, J. Memb. Sci. 379 (2011) 52–59. doi:10.1016/j.memsci.2011.05.046.

[44] S. Mondal, A. Elkamel, D. Reinalda, K. Wang, Preparation and morphology study of carbon molecular sieve membrane derived from polyimide, Can. J. Chem. Eng. 95 (2017) 1993–1998. doi:10.1002/cjce.22881.

[45] L.B. Adams, C.R. Hall, R.J. Holmes, R.A. Newton, An examination of how exposure to humid air can result in changes in the adsorption properties of activated carbons, Carbon N. Y. 26 (1988) 451–459. doi:10.1016/0008-6223(88)90143-1.

[46] T. Hasell, M. Miklitz, A. Stephenson, M.A. Little, S.Y. Chong, R. Clowes, L. Chen, D. Holden, G.A. Tribello, K.E. Jelfs, A.I. Cooper, Porous organic cages for sulfur hexafluoride separation, J. Am. Chem. Soc. 138 (2016) 1653–1659. doi:10.1021/jacs.5b11797.

Chapter III

Chapter 3 - High performing CMS adsorbent for O_2 / N_2 separation[1]

Graphical abstract

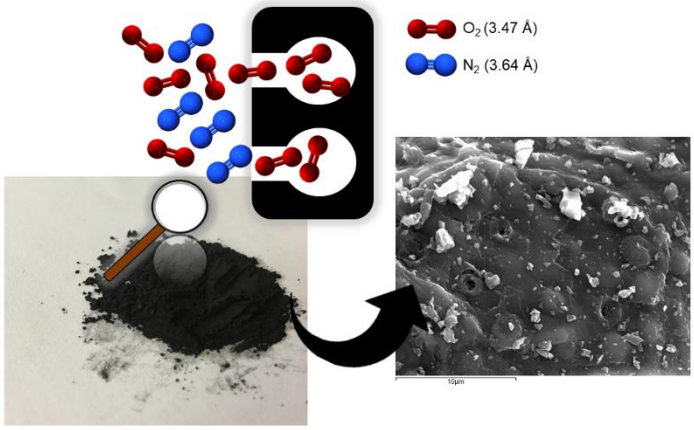

3.1. Abstract

The synthesis of a low particle size carbon molecular sieve (CMS) adsorbent was optimized for the O_2 / N_2 separation. The best performing CMS displayed an O_2 / N_2 adsorption kinetic selectivity of 123 and an inverse of apparent diffusion time constant of *ca.* 9×10^{-2} s^{-1}; these are the highest values reported for an oxygen chemisorption stabilized sample. The adsorbent was prepared from the carbonization of a cellulosic precursor at 1000 ºC followed by milling and stabilization steps. The sample structure, morphology and performance were further examined by scanning electron microscopy, thermogravimetric analysis, Fourier transform infrared spectroscopy, CO_2 adsorption and adsorption capacity and kinetics of O_2, N_2, Ar and SF_6 at 25 ºC. SEM micrographs showed very fine powder particles with stomas. CO_2 adsorption isotherms revealed that the CMS adsorbent has a well-developed microporous structure. The obtained results were well above the ones reported on literature for similar conditions opening the door for the preparation of stable carbon molecular sieve adsorbents with extraordinary O_2 / N_2 separation performance.

---

[1]M. Andrade, S. C. Rodrigues, A. Mendes, High performing CMS adsorbent for O_2 / N_2 separation, Microporous Mesoporous Mater. 296 (2020) 11. doi:10.1016/j.micromeso.2019.109989.

3.2. Introduction

Gas separation processes play an important role in several industries such as chemical, food, medical and petrochemical. The search for more efficient separation processes, with less energy-consumption, as well as less environmental impacts and cost has been a long-term challenge [1]. The most used gas separation process is the cryogenic distillation [1,2]. Despite being a process suitable for treating large feed flowrates with high purities it is an energy-intensive and very expensive process [1,3]. Absorption technology for gas separation appeared as a simple process but with poor separation performances exhibiting low purities and recoveries [4,5]. On the other hand, adsorption-based processes, such as, pressure swing adsorption (PSA), emerged as an energy and efficient process, suitable for several gas separations and purification applications [1,6,7]. PSA is a cyclic adsorption process in which gas species are separated by differences in adsorption capacity and/or adsorption rates [1,8,9]. Membrane technology also appeared as a new solution for gas mixtures separation displaying promising results and being a low cost and energy saving process [5].

Zeolites and carbon molecular sieve (CMS) adsorbents are the most commonly used materials in gas separation processes. Zeolites are highly efficient materials but expensive and weak under acid or basic conditions and high temperatures [8]. On the other hand, CMS adsorbents exhibit excellent performances in gas separation processes and are cheap, highly resistant to both alkaline and acid media and display thermal stability under inert atmospheres [8,10,11]. CMS materials are a special class of activated carbon (AC) materials [9] characterized by a very narrow micropore size distribution (ranging from 0.4 nm to 0.9 nm) [5,12]; they have smaller pore surface area and narrower pore size distributions than AC. CMS adsorbents are normally used for kinetic separations since they display high adsorption kinetic selectivities [13]. An effective CMS adsorbent is defined by two properties: adsorption capacity and kinetic selectivity [14]. The adsorption capacity is developed during the production of the carbon material while the selectivity is induced by tailoring the pore entrance [11,15]. The selectivity is provided by a narrow pore size distribution and the adsorption capacity is related to the micropores volume [14,15]. Therefore, selectivity arises from differences in the shape and dimensions of the adsorbate species originating different adsorption kinetics [15,16]. Then, generally, CMS gas separation is based on the differences of the diffusion

rates of the involved gas species [15,16] whereas species with a molecular size smaller than the pore entrance are preferentially adsorbed [15–17]. The gas species penetrate the microporous structure filling up the micropores until the sorption equilibrium is achieved [15,17]; therefore, the adsorption process is controlled either by adsorption equilibrium or the diffusion time constant [15–17].

The preparation of CMS adsorbents generally involves five main steps: i) precursor material selection ii) pre-treatments iii) controlled carbonization of the precursor material; iv) activation of the carbonized product (char) and; v) post-treatments/modification of the porosity through chemical vapor deposition (CVD) [11,15,18]. Among these, the precursor selection and the carbonization are the most important steps in the carbon molecular sieve materials preparation. The main operating parameters in the carbonization step are the carbonization end temperature, heating rate, inert gas flowrate and the precursor material [15]. High carbonization temperatures result in a greater amount of volatiles released from the precursor material with a direct influence in the pore size distribution of the adsorbent. Normally, the carbonization end temperature ranges between 500 ^{o}C and 1100 ^{o}C [19–23]. However, the precursor plays the main role on the final structure of the CMS adsorbents since different precursors carbonized in the same operating conditions lead to carbon adsorbents with different properties [24,25]. Several lignocellulosic biomass materials such as coconut shell, pistachio shell, walnut shell, tropical wood, among others, have been used as precursor materials to produce CMS adsorbents [23]. The carbonization of lignocellulosic biomass results in the formation of three main phases: i) char, ii) oils (tar) and iii) gases. During the thermal treatment, moisture and volatile compounds are removed from the biomass and solid chars are generated [15,26]. Thus, char phase corresponds to the resultant carbonaceous material from carbonization process after removing non-carbon elements such as hydrogen and oxygen from the precursor material [15].

Many authors have been focused on tailoring the molecular sieve properties of carbon materials to obtain CMS adsorbents with high separation performance [27–30]; nevertheless, there are not many studies addressing the CMS stability [29,31–34]. CMS materials are mechanically stable but can be susceptible to chemical aging, due to the oxygen chemisorption and humidity blockage of the pores [29,32–34]. Several studies

regarding water adsorption reported that it reduces the carbon materials performance [29,34,35]. Furthermore, Jones and Koros [31] reported also that when carbon materials are exposed to organic contaminants a significant loss of performance is observed [29]; however, when the CMS are post-treated with a propylene atmosphere it acts like a cleaning agent of organic contaminants enabling its use as a regenerating entity. Lagorsse *et al.* [32] studied hydrogen passivation for carbon membranes regeneration and observed that hydrogen stabilized an extent number of carbon active sites, however, this technique was not completely efficient by leaving still some reactive sites capable to re-adsorb oxygen. Furthermore, Largorsse *et al.* [32] mentioned that even when hydrogen passivation is applied, a stabilization technique is needed, *e.g.* propylene storage. Research on aging of carbonized phenolic films on porous alumina tubes under several environments (air, nitrogen and propylene) was also reported by Menendez and Fuertes [33]. The authors concluded that oxygen exposure was the major cause of aging on the carbon materials [29,33]. Moreover, they suggested that oxygen selectively adsorbs on the "edges" of the ultramicropores and in the defects of the carbon structure [33]. When carbon materials with reactive edges are exposed to air, even at room temperature, oxygen chemisorption begins to take place slowly [29,33,36]. Jones and Koros [37] showed that carbon microvoids are generally hydrophobic; however, some oxygen-containing surface groups can act as primary sites to attract water molecules [29,37]. Even in relatively hydrophobic micropores, when high activities occur, the formation of water clusters may eventually occur [38,39].

This work reports the optimization of CMS adsorbents for the kinetic separation of O_2 / N_2. High selective CMS adsorbents were prepared from the carbonization of a cellulosic precursor with subsequent milling of the carbonized product and stabilization in a propylene atmosphere. Morphological and structural characterizations of the optimized samples were obtained. Adsorption experiments were also performed to obtain the adsorption capacity and kinetics to oxygen and nitrogen.

3.3. Experimental

3.3.1. Materials

The cellulosic precursor material, GC-AP, was supplied by Air Products and Chemicals Inc. displaying a mean particle size of 58 µm. Oxygen (99.995 % pure), nitrogen (99.999 % pure), argon (99.999 % pure), carbon dioxide (99.9 % pure) and helium (99.999 % pure) were supplied by Air Liquide. Propylene (99.5 % pure) and sulfur hexafluoride (99.9 % pure) was from Praxair.

3.3.2. Carbonization, milling and stabilization

The carbonization step was performed in an alumina tube (954 cm^3 of volume) inside a tubular horizontal Termolab TH furnace under a nitrogen atmosphere with a flowrate of 170 $mL \cdot min^{-1}$ and a heating rate of 0.5 $^oC \cdot min^{-1}$. To guarantee the temperature homogeneity along the tube, the furnace was equipped with three heating elements (Figure 3.1). The end temperature varied between 900 ^oC and 1100 ^oC and a soaking time of 120 min was applied. After the carbonization step, the system was allowed to cool naturally until room temperature and after that the samples were removed from the furnace.

After carbonization, the samples were milled in a planetary ball mill (Retsch PM 100) at different wheel speeds (100-200 min^{-1}). To protect the samples from oxygen chemisorption, the samples were subsequently stored in a propylene atmosphere (1-10 days) at 2 bar.

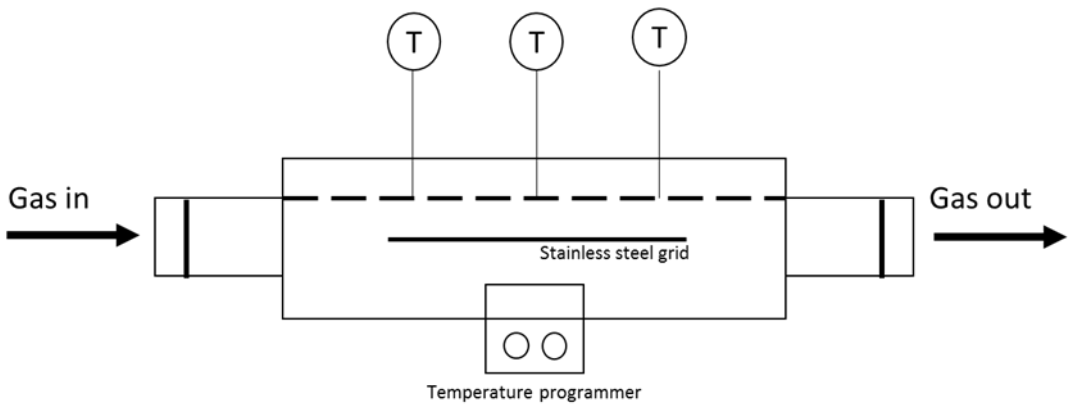

Figure 3.1. Scheme of the carbonization setup.

3.3.3. Experimental design

Statistical design of experiments (DoE) consists in a matrix-based multifactor method that measures interaction effects of the multidimensional experimental region [40]. DoE has several methodologies such as Screening Design, Full Factorial Design, Mixture Design, Taguchi Design, Non-linear Design, Response Surface Design, among others. In this work, the Response Surface Design methodology (RSM) was used; it consists in a group of mathematical and statistical techniques based on empirical models used to fit the obtained experimental data achieved by the experimental design [41]. Accordingly, linear or polynomial functions are used for describing the experimental results and consequently to explore new experimental conditions (modeling and/or deleting) even before its optimization [41]. Response Surface Design method has several designs; the central composite design and the Box-Behnken are the most used. The Central Composite Design involves three parts i) a full factorial or fractional factorial design; ii) an additional design, often a star design where experimental points are at a distance α from its center and iii) a central point [41].

The CMS adsorbents performance for a given gas separation is generally measured by the kinetics of adsorption ($D \cdot r^{-2}$), adsorption capacity (q_{ads}) and kinetic selectivity (S_{O_2/N_2}). In this work, the influence of carbonization end temperature (T_{end}), particle size (R_{speed}) and propylene time exposure ($t_{C_3H_6}$) on the CMS performance was carefully studied. The significance parameters were characterized by the *p*-value and the coefficient of determination (R^2); the model fitness and accuracy was characterized by the root-mean-square error (RMSE) and lack of fit test [42]. An experimental design was constructed using the Response Surface Design method based on JMP 12.0 from SAS. The Central Composite Design was chosen which for 3 factors includes 17 experiments as shown in Table 3.2. The factors considered were: i) carbonization end temperature (900 -1100 ºC), ii) rotation speed of the milling step (100-200 rpm) and iii) samples stabilization period (5 -10 days).

3.3.4. Adsorption capacity and gas uptake experiments

The adsorption isotherms and uptake curves of O_2, N_2, Ar, CO_2 and SF_6 on the prepared CMS adsorbents were obtained using the volumetric method. This method is based on the pressure variation of the gas after an expansion; knowing the pressure

decrease and assuming for the system an ideal gas behaviour, the amount of adsorbed solute can be determined [43,44]. Figure 3.2 shows a schematic representation of the used volumetric unit. Briefly, the experimental setup consists on a gas tank (Tank A) and a tank where the sample is located (Tank B). For obtaining the mono-component adsorption equilibrium isotherms, the equilibrium pressure of the Tank A is measured after opening valve V1 [43]. For pressures until 2 bar, a 2 bar Drück pressure sensor (reading error of 0.1 % of full scale) was used while for higher pressures, a 7 bar Drück pressure sensor (reading error of 0.1 % of full scale) was implemented. Both tanks were immersed in a thermostatic water bath (Huber, K12-cc-NR) for constant temperature operation. An Alcatel 1004A rotary vacuum pump was also used to evacuate the tanks. The sample was regenerated at 70 ^{o}C during 4 h under < 2 mbar.

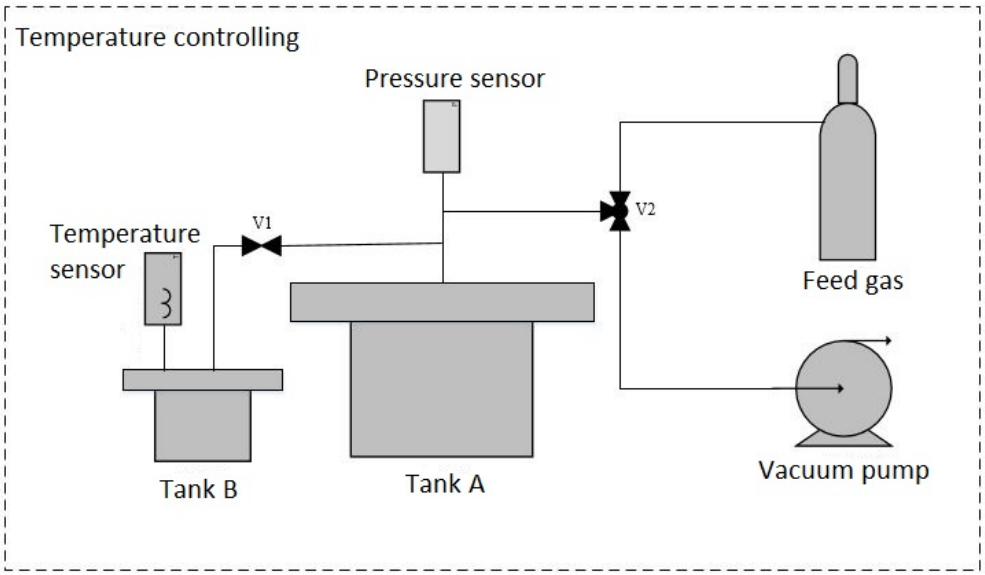

Figure 3.2. Volumetric unit setup.

Langmuir, dual-site Langmuir, Toth and Langmuir-Freundlich (SIPS) equations are commonly used to fit the adsorption equilibrium isotherms. Langmuir, dual-site Langmuir and Toth equations display simple mathematical formulations that are thermodynamically consistent. Besides, dual-site Langmuir (Eq. 3.2) and Toth equations (Eq. 3.3) have one more parameter than Langmuir equation (Eq. 3.1) which becomes an alternative to Langmuir when this model does not fit well the experimental data [16]. Further, Toth and SIPS (Eq. 3.4) take into account the heterogeneity of the adsorption

surface. However, SIPS model is not valid for low end pressure range since this model does not displays a Henry law type behaviour [5,16].

$$q = q_s \frac{bP}{1+bP} \tag{3.1}$$

$$q = q_{s,1} \frac{b_1 P}{1+b_1 P} + q_{s,2} \frac{b_2 P}{1+b_2 P} \tag{3.2}$$

$$q = q_s \frac{bP}{\left(1+(bP)^t\right)^{1/t}} \tag{3.3}$$

$$q = q_s \frac{(bP)^{1/n}}{1+(bP)^{1/n}} \tag{3.4}$$

where q represents the adsorbed solute concentration at pressure P, q_s is the adsorbed saturation capacity, b is the adsorption affinity constant and t and n are parameters used to characterize the heterogeneity of the system. Generally, t is less than the unity; for t = 1, Toth equation reduces to Langmuir equation [16].

The inverse of apparent diffusion time constant ($D \cdot r^{-2}$) was obtained fitting a mathematical model to the experimental uptake curves. The selected model (Eq. 3.5), was developed for accounting with the adsorption release of heat (non-isothermal model) and for the initial pressure after pressure equilibration between the two tanks and assuming no adsorption [45]:

$$F = 1 - \sum_{n=1}^{\infty} \frac{9\left(1+\alpha^*\right)\left[\frac{Y_n}{-q_n^2}\right]^2 \exp\left(-q_n^2 \tau\right)}{\frac{1}{\beta_n^*} + \frac{3}{2}\frac{\beta}{\beta_n^*}\left[q_n \cot q_n \left(\frac{Y_n}{q_n^2}\right)+1\right] + \frac{3}{2}\frac{\alpha^* B_n}{q_n^4 \beta_n^*}} \tag{3.5}$$

where where $B_n = Y_n\left[(q_n^2 - \alpha)\, q_n \cot q_n - 2\alpha\right] + q_n^2(q_n^2 - \alpha)$, $Y_n = q_n \cot q_n - 1$ and $\alpha^* = KV$. Considering that $V = V_s / V_g$ and V_s and V_g are the structural volume of the adsorbent sample and the total gas phase volume (in both tanks), respectively.

3.3.5. Thermogravimetric analysis

Thermogravimetric analysis (TGA) was performed in a Netzsch STA 449 F3 Jupiter thermogravimetric balance. A proximate analysis was performed for determining moisture, volatile matter, fixed carbon and ashes. The feed gases used in the analysis were N_2 and O_2. The program included a heating rate of 25 $^oC \cdot min^{-1}$, with several dwells at 50 ^oC, 110 ^oC and 950 ^oC. The dwells at 50 ^oC and 110 ^oC are related to O_2 removal for preventing CMS oxidation at higher temperatures; the dwell at 110 ^oC is also applied to ensure that all water in the carbon materials is released. At 950 ^oC, the applied dwell has a duration of 20 min and is divided in two sub-dwells: a first one of 9 min under N_2 for measuring the release of volatile matter and a second one of 11 min under O_2 for assessing the ash content [46].

3.3.6. Pore size distribution

The pore size distribution of the CMS adsorbents was obtained based on the adsorption equilibrium isotherm of carbon dioxide at 0 ^oC following the methodology described by Do *et al.* [47].

3.3.7. Scanning electron microscopy (SEM) and Energy dispersive X-ray spectroscopy analysis (EDS)

SEM/EDS analyses were performed in a JEOL JSM 6301F/ Oxford INCA Energy 350 using a high-resolution scanning electron microscope with X-ray microanalysis. The samples were previously sputtered with Au/Pd using a SPI Module Sputter Coater equipment.

3.3.8. Fourier transform infrared spectroscopy (FTIR)

The infrared spectra were recorded using a VERTEX 70 FTIR spectrometer (BRUKER) in transmittance mode with a high sensitivity DLaTGS detector at room temperature. Samples were measured in transmission mode, using pellets of potassium bromide (KBr) with 1 % (w/w) of compound. The spectra were recorded from 4000 cm^{-1} to 400 cm^{-1} with a resolution of 4 cm^{-1}.

3.4. Results and discussion

3.4.1. Adsorption equilibrium isotherms and adsorption rate

A pre-screen set of experiments were performed to identify the searching domain of the selected factors. The best performing sample was obtained carbonizing the GC-AP precursor material at 1000 ºC carbonization end temperature and applying a soaking time of 120 min; after that, the carbonized sample was milled at 160 rpm and stored in a propylene atmosphere for 5 days – GC-AP-HP-5. Figure 3.3 shows the adsorption equilibrium isotherms for oxygen and nitrogen on the GC-AP-HP-5 CMS sample at 25 ºC.

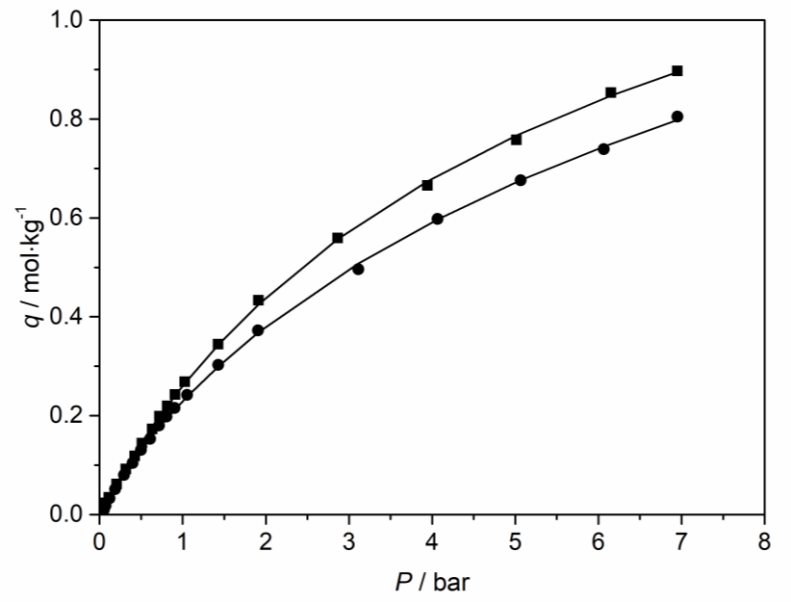

Figure 3.3. O_2 (■) and N_2 (●) adsorption equilibrium isotherms at 25 ºC on GC-AP-HP-5. The solid lines represent Toth isotherm fitting.

Table 3.1 shows the inverse of the apparent diffusion time constants for O_2 and N_2 and the kinetic selectivity of GC-AP-HP-5 at *ca.* 1 bar and 25 ºC.

Table 3.1. GC-AP-HP-5 adsorption kinetic parameters at *ca.* 1 bar and 25 ºC.

Sample		T_{end} / ºC	R_{speed} / rpm	$t_{C_3H_6}$ / days	$D \cdot r^{-2}$ / s^{-1}	$S_{O2/N2}$
GC-AP-HP-5	O_2 N_2	1000	160	5	9.25×10^{-2} 1.64×10^{-3}	56.4

To optimize the GC-AP-HP-5 CMS performance, a Design of Experiments (DoE) was performed. Table 3.2 shows the obtained DoE and the corresponding characterization results.

Table 3.2 Design of Experiments given by JMP software and respective experimental results.

Run	T_{end} / ºC	R_{speed} / rpm	$t_{C_3H_6}$/ days	$D \cdot r^{-2}$ / s^{-1}	S_{O_2/N_2}	q_{ads} / mol·kg^{-1}
1	1100	200	10	7.03×10^{-4}	1.79	0.204
2	1100	100	5	2.79×10^{-4}	42.80	0.264
3	900	200	5	3.66×10^{-2}	7.18	0.262
4	900	100	5	9.46×10^{-3}	13.90	0.197
5	900	200	10	2.79×10^{-2}	2.80	0.268
6	1000	150	7.5	9.74×10^{-3}	23.70	0.156
7	1000	150	10	5.02×10^{-2}	3.42	0.201
8	1100	100	10	9.16×10^{-4}	51.17	0.220
9	1100	150	7.5	5.37×10^{-4}	12.64	0.175
10	1000	150	7.5	1.44×10^{-2}	27.43	0.120
11	1100	200	5	2.21×10^{-3}	14.44	0.269
12	1000	150	5	1.04×10^{-1}	48.37	0.182
13	1000	200	7.5	2.64×10^{-2}	20.78	0.192
14	900	100	10	1.71×10^{-2}	21.81	0.155
15	1000	150	7.5	9.12×10^{-3}	21.45	0.158
16	1000	100	7.5	1.37×10^{-2}	47.74	0.157
17	900	150	7.5	3.46×10^{-2}	106.46	0.223

The obtained results for each response variable, namely, oxygen inverse of the apparent diffusion time constant ($D \cdot r^{-2}$), oxygen adsorption capacity (q_{ads}) and kinetic selectivity (S_{O_2/N_2}) indicated that the model did not described well the experimental results. For oxygen inverse apparent diffusion time constant, a *p*-value of 0.26 and a R^2 = 0.68 were obtained; for the O_2 / N_2 kinetic selectivity a *p*-value 0.83 and a R^2 = 0.39 were obtained; and for oxygen adsorption capacity, a *p*-value = 0.04 and a R^2 = 0.84 were obtained. Therefore, the Response Surface Design cannot be used to predict the experimental data. Nevertheless, from Table 3.2, it can be observed that Run #12 displays the CMS adsorbent with best separation properties. Also, it is interesting to note that this material has preparation conditions very close to the preparation conditions of GC-AP-HP-5, which displays slightly better gas separation properties. The preparation conditions of GC-AP-HP-5 were then taken as reference. From Table 3.2 it is evident that the contacting time with propylene plays a small role on the properties

of the adsorbents. It was then decided to assess its role for smaller contact times. Table 3.3 shows the separation properties of absorbents prepared at the reference conditions with propylene contact times increasing from 1 to 5 days.

Table 3.3. Adsorption variables for GC-AP-HP samples exposed to a propylene atmosphere for different time periods.

Sample	$t_{C_3H_6}$ / days	$O_2D \cdot r^{-2}$ / s^{-1}	O_2D / $cm^2 \cdot s^{-1}$	S_{O_2/N_2}	O_2q_{ads} / $mol \cdot kg^{-1}$
GC-AP-HP-1	1	2.15×10^{-2}	1.34×10^{-9}	136.1	0.268
GC-AP-HP-2	2	2.99×10^{-2}	1.87×10^{-9}	133.5	0.228
GC-AP-HP-3	3	7.05×10^{-2}	4.41×10^{-9}	79.80	0.188
GC-AP-HP-4	4	9.11×10^{-2}	5.69×10^{-9}	123.4	0.197
GC-AP-HP-5	5	9.25×10^{-2}	5.78×10^{-9}	56.40	0.194

Table 3.3 shows that the sample with a contact time of 4 days (GC-AP-HP-4) displays the best separation properties; therefore, a more detailed characterization was performed only for this carbon sample.

3.4.2. Thermogravimetric analysis

The TGA characteristic curve is plotted in Figure 3.4. From 30 ºC to 110 ºC a weight loss of 3.8 % related to the release of physically adsorbed water is observed. Between 110 ºC and 950 ºC the sample loses *ca.* 74 % of its original weight which was assigned to the release of heteroatoms and non-fixed carbon.

In the present work, the carbon yield is the most important variable since it provides information about the fraction of carbon content in the final material. Furthermore, higher fixed carbon contents indicate that the resultant carbon materials are mechanically more stable. Usually, carbon materials have 25 % - 50 % of fixed carbon depending on the precursor material [5,48]. Some reported materials have carbon yields higher than 60 % such as PBO fibres [49] (69 %) [50] and hyperbranched polyborate and paraformaldehyde (75 % - 80 %) [51]. Table 3.4 shows the proximate analysis results. The precursor presents *ca.* 18 % of fixed carbon. Carbon yields of 18 % - 20 % have been reported for similar raw materials; in agreement with this, the obtained result is situated in the expected range [52–54].

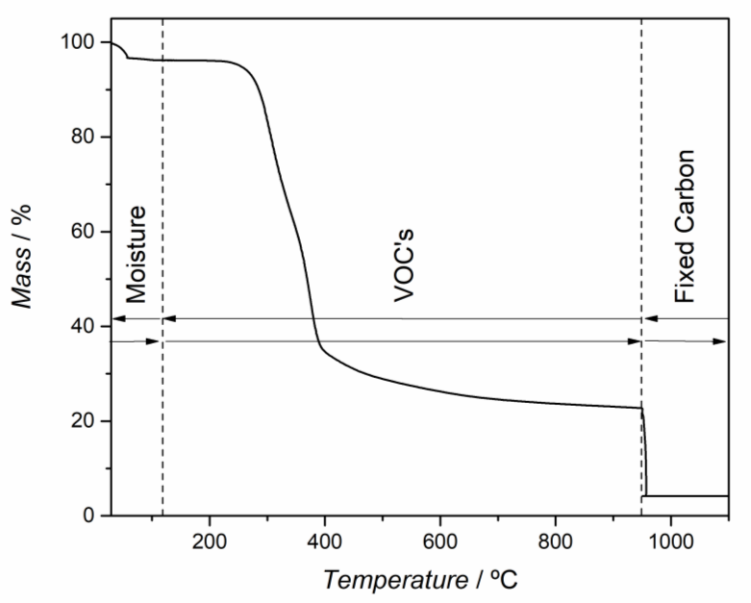

Figure 3.4. TGA characteristic curve of GC-AP precursor.

Table 3.4. Proximate analysis of the GC-AP precursor.

	GC-AP precursor
Humidity / %	3.8
Volatile matter / %	73.8
Fixed carbon / %	18.3
Ashes / %	4.1

3.4.3. Pore size characterization

Carbon dioxide at 0 ºC can be used to access very narrow porosity in the range of 0.3 nm–1 nm [25,55–59] due to its small diameter and ability to be highly adsorbed by porous carbons. The adsorption equilibrium isotherm of carbon dioxide at 0 ºC on GC-AP-HP-4 CMS sample is plotted in Figure 3.5.

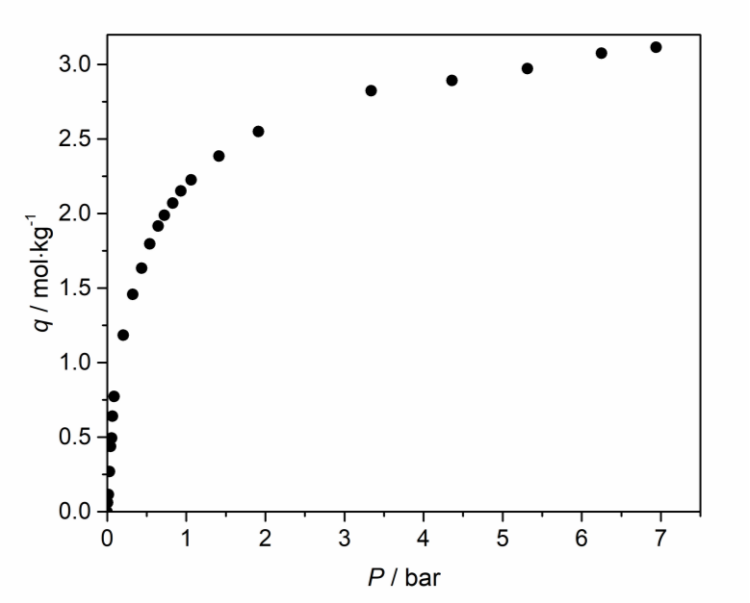

Figure 3.5. Adsorption equilibrium isotherm for CO_2 at 0 ºC of GC-AP-HP-4 CMS sample.

Dubinin-Astakhov (DA) equation (Eq. 3.6) was used to fit the experimental data and determining the micropore volume (W_0) and the characteristic energy of adsorption (E_0) [25]:

$$\frac{W}{W_0} = \exp\left[-\left(\frac{RT\ln(P_0/P)}{E_0}\right)^n\right] \tag{3.6}$$

where W is the micropore volume, P is the pressure, W_0 is the total micropore volume, E_0 is the characteristic energy for adsorption, P_0 is the vapor pressure of the free liquid, R is the gas constant and T is the absolute temperature and n is an adjustable parameter. Dubinin-Radushkevitch (DR) equation is a particular case of DA equation for $n = 2$ providing only a reasonable description of adsorption in micropores of CO_2 for linear characteristic curves. In the present work, the CO_2 characteristic curve was not linear. As result, DA equation was used to fit the experimental data and to obtain the micropore volume and the characteristic energy of adsorption. Figure 3.6 presents the CO_2 characteristic curve for GC-AP-HP-4 CMS adsorbent. A DA equation with $n = 2.8$ provides a good fitting for the experimental data. It is important to note that the slope of the plot gives E_0 and the interception is related to W_0. Table 3.5 summarizes the obtained structural parameters.

Usually, empiric correlations developed by Stoeckli *et al.* [60] are used to determine the mean pore width (*l*). However, Stoeckli equation can only be used when the DR equation applies. Therefore, in the present work the mean pore width was obtained by a weighted average [25].

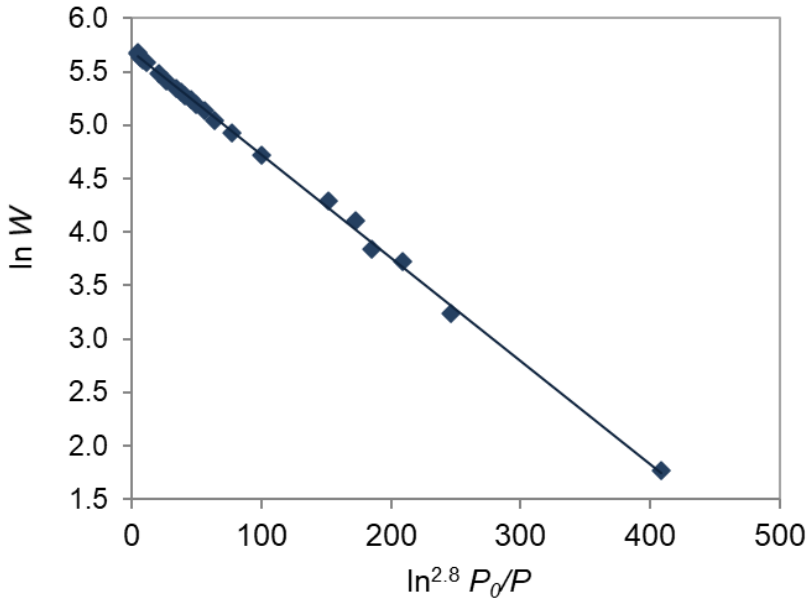

Figure 3.6. CO_2 characteristic curve of GC-AP-HP-4 CMS sample at 0 ºC. The points represent the experimental data and the solid line represents the DA fitting.

Table 3.5. Structural parameters of GC-AP-HP-4 CMS sample.

Parameter	GC-AP-HP-4
W_0 / $cm^3 \cdot kg^{-1}$	291.2
E_0 / $kJ \cdot mol^{-1}$	12.0
l / nm	0.70

From Table 3.5, it can be observed that the GC-AP-HP-4 sample has a micropore volume of *ca.* 291 $cm^3 \cdot kg^{-1}$ which is in agreement with reported values for similar carbon materials [61,62]. The mean pore width (obtained by weighted average) has also the usual value found for carbon molecular sieves [5,61,62].

Pore size distribution was obtained applying the method proposed by Do *et al.* [25,47,63] for determination of micropore size distribution in carbonaceous materials. Figure 3.7 shows the obtained micropore size distribution of GC-AP-HP-4 CMS adsorbent.

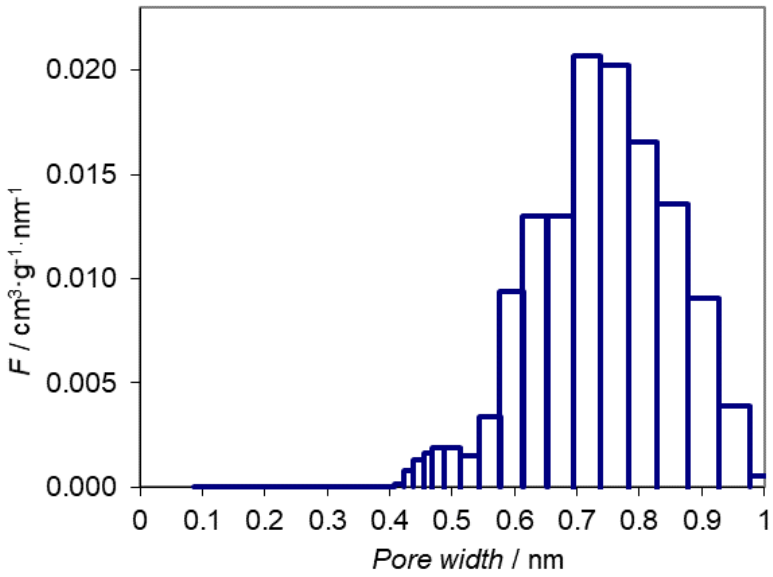

Figure 3.7. Micropore size distribution of GC-AP-HP-4 sample.

The studied sample presents ultramicropores (0.4 nm – 0.7 nm) and larger micropores (0.7 nm – 1 nm). There is a well-defined fraction of pores in 0.4 nm – 0.54 nm diameter range related with the so-called constrictions, responsible for the high kinetic selectivity [5,48]. Despite the existence of some larger micropores, the resistance to mass transfer is mostly conducted by pores with the size close to the molecule dimensions and, the determination of micropore size distribution from adsorption equilibrium data may not be enough to entirely explain the mass transport mechanism; the way that pores are connected with each other may also play an important role [5,63,64].

3.4.4. Morphological and elemental analysis

The morphology and qualitative elemental composition of the samples was examined by SEM/EDS. Figures 3.8 and 3.9 show scanning electron micrographs of the surface view of the precursor and derived CMS adsorbent, respectively.

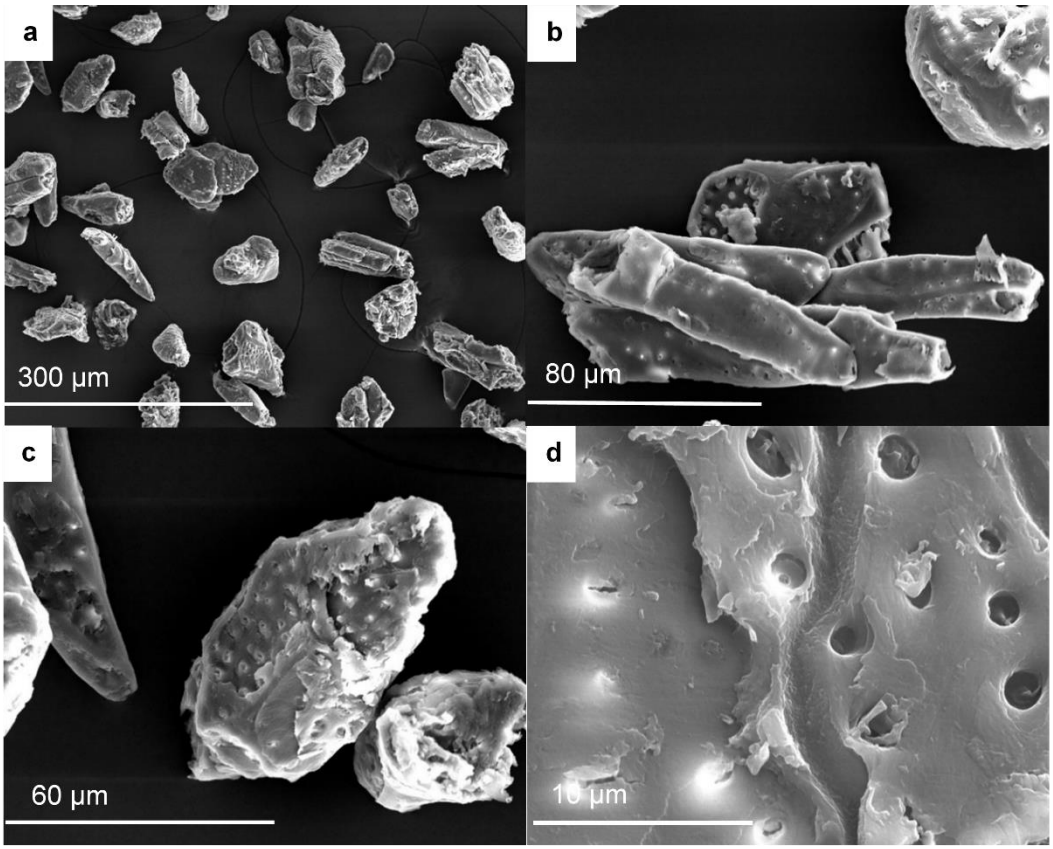

Figure 3.8. Surface scanning electron micrographs of GC-AP-HP-4 precursor. Magnification: (a) 200×, (b) 700×, (c) 1000× and (d) 5000×.

Particle size measurements indicated that the precursor material has an average particle size of *ca.* 58 µm (data not shown). SEM micrographs show that some particles have diameters higher than 58 µm indicating that some particle agglomeration occurred (Figure 3.8). The presence of stomas was also observed; stomas are present on vegetal cells and are responsible for the cellular respiration [65]. These structures are porous entities that may significantly influence the final gas separation properties of the prepared CMS.

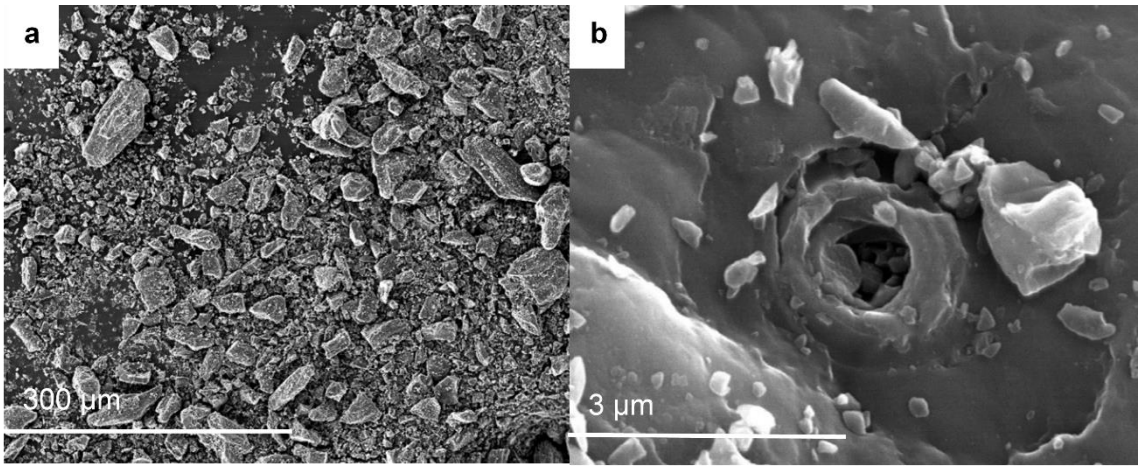

Figure 3.9. Surface scanning electron micrographs of GC-AP-HP-4 adsorbent. Magnification: (a) 200× and (b) 20000×.

The average particle size of the CMS adsorbent was previously determined and it was observed that the carbonized material has *ca.* 1.6 µm (data not shown). Again, some particle agglomeration is evident (Figure 3.9a) and the presence of stomas was also observed (Figure 3.9b). Comparing Figures 3.8 and 3.9, it can be observed that CMS adsorbent has a significant smaller particle size than the precursor due to the carbonization and milling steps.

X-ray microanalysis indicated that the main composition of the samples is carbon and oxygen. The precursor exhibited a lower C / O ratio than the CMS adsorbent which is expected since during the carbonization step oxygenated functional groups are released and a carbon matrix is formed [5].

3.4.5. FTIR characterization

The chemical structure of the samples was investigated by FTIR. Figures 3.10 and 3.11 show the FTIR spectra of the precursor and derived GC-AP-HP-4 CMS adsorbents (with and without propylene treatment), respectively.

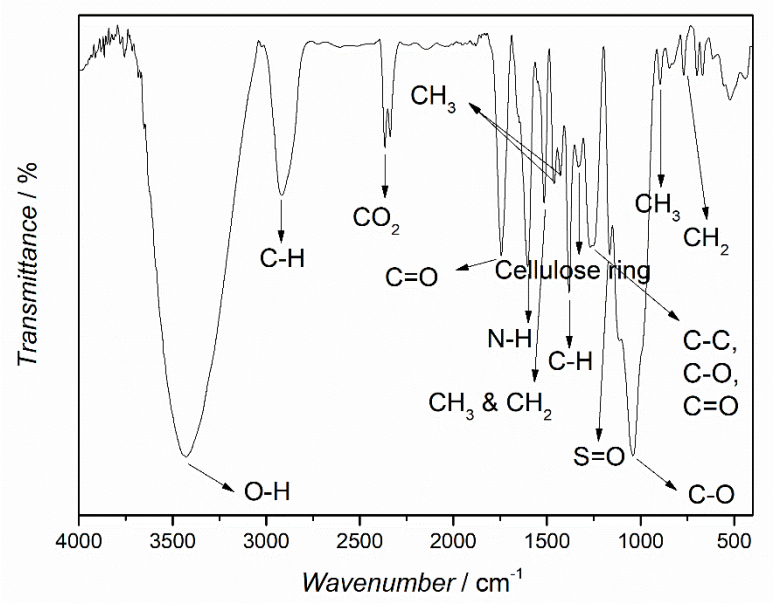

Figure 3.10. FTIR spectrum of the GC-AP precursor material.

The precursor spectrum shows the presence of a O-H stretch vibration band at 3429 cm^{-1} related to adsorbed water on the samples surface and a C-H (alkene) stretch vibration band at 2914 cm^{-1}. The twin bands situated at 2366 cm^{-1} and at 2336 cm^{-1} are attributed to the presence of CO_2 in the beam and at 1740 cm^{-1} a C=O stretching vibration band assigned to esters is observed. A N-H band ascribed to primary amines was observed at 1604 cm^{-1}; the band at 1520 cm^{-1} is attributed to CH_3 and CH_2 sp^3 groups. The band at 1379 cm^{-1} can be ascribed to C-H in alkanes or C-H in methyl and phenolic alcohols and at 1330 cm^{-1} is registered a band ascribed to the vibration of the cellulose ring. The band at 1250 cm^{-1} is attributed to C-C, C-O and C=O stretching vibration and at 1167 cm^{-1} a S=O stretch vibration band is detected. A C-O stretching vibration band assigned to alkoxy groups appeared at 1035 cm^{-1}; and, finally, the bands at 895 cm^{-1} and 771 cm^{-1} are ascribed to CH_3 and CH_2 groups, respectively [66–70].

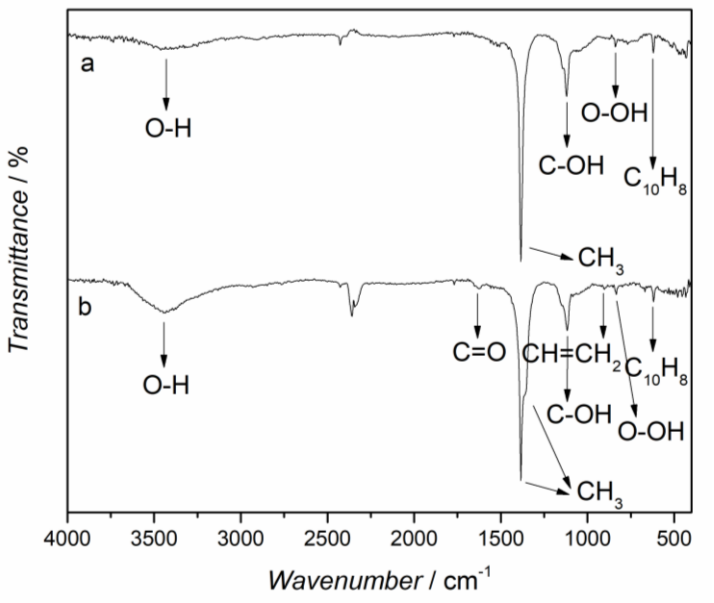

Figure 3.11. FT-IR spectra of GC-AP sample carbonized at 1000 ºC and milled at 160 rpm without propylene treatment (a) and of GC-AP-HP-4 sample (b).

From Figure 3.11 it can be concluded that the propylene treatment induced changes on the surface chemistry of the samples. Two new functional groups appeared in the treated sample, namely C=O stretch vibration in β-keto esters at 1633 cm^{-1} and a $CH=CH_2$ out-of-plane deformation in vinyl compounds at 908 cm^{-1}. Besides, both spectra show a broad band at 3200 cm^{-1}–3600 cm^{-1} which was ascribed to the O-H stretching vibrations in hydroxyl or carbonyl groups and a band at 1380 cm^{-1}–1370 cm^{-1} ascribed to the CH_3 symmetric stretch deformation in aliphatic compounds. The treated and untreated samples showed also a band at 1120 cm^{-1} – 1080 cm^{-1} related to the C-O stretching vibrations (C-OH group of secondary or tertiary alcohols); the band at 860 cm^{-1} – 840 cm^{-1} was attributed to O-OH stretching vibrations from hydroperoxides and the band at 645 cm^{-1} – 615 cm^{-1} corresponds to the $C_{10}H_8$ in-plane ring deformation derived from naphthalenes [66,67].

3.4.6. Adsorption equilibrium isotherms and kinetics

The adsorption capacity of an adsorbent material is strongly dependent of the amount of micropores and surface area [18,71]. The gas adsorption occurs mainly in the micropores; a little fraction of the adsorption occurs in mesopores and macropores since they act as highways for distributing the feeding molecules to the micro-/mesoporous domains inside the activated carbon [17]. One technique to estimate the pore

dimensions present in an adsorbent material consists in analysing its adsorption isotherm curves [11]. Figure 3.12 shows the oxygen, argon, nitrogen, and sulfur hexafluoride adsorption equilibrium isotherms at 25 ºC on GC-AP-HP- 4 CMS.

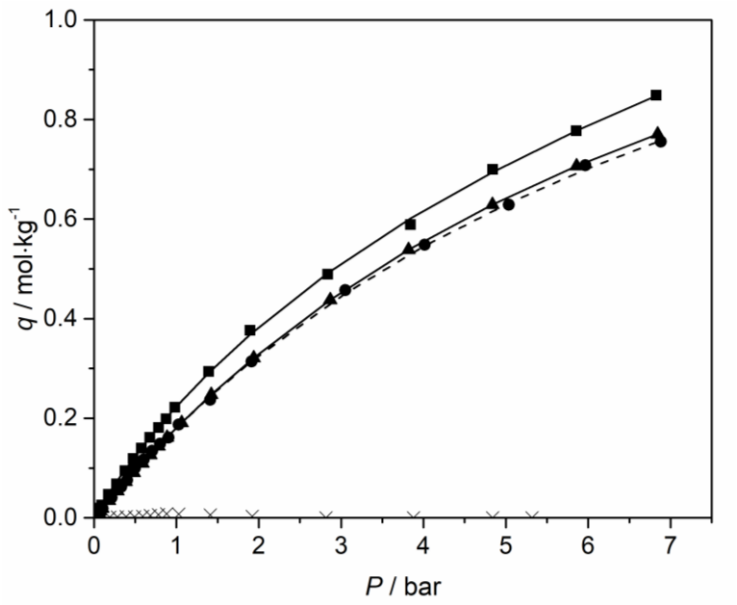

Figure 3.12. O_2 (■), N_2 (●), Ar (▲), and SF_6 (×) adsorption equilibrium isotherms at 25 ºC for GC-AP-HP-4. The solid lines represent Toth isotherm fitting; the dashed line represents the dual-site Langmuir isotherm fitting.

Table 3.6 shows the Toth and dual-site Langmuir equations parameters for oxygen, argon and nitrogen.

Table 3.6. Toth and dual-site Langmuir equation parameters for O_2, Ar; and N_2.

	Toth equation			
	q_s / mol·kg^{-1}	b / bar^{-1}	t	$\sum\left(q-q^*\right)^2$
O_2	2.828	0.107	0.666	2.99×10^{-4}
Ar	1.468	0.133	1.164	3.48×10^{-4}
	Dual-site Langmuir equation				
	$q_{s,1}$ / mol·kg^{-1}	b_1 / bar^{-1}	$q_{s,2}$ / mol·kg^{-1}	b_2 / bar^{-1}	$\sum\left(q-q^*\right)^2$
N_2	-	17.449	1.6560	0.1226	2.89×10^{-4}

The surface of carbonaceous materials is mainly non-polar and, for that reason, their interaction with non-polar or weakly polar species such as O_2, Ar, N_2 and SF_6, occur through Van der Walls forces [5]. The adsorption of a specific gas molecule on an

adsorbent does not depend only on its microporous volume; several other factors such as the diameter and geometry of the gas molecule and its chemistry; the surface chemistry of the adsorbent and the dimension and shape of its pores, also influence the adsorption behaviour [13,72]. From Figure 3.12 it can be concluded that GC-AP-HP-4 presents a higher adsorption capacity towards oxygen when compared to the adsorption of the other gas species. Moreover, sulfur hexafluoride does not adsorb on GC-AP-HP-4 due its large kinetic diameter (0.550 nm [73]), compared with the other gases – N_2 (0.364 nm), Ar (0.354 nm), O_2 (0.347 nm) [74,75]. Sulfur hexafluoride has an octahedral geometry unlike the other gas species that are linear or spherical (argon). Oxygen is the specie that adsorbs the most, followed by argon and nitrogen that show almost identical adsorption capacity. Toth equation describes quite well the experimental data for oxygen and argon; dual-site Langmuir equation was used for fitting the adsorption isotherm of nitrogen.

Experimental oxygen and nitrogen uptake curves were determined at *ca.* 1 bar, with a step pressure perturbation of 1.2 bar, and 25 ºC, using the experimental setup depicted in Figure 3.2. Figure 3.13 shows the oxygen and nitrogen experimental uptake curves and Figure 3.14 shows 80 % of the fractional uptake with the respective fitting model (Eq. 3.5).

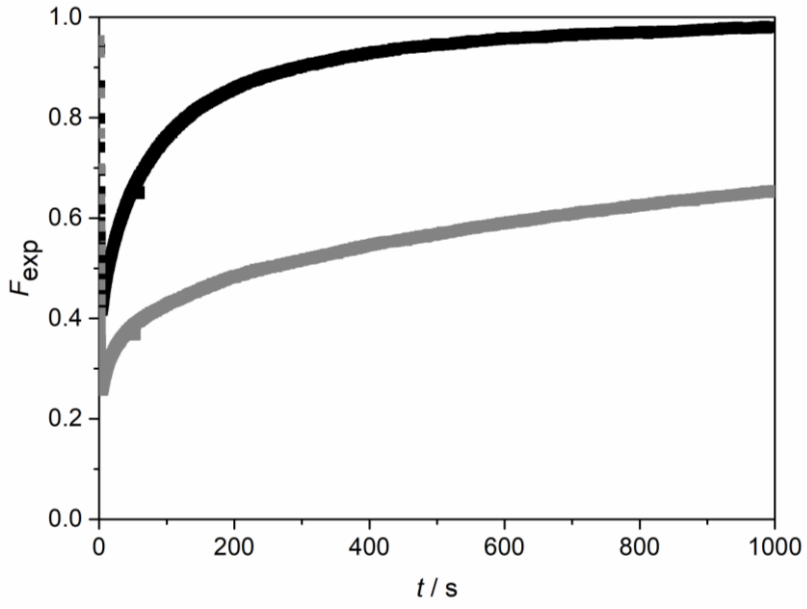

Figure 3.13. Experimental uptake curves for O_2 (black symbols) and N_2 (grey symbols) at 25 ºC and *ca.* 1 bar, with a step perturbation of 1.2 bar.

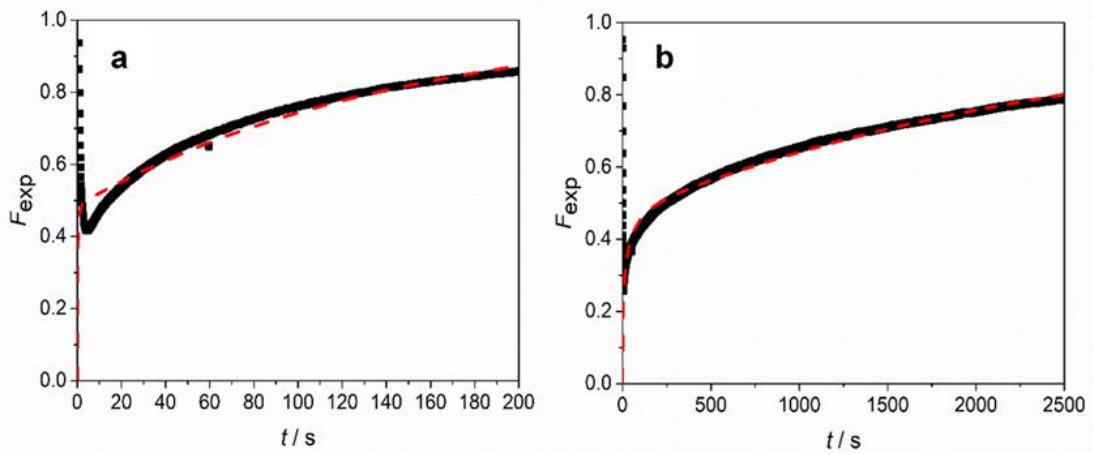

Figure 3.14. Experimental uptake curves (black lines) and respective fitting model (red dashed lines) for O_2 (a) and N_2 (b) in GC-AP-HP-4 CMS sample at 25 ºC and *ca.* 1 bar, with a step perturbation of 1.2 bar.

GC-AP-HP-4 displays a very high oxygen inverse of apparent diffusion time constant, 9.11×10^{-2} s^{-1}, and an O_2 / N_2 kinetic selectivity of *ca.* 123. The fractional uptake curves for both gases have two distinct behaviours: i) until 0.8 of the fractional uptake, the gas kinetics is faster ii) from 0.8 to 1 of the fractional uptake, the diffusivity is lower [76]. As a result, for both gases, the fitting was performed until 0.8 of the factional uptakes.

To test the CMS reproducibility new samples were prepared and both adsorption capacity and kinetics were measured. The reproducibility was assessed, and the adsorption equilibrium and kinetic behaviour was the same, as can be concluded from Table 3.7.

Table 3.7. Results replication of GC-AP-HP-4 CMS sample.

Sample		$D\cdot r^{-2}$ / s^{-1}	D / $cm^2\cdot s^{-1}$	S_{O_2/N_2}	q_{ads} / $mol\cdot kg^{-1}$
GC-AP-HP-4	O_2	9.11×10^{-2}	5.69×10^{-9}	123	0.197
	N_2	7.38×10^{-4}	4.61×10^{-11}		0.190
GC-AP-HP-4[1]	O_2	9.12×10^{-2}	5.70×10^{-9}	129	0.196
	N_2	7.05×10^{-4}	4.41×10^{-11}		0.198

[1]new prepared sample

Table 3.8 and Figure 3.15 show the kinetics of adsorption data obtained in this work and a brief comparison with other reported CMS in literature (some tested in similar conditions).

Table 3.8. Comparison of the kinetics data obtained for the prepared CMS in this work with several carbon adsorbents reported in literature.

Reference	Method	Sorbate	T / °C	P / bar	$D \cdot r^{-2}$ / s^{-1}	S_{O_2/N_2}
[77]	Volumetric	O_2	27	1	1.7×10^{-4}	24
		N_2			7.0×10^{-6}	
[78]	Gravimetric	O_2	30		5.2×10^{-3}	26
		N_2			2.0×10^{-4}	
[79]	Volumetric[2]	O_2			1.0×10^{-3}	100
		N_2			1.0×10^{-5}	
		O_2			3.2×10^{-2}	30
		N_2			1.1×10^{-3}	
		O_2			7.5×10^{-3}	50
		N_2			1.5×10^{-4}	
[80]	Gravimetric	O_2	0		2.4×10^{-4}	68
		N_2			3.5×10^{-6}	
[81]	DAB	O_2	27		3.5×10^{-4}	35
		N_2			1.0×10^{-5}	
[82]	IET[2]	O_2	30		6.0×10^{-2}	22
		N_2			3.2×10^{-3}	
[9]	Gravimetric	O_2	25		0.99×10^{-4}	10
		N_2			1.0×10^{-5}	
[83]	Volumetric	O_2	20		3.8×10^{-3}	38
		N_2			1.0×10^{-4}	
[13]	Manometric[2]	O_2	25	0.955	4.04×10^{-2}	∞
This work	Volumetric	O_2	25	1	1.18×10^{-1}	∞[3]
		N_2			n.d.	
		O_2			9.11×10^{-2}	123[4]
		N_2			7.38×10^{-4}	

[2] Mass-transfer coefficients

[3] CMS adsorbent with oxygen chemisorption

[4] GC-AP-HP-4 CMS adsorbent

Comparing GC-AP-HP-4 adsorbent with other CMS materials reported in literature, it can be concluded that GC-AP-HP-4 has the highest kinetic selectivity to O_2 / N_2 and oxygen inverse time constant for an oxygen chemisorption stabilized adsorbent. Nabais *et al.* [13] developed a CMS with a high O_2 inverse time constant and infinite O_2 / N_2 kinetic selectivity (Table 3.8 and Figure 3.15); however, the stability of the material was not evaluated.

A CMS from GC-AP precursor material with very high oxygen inverse time constant and infinite O_2 / N_2 kinetic selectivity was also obtained by the authors; however, the obtained adsorbent was susceptible to oxygen chemisorption.

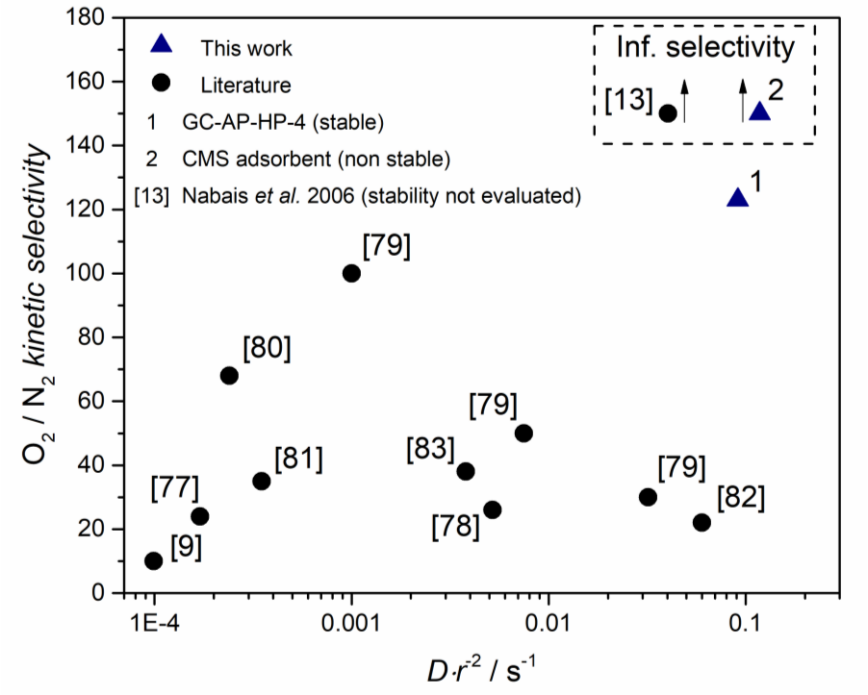

Figure 3.15. Comparison between O_2 inverse of diffusion time constant vs. O_2 / N_2 kinetic selectivity for results obtained in literature and this work.

3.5. Conclusions

Carbon molecular sieve adsorbents with high O_2 / N_2 separation performance and stable towards oxygen chemisorption were successfully prepared. The CMS adsorbents were prepared from the carbonization of a low-cost cellulosic precursor under nitrogen atmosphere followed by milling and stabilization steps. Optimization studies performed on CMS adsorbents revealed that a carbonization end temperature of 1000 ^oC, a soaking time of 120 min, a milling rotation speed of 160 rpm and a propylene treatment for 4 days were the best preparation conditions. The full characterization of the best performing material was performed and an O_2 / N_2 kinetic selectivity of *ca.* 123 and an oxygen inverse apparent diffusion time constant of *ca.* 9×10^{-2} s^{-1} were obtained. Comparing the prepared CMS adsorbents with similar materials reported in literature, it was concluded that the CMS prepared in this work have a better separation performance making them very attractive materials for several industrial applications in special attention for separation of nitrogen from air.

3.6. Acknowledgments

This work was financially supported by: project UID/EQU/00511/2019 - Laboratory for Process Engineering, Environment, Biotechnology and Energy – LEPABE funded by national funds through FCT/MCTES (PIDDAC); Project “LEPABE-2-ECO-INNOVATION” – NORTE-01-0145-FEDER-000005, funded by North Portugal Regional Operational Programme (NORTE 2020), under PORTUGAL 2020 Partnership Agreement, through the European Regional Development Fund (ERDF).

S.C. Rodrigues is grateful to the Portuguese Foundation for Science and Technology (FCT) for the doctoral grant (reference SFRH/BD/93779/2013) supported by funding POPH/FSE.

The authors are thankful to Air Products and Chemicals, Inc. for generously providing the precursor material.

The authors are thankful to CEMUP for the SEM/EDS analyses.

3.7. References

[1] D.A.S.S. Ferreira, High-purity oxygen production by VPSA, University of Porto, 2015.

[2] R.B. Bird, W.E. Stewart, E.N. Lightfoot, Transport Phenomena, John Wiley & Sons, 2002. doi:10.1016/j.ijhydene.2006.08.059.

[3] R.T. Yang, Gas separation by adsorption processes, Imperial College Press, London, 1997.

[4] M.T. Ravanchi, T. Kaghazchi, A. Kargari, Application of membrane separation processes in petrochemical industry: a review, Desalination. 235 (2009) 199–244. doi:10.1016/j.desal.2007.10.042.

[5] M.M.C.C. Santos, Carbon molecular sieve membranes for gas separation: study, preparation and characterization, University of Porto, 2009.

[6] S. Sircar, Pressure swing adsorption, Ind. Eng. Chem. Res. 41 (2002) 1389–1392. doi:10.1021/ie0109758.

[7] D.M. Ruthven, S. Farooq, K.S. Knaebel, Pressure Swing Adsorption, VCH Publishers, New York, 1994.

[8] T. Horikawa, J. Hayashi, K. Muroyama, Preparation of molecular sieving carbon from waste resin by chemical vapor deposition, Carbon N. Y. 40 (2002) 709–714. doi:10.1016/S0008-6223(01)00157-9.

[9] R.F.P.M. Moreira, H.J. José, A.E. Rodrigues, Modification of pore size in activated carbon by polymer deposition and its effects on molecular sieve selectivity, Carbon N. Y. 39 (2001) 2269–2276. doi:10.1016/S0008-6223(01)00046-X.

[10] G. Bello, R. García, R. Arriagada, A. Sepúlveda-Escribano, F. Rodríguez-Reinoso, Carbon molecular sieves from Eucalyptus globulus charcoal, Microporous Mesoporous Mater. 56 (2002) 139–145. doi:10.1016/S1387-1811(02)00465-1.

[11] D. Adinata, W.M.A.W. Daud, M.K. Aroua, Production of carbon molecular sieves from palm shell based activated carbon by pore sizes modification with benzene

for methane selective separation, Fuel Process. Technol. 88 (2007) 599–605. doi:10.1016/j.fuproc.2007.01.009.

[12] Z. Hu, E.F. Vansant, Carbon molecular sieves produced from walnut shell, Carbon N. Y. 33 (1995) 561–567. doi:10.1016/0008-6223(94)00141-L.

[13] J.M.V. Nabais, P.J.M. Carrott, M.M.L. Ribeiro Carrott, A.M. Padre-Eterno, J.A. Menéndez, A. Dominguez, A.L. Ortiz, New acrylic monolithic carbon molecular sieves for O_2/N_2 and CO_2/CH_4 separations, Carbon N. Y. 44 (2006) 1158–1165. doi:10.1016/j.carbon.2005.11.005.

[14] S. Villar-Rodil, R. Navarrete, R. Denoyel, A. Albiniak, J.I. Paredes, A. Martínez-Alonso, J.M.D. Tascón, Carbon molecular sieve cloths prepared by chemical vapour deposition of methane for separation of gas mixtures, Microporous Mesoporous Mater. 77 (2005) 109–118. doi:10.1016/j.micromeso.2004.08.017.

[15] A.R. Mohamed, M. Mohammadi, G.N. Darzi, Preparation of carbon molecular sieve from lignocellulosic biomass: a review, Renew. Sustain. Energy Rev. 14 (2010) 1591–1599. doi:10.1016/j.rser.2010.01.024.

[16] D.D. Do, Adsorption analysis: equilibria and kinetics, Queensland, 1998. doi:10.1142/p111.

[17] R.C. Bansal, M. Goyal, Activated carbon adsorption, CRC Press, Boca Raton, 2005.

[18] K. Yang, J. Peng, C. Srinivasakannan, L. Zhang, H. Xia, X. Duan, Preparation of high surface area activated carbon from coconut shells using microwave heating, Bioresour. Technol. 101 (2010) 6163–6169. doi:10.1016/j.biortech.2010.03.001.

[19] H. Marsh, B. Rand, The process of activation of carbons by gasification with CO_2-I. Gasification of pure polyfurfuryl alcohol carbon, Carbon N. Y. 9 (1971) 47–61. doi:10.1016/0008-6223(71)90143-6.

[20] R.A. Guedes de Carvalho, C.G. González Beça, M.N. Sampaio, O. Neves, M.C. Sol Pereira, A. Macedo, Use of pine bark for preparation of activated carbon and as a soil conditioner, Agric. Wastes. 9 (1984) 231–238. doi:10.1016/0141-4607(84)90082-9.

[21] K. Kutics, L. Kotsis, P. Szolcsányi, J. Argyelán, Production of activated carbon from walnut shell I. Adsorption investigations and study of application characteristics, Hungarian J. Ind. Chem. 12 (1984) 319–327.

[22] G.Q. Lu, D.D. Do, Physical structure and adsorption properties of coal washery reject, Fuel. 71 (1992) 809–813. doi:10.1016/0016-2361(92)90134-A.

[23] W.M.A.W. Daud, W.S.W. Ali, Comparison on pore development of activated carbon produced from palm shell and coconut shell, Bioresour. Technol. 93 (2004) 63–69. doi:10.1016/j.biortech.2003.09.015.

[24] W.N.W. Salleh, A.F. Ismail, Carbon membranes for gas separation processes: recent progress and future perspective, J. Membr. Sci. Res. 1 (2015) 2–15. doi:10.22079/JMSR.2015.12301.

[25] S.C. Rodrigues, R. Whitley, A. Mendes, Preparation and characterization of carbon molecular sieve membranes based on resorcinol–formaldehyde resin, J. Memb. Sci. 459 (2014) 207–216. doi:10.1016/j.memsci.2014.02.013.

[26] O. Ioannidou, A. Zabaniotou, Agricultural residues as precursors for activated carbon production-a review, Renew. Sustain. Energy Rev. 11 (2007) 1966–2005. doi:10.1016/j.rser.2006.03.013.

[27] M. Rungta, L. Xu, W.J. Koros, Carbon molecular sieve dense film membranes derived from Matrimid® for ethylene ethane separation, Carbon N. Y. 50 (2012) 1488–1502. doi:10.1016/j.carbon.2011.11.019.

[28] L. Xu, M. Rungta, M.K. Brayden, M. V Martinez, B.A. Stears, G.A. Barbay, W.J. Koros, Olefins-selective asymmetric carbon molecular sieve hollow fiber membranes for hybrid membrane-distillation processes for olefin/paraffin separations, J. Memb. Sci. 423–424 (2012) 314–323. doi:10.1016/j.memsci.2012.08.028.

[29] L. Xu, M. Rungta, J. Hessler, W. Qiu, M. Brayden, M. Martinez, G. Barbay, W.J. Koros, Physical aging in carbon molecular sieve membranes, Carbon N. Y. 80 (2014) 155–166. doi:10.1016/j.carbon.2014.08.051.

[30] M. Kiyono, P.J. Williams, W.J. Koros, Effect of pyrolysis atmosphere on separation performance of carbon molecular sieve membranes, J. Memb. Sci. 359 (2010) 2–10. doi:10.1016/j.memsci.2009.10.019.

[31] C.W. Jones, W.J. Koros, Carbon molecular sieve gas separation membranes-II. Regeneration following organic exposure, Carbon N. Y. 32 (1994) 1427–1432. doi:10.1016/0008-6223(94)90136-8.

[32] S. Lagorsse, F.D. Magalhães, A. Mendes, Aging study of carbon molecular sieve membranes, J. Memb. Sci. 310 (2008) 494–502. doi:10.1016/j.memsci.2007.11.025.

[33] I. Menendez, A.B. Fuertes, Aging of carbon membranes under different environments, Carbon N. Y. 39 (2001) 733–740. doi:10.1016/S0008-6223(00)00188-3.

[34] C.W. Jones, W.J. Koros, Carbon composite membranes: a solution to adverse humidity effects, Ind. Eng. Chem. Res. 34 (1995) 164–167. doi:10.1021/ie00040a015.

[35] M. Kiyono, Carbon molecular sieve membranes for natural gas separations, Georgia Institute of Technology, 2010.

[36] H.P. Boehm, Surface oxides on carbon and their analysis: a critical assessment, Carbon N. Y. 40 (2002) 145–149. doi:10.1016/S0008-6223(01)00165-8.

[37] C.W. Jones, W.J. Koros, Characterization of ultramicroporous carbon membranes with humidified feeds, Ind. Eng. Chem. Res. 34 (1995) 158–163. doi:10.1021/ie00040a014.

[38] L. Chen, D. Ma, X. Li, X. Bao, Silver catalysts supported over activated carbons for the selective oxidation of CO in excess hydrogen: effects of different treatments on the supports, Catal. Letters. 111 (2006) 133–139. doi:10.1007/s10562-006-0139-2.

[39] M.C. Campo, S. Lagorsse, F.D. Magalhães, A. Mendes, Comparative study between a CMS membrane and a CMS adsorbent: part II. Water vapor adsorption

and surface chemistry, J. Memb. Sci. 346 (2010) 26–36. doi:10.1016/j.memsci.2009.09.004.

[40] N.I. Bukhari, S. Kaur, S.H. Bai, Y.K. Hay, A. Bakar, A. Majeed, Y.B. Kang, M. Anderson, Statistical design of experiments on fabrication of starch nanoparticles – a case study for application of Response Surface Methods (RSM), Pharm. Int. (2009) 1–10.

[41] M.A. Bezerra, R.E. Santelli, E.P. Oliveira, L.S. Villar, L.A. Escaleira, Response surface methodology (RSM) as a tool for optimization in analytical chemistry, Talanta. 76 (2008) 965–977. doi:10.1016/j.talanta.2008.05.019.

[42] F. Relvas, R.D. Whitley, C. Silva, A. Mendes, Single-stage pressure swing adsorption for producing fuel cell grade hydrogen, Ind. Eng. Chem. Res. 57 (2018) 5106–5118. doi:10.1021/acs.iecr.7b05410.

[43] J.C. Santos, F.D. Magalhães, A. Mendes, Contamination of zeolites used in oxygen production by PSA: effects of water and carbon dioxide, Ind. Eng. Chem. Res. 47 (2008) 6197–6203. doi:10.1021/ie800024c.

[44] D. Ferreira, R. Magalhães, P. Taveira, A. Mendes, Effective adsorption equilibrium isotherms and breakthroughs of water vapor and carbon dioxide on different adsorbents, Ind. Eng. Chem. Res. 50 (2011) 10201–10210. doi:10.1021/ie2005302.

[45] M. Kočiřík, P. Struve, M. Bülow, Analytical solution of simultaneous mass and heat transfer in zeolite crystals under constant-volume/variable-pressure conditions, J. Chem. Soc. Faraday Trans. 1. 80 (1984) 2167–2174. doi:10.1039/F19848002167.

[46] M. Ottaway, Use of thermogravimetry for proximate analysis of coals and cokes, Fuel. 61 (1982) 713–716. doi:10.1016/0016-2361(82)90244-7.

[47] C. Nguyen, D.D. Do, Adsorption of supercritical gases in porous media: determination of micropore size distribution, J. Phys. Chem. B. 103 (1999) 6900–6908. doi:10.1021/jp9906536.

[48] H.C. Foley, Carbogenic molecular sieves: synthesis, properties and applications, Microporous Mater. 4 (1995) 407–433. doi:10.1016/0927-6513(95)00014-Z.

[49] Y. Kawahara, S. Otoyama, K. Yamamoto, W. Hiroyuki, Y. Shinahara, H. Hoshiro, N. Ishibashi, N. Iwashita, Direct carbonization of high-performance aromatic polymers and the production of activated carbon fibers, J. Text. Sci. Eng. 5 (2015) 1–5. doi:10.4172/2165-8064.1000219.

[50] J.P. Chen, High carbon yield phenolic resole, WO03/051948A1, 2003.

[51] P. Xu, X. Jing, High carbon yield thermoset resin based on phenolic resin, hyperbranched polyborate, and paraformaldehyde, Polym. Adv. Technol. 22 (2011) 2592–2595. doi:10.1002/pat.1806.

[52] S. Ouyang, S. Xu, N. Song, S. Jiao, Coconut shell-based carbon adsorbents for ventilation air methane enrichment, Fuel. 113 (2013) 420–425. doi:10.1016/j.fuel.2013.06.004.

[53] W. Li, J. Peng, L. Zhang, K. Yang, H. Xia, S. Zhang, S. Guo, Preparation of activated carbon from coconut shell chars in pilot-scale microwave heating equipment at 60 kW, Waste Manag. 29 (2009) 756–760. doi:10.1016/j.wasman.2008.03.004.

[54] K. Promdee, J. Chanvidhwatanakit, S. Satitkune, C. Boonmee, T. Kawichai, S. Jarernprasert, T. Vitidsant, Characterization of carbon materials and differences from activated carbon particle (ACP) and coal briquettes product (CBP) derived from coconut shell via rotary kiln, Renew. Sustain. Energy Rev. 75 (2017) 1175–1186. doi:10.1016/j.rser.2016.11.099.

[55] M.C. Campo, F.D. Magalhães, A. Mendes, Comparative study between a CMS membrane and a CMS adsorbent: part I-morphology, adsorption equilibrium and kinetics, J. Memb. Sci. 346 (2010) 15–25. doi:10.1016/j.memsci.2009.08.045.

[56] M.C. Campo, F.D. Magalhães, a. Mendes, Carbon molecular sieve membranes from cellophane paper, J. Memb. Sci. 350 (2010) 180–188. doi:10.1016/j.memsci.2009.12.026.

[57] S.-J. Park, W.-Y. Jung, Preparation and structural characterization of activated carbons based on polymeric resin., J. Colloid Interface Sci. 250 (2002) 196–200. doi:10.1006/jcis.2002.8337.

[58] T. Yamamoto, T. Sugimoto, T. Suzuki, S.R. Mukai, H. Tamon, Preparation and characterization of carbon cryogel microspheres, Carbon N. Y. 40 (2002) 1345–1351. doi:10.1016/S0008-6223(01)00294-9.

[59] Y.D. Chen, R.T. Yang, Preparation of carbon molecular sieve membrane and diffusion of binary mixtures in the membrane, Ind. Eng. Chem. Res. 33 (1994) 3146–3153. doi:10.1021/ie00036a033.

[60] F. Stoeckli, A. Slasli, D. Hugi-Cleary, A. Guillot, The characterization of microporosity in carbons with molecular sieve effects, Microporous Mesoporous Mater. 51 (2002) 197–202.

[61] D. Cazorla-Amorós, J. Alcañiz-Monge, M.A. de la Casa-Lillo, A. Linares-Solano, CO_2 as an adsorptive to characterize carbon molecular sieves and activated carbons, Langmuir. 14 (1998) 4589–4596. doi:10.1021/la980198p.

[62] S. Lagorsse, F.D. Magalhães, A. Mendes, Carbon molecular sieve membranes: sorption, kinetic and structural characterization, J. Memb. Sci. 241 (2004) 275–287. doi:10.1016/j.memsci.2004.04.038.

[63] C. Nguyen, D.D. Do, K. Haraya, K. Wang, The structural characterization of carbon molecular sieve membrane (CMSM) via gas adsorption, J. Memb. Sci. 220 (2003) 177–182. doi:10.1016/S0376-7388(03)00219-9.

[64] D. Cazorla-Amorós, J. Alcañiz-Monge, A. Linares-Solano, Characterization of activated carbon fibers by CO_2 adsorption, Langmuir. 12 (1996) 2820–2824. doi:10.1021/la960022s.

[65] M. Toral, A. Manríquez, R. Navarro-Cerrillo, D. Tersi, P. Naulin, Características de los estomas, densidad e índice estomático en secuoya (Sequoia sempervirens) y su variación en diferentes plantaciones de Chile, Bosque (Valdivia). 31 (2010) 157–164. doi:10.4067/S0717-92002010000200009.

[66] R.M. Silverstein, G.C. Bassler, T.C. Morrill, Spectrometric identification of organic compounds, in: Wiley, New York, 1981.

[67] H.F. Shurvell, Spectra-structure correlations in the mid- and far-infrared, Handb. Vib. Spectrosc. (2006). doi:10.1002/0470027320.s4101.

[68] R. Boopathy, S. Karthikeyan, A.B. Mandal, G. Sekaran, Adsorption of ammonium ion by coconut shell-activated carbon from aqueous solution: kinetic, isotherm, and thermodynamic studies, Environ. Sci. Pollut. Res. 20 (2013) 533–542. doi:10.1007/s11356-012-0911-3.

[69] A. Sartape, A. Mandhare, P. Salvi, D. Pawar, P. Raut, M. Anuse, S. Kolekar, Removal of Bi (III) with adsorption technique using coconut shell activated carbon, Chinese J. Chem. Eng. 20 (2012) 768–775. doi:10.1016/S1004-9541(11)60247-4.

[70] C. Rolence, R.L. Machunda, K.N. Njau, Water hardness removal by coconut shell activated carbon, Int. J. Sci. Technol. Soc. 2 (2014) 97–102. doi:10.11648/j.ijsts.20140205.11.

[71] F. Caturla, M. Molina-Sabio, F. Rodríguez-Reinoso, Preparation of activated carbon by chemical activation with $ZnCl_2$, Carbon N. Y. 29 (1991) 999–1007. doi:10.1016/0008-6223(91)90179-M.

[72] K. Kaneko, Molecular assembly formation in a solid nanospace, Colloids Surfaces A Physicochem. Eng. Asp. 109 (1996) 319–333. doi:10.1016/0927-7757(95)03464-1.

[73] T. Hasell, M. Miklitz, A. Stephenson, M.A. Little, S.Y. Chong, R. Clowes, L. Chen, D. Holden, G.A. Tribello, K.E. Jelfs, A.I. Cooper, Porous organic cages for sulfur hexafluoride separation, J. Am. Chem. Soc. 138 (2016) 1653–1659. doi:10.1021/jacs.5b11797.

[74] S. Sircar, Basic research needs for design of adsorptive gas separation processes, Ind. Eng. Chem. Res. 45 (2006) 5435–5448. doi:10.1021/ie051056a.

[75] N. Mehio, S. Dai, D. Jiang, Quantum mechanical basis for kinetic diameters of small gaseous molecules, J. Phys. Chem. A. 118 (2014) 1150–1154. doi:10.1021/jp412588f.

[76] A.I. Sarker, A. Aroonwilas, A. Veawab, Equilibrium and kinetic behaviour of CO2 adsorption onto zeolites, carbon molecular sieve and activated carbons, Energy Procedia. 114 (2017) 2450–2459. doi:10.1016/j.egypro.2017.03.1394.

[77] K. Knoblauch, Pressure-swing adsorption: geared for small volume users, Chem Eng. 87 (1978) 237–41.

[78] H.M. Yi, S. Weiruo, B. Maruti, W. Jinqu, G.W. Miller, Adsorption and diffusion of nitrogen, oxygen, argon, and methane in molecular sieve carbon at elevated pressures, Sep. Technol. 1 (1991) 90–98. doi:10.1016/0956-9618(91)80004-J.

[79] T.R. Gaffney, J.N. Armor, A.L. Cabrera, T.S. Farris, Modified carbon molecular sieves for gas separation, CA2049806A1, 1991.

[80] D.M. Ruthven, Diffusion of oxygen and nitrogen in carbon molecular sieve, Chem Eng Sci. 47 (1992) 4305–4308. doi:10.1016/0009-2509(92)85108-N.

[81] Y.D. Chen, R.T. Yang, P. Uawithya, Diffusion of oxygen, nitrogen and their mixtures in carbon molecular sieve, AlChE J. 40 (1994) 577–585.

[82] R.M. Rynders, M.B. Rao, S. Sircar, Isotope exchange technique for measurement of gas adsorption equilibria and kinetics, AlChE J. 43 (1997) 2456–2470. doi:10.1002/aic.690431009.

[83] Y.-S. Bae, J.-H. Moon, H. Ahn, C.-H. Lee, Effects of adsorbate properties on adsorption mechanism in a carbon molecular sieve, Korean J. Chem. Eng. 21 (2004) 712–720. doi:10.1007/BF02705510.

Chapter IV

Chapter 4 - Highly propylene equilibrium selective carbon molecular sieve adsorbent[1]

Graphical abstract

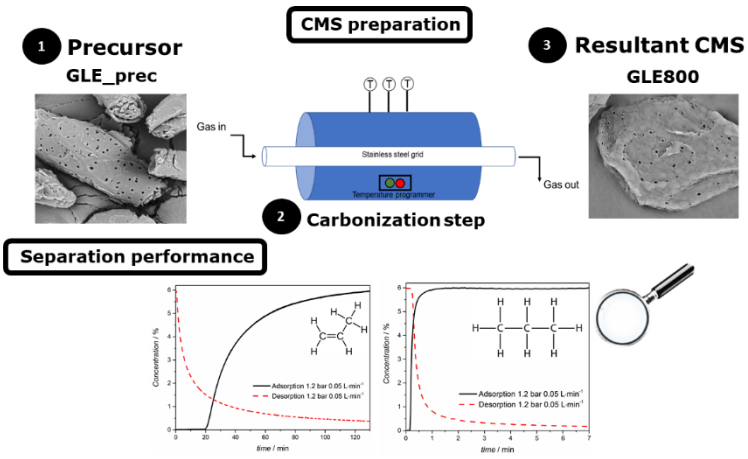

4.1. Abstract

Propylene-propane separation is one of the most difficult and relevant separations in the industrial field. Since this separation is high energy demanding the research for new processes and/or materials able to efficiently separate these components with lower energy consumption is encouraged. The present work reports a new carbon molecular sieve adsorbent highly equilibrium selective towards propylene – GLE800. This adsorbent was prepared in a single-step pyrolysis under nitrogen atmosphere. The pore size distribution, obtained based on the CO_2 adsorption equilibrium isotherm at 0 ºC, revealed a well-developed pore structure in the micropore range. Adsorption equilibrium isotherms were obtained at 25 ºC, 35 ºC and 45 ºC. GLE800 adsorbent displayed a very high propylene / propane adsorbed concentration ratio of *ca.* 140 at 1 bar and 25 ºC. The breakthrough curves, mono- and multicomponent, confirmed the high adsorption selectivity obtained from the adsorption equilibrium isotherms.

[1]M. Andrade, F. Relvas, A. Mendes, Highly propylene equilibrium selective carbon molecular sieve adsorbent, submitted, (2019).

4.2. Introduction

One of the most difficult and complex industrial separations is the olefin purification from an olefin / paraffin mixture, which is currently accomplished by cryogenic distillation [1,2]; this difficulty arises from the close boiling points of both components. A great research effort has been then put on for developing new processes to accomplish this energy demanding separation. Adsorption based separation processes are very attractive, but they require selective adsorbents. Several studies have been published reporting new adsorbents for the pressure swing adsorption (PSA) separation of olefins/paraffins [3–7].

Propylene is a very important raw material for the petrochemical industry where the primary use is for polypropylene production [8,9]. Polypropylene synthesis requires a propylene purity better than 99.5 wt. %, whereas other applications within the petrochemical industry require a propylene purity of 92 wt. % [9]. Olefins are currently produced by steam cracking [2,10]; naphtha and alkanes (such as propane and ethane) are heated up to 750-900 ^{o}C producing light olefins and paraffins with small amounts of hydrogen, methane, acetylene, benzene, toluene, xylene, among other small molecules [2,10]. Propylene is then obtained from this product stream by cryogenic distillation in a column with over *ca*. 150 theoretical distillation plates [11], where its purity depends mainly on the efficient removal of propane [9].

Most of the reported adsorbents are equilibrium and kinetic selective to propylene over propane; however, some adsorbents display an inverted selectivity [12–14] where probably the most referred is ZIF-7, a metal organic framework (MOF) adsorbent [13,15]. Zeolites, carbon molecular sieves (CMS) and MOFs adsorbents have been studied for propylene / propane separation and zeolites 4A and 13X are the most studied for using with pressure swing adsorption (PSA) technology [3,16–20]. Silva *et al.* [16] studied and compared the performance of zeolites 13X (CECA) and 4A (Rhöne-Poulene) for the propylene / propane separation. Zeolite 4A exhibited a propylene adsorption capacity of 1.9 mol·kg^{-1} and a propane a capacity lower than 0.2 mol·kg^{-1}, at *ca.* 1 bar and 30 ^{o}C. On the other hand, zeolite 13X displayed an adsorption capacity of 2.6 mol·kg^{-1} for propylene and a 2.0 mol·kg^{-1} adsorption capacity for propane, again at *ca.* 1 bar and 30 ^{o}C. Also, these authors calculated the propylene / propane selectivity over 13X and 4A zeolites using the Toth isotherm and respective fitting parameters

reporting a selectivity of *ca.* 10 for zeolite 13X and a much higher selectivity of 100-1000 for zeolite 4A, in the range of 30-150 ºC. Silva *et al.* [18] reported a 5-steps vacuum swing adsorption (VPSA) using a zeolite 4A obtaining a propylene purity of 96.9 %, a recovery of 25.7 % and a productivity of 1.03 $mol \cdot kg^{-1} \cdot h^{-1}$. Regarding 13X zeolite, Silva *et al*. [17] proposed a 5-steps VPSA and obtained a 98 % of purity, 19 % of recovery and a propylene productivity of 0.785 $mol \cdot kg^{-1} \cdot h^{-1}$. Also, Grande *et al.* [21] studied a Li-exchanged 13X zeolite that displayed a 2.5 $mol \cdot kg^{-1}$ propylene adsorption capacity and a 2.0 $mol \cdot kg^{-1}$ propane capacity, at 1 bar and 50 ºC. Campo *et al.* [3] proposed a 5-steps VPSA using a 13X zeolite and obtained a propylene purity of 99.54 %, a recovery of 85 % and a productivity of 1.46 $mol \cdot kg^{-1} \cdot h^{-1}$. Other types of zeolites have been also proposed and namely Padin *et al.* [22] prepared an $AlPO_4$-14 zeolite suitable to sterically exclude propane. These authors performed a four-step PSA simulation with co-current high-pressure purge and a 1:1 propylene / propane feed mixture. Despite the adsorbent displaying infinite adsorption selectivity, simulation results computed a propylene purity of only 99.38 %, a recovery of 52.59 % and a productivity of 0.91 $kg \cdot kg^{-1} \cdot h^{-1}$.

Few activated carbons and carbon molecular sieve adsorbents are reported in literature for the propylene / propane separation, mainly because the small separation selectivity displayed by these materials [23–26]. Grande *et al.* [5] studied the separation of propylene / propane by using a CMS Takeda 4A [27] (adsorption capacity of 1.2 $mol \cdot kg^{-1}$ for propylene and a 0.8 $mol \cdot kg^{-1}$ adsorption capacity for propane, at *ca.* 1 bar and 100 ºC) and a zeolite 4A in a 5-steps VPSA unit. The results clearly showed that the best separation performance results were obtained with the zeolite. Namely, VPSA experiments showed a purity of 83.6 % and 98.6 %, and a recovery of 84.4 % and 92.2 %, respectively for the CMS 4A and the zeolite 4A. More recently, Liu *et al.* [6] reported a carbon molecular sieve material resultant from the carbonization of a gel-type strong acid cation exchange resin with a propylene adsorption capacity of 45.5 $cm^3 \cdot g^{-1}$ and a propylene / propane adsorbed concentration ratio of 2.3, at 1 bar and 90 ºC. Also, this adsorbent exhibited a propylene / propane kinetic selectivity of 99 with a propylene diffusivity of 1×10^{-9} $cm^2 \cdot s^{-1}$, at 1 bar and 90 ºC. Liu *et al.* [28] reported also a polyvinylidene chloride copolymer (PVDC) derived carbon material – CMS-18 – with a separation factor 8.5 times higher than for MSC-4K CMS adsorbent (34 *vs*. 4) and

displaying a propylene adsorbed concentration 1.5 times higher (0.131 $g_{C3H6}{\cdot}g_{CMS}^{-1}$ vs. 0.088 $g_{C3H6}{\cdot}g_{CMS}^{-1}$) at 4.5 bar at 35 ºC.

Metal organic frameworks (MOFs) exhibit a great potential for propylene / propane separation: i) equilibrium-based [29–31], ii) kinetic-based [32,33] and iii) taking advantage of the so-called gate-opening mechanism [12,13]. Literature reports that open metal sites have an important role in the equilibrium separation of propylene / propane mixtures [30,31,34]. Lamia *et al.* [30] showed that open Cu^{2+} sites in CuBTC MOF adsorbent interact preferentially with propylene displaying a propylene adsorption capacity of *ca.* 7.9 $mol{\cdot}kg^{-1}$ and a propane capacity of *ca.* 6.2 $mol{\cdot}kg^{-1}$, at 1 bar and 50 ºC [30,31]. Bae *et al.* [31] studied a Co-MOF-74 adsorbent and a reported propylene and propane adsorption capacity of 7.3 $mol{\cdot}kg^{-1}$ and 5 $mol{\cdot}kg^{-1}$, respectively, at 1 bar and 25 ºC. Also, these authors predicted a propylene / propane IAST selectivity of *ca.* 45 for an equimolar mixture. Cadiau *et al*. [9] prepared a fluorinated MOF adsorbent – KAUST-7 – that showed full exclusion of propane molecules, at 1 bar and 25 ºC. KAUST-7 exhibited a propylene adsorption capacity of *ca.* 60 $mg_{C3H6}{\cdot}g_{CMS}^{-1}$ and a propane adsorption capacity close to zero. Lee *et al.* [33] prepared a BTO MOF that exhibited a propylene / propane kinetic selectivity of 12 and a propylene inverse of apparent diffusion time constant of $1.3{\times}10^{-4}\ s^{-1}$, at 0.3 bar and 25 ºC. Wang *et al.* [35] produced a MOF NJU-Bai8 for separating propylene / propane with an adsorbed concentration ratio of 43.2 (propylene adsorbed concentration of 60.5 $cm^3{\cdot}g^{-1}$ and propane adsorbed concentration of 1.4 $cm^3{\cdot}g^{-1}$) at 0.2 bar and 25 ºC; NJU-Bai8 adsorbent displayed a gate-opening mechanism.

Membrane-based processes emerged also as promising candidates to be energy-efficient for this separation [36–38]. Steel and Koros [39] showed that CMS membranes derived from 6-FDA-based polyimide precursor exhibited a *ca.* 1.1 propylene / propane adsorbed concentration ratio and a kinetic selectivity to propylene of *ca*. 90, resulting in an ideal permeselectivity of *ca*. 100 and a permeability of 196 barrer at 35 ºC. Teixeira *et al.* [40] prepared carbon-Al_2O_3-Ag composite molecular sieve membranes that displayed a propylene permeability of 69.3 barrer and a propylene / propane permeselectivity of 37.8, at 20 ºC. Afterwards, Teixeira *et al.* [41] reported boehmite-phenolic resin carbon molecular sieve membranes with a propylene permeability of 420 barrer and a propylene / propane permeselectivity of 18.1, at 20 ºC.

The present work reports a carbon molecular sieve adsorbent, derived from a low-cost cellulosic precursor material (GLE_prec), with very high propylene / propane adsorbed concentration ratio of *ca.* 140 and a propylene adsorption capacity of 2.5 mol·kg^{-1}, at 1 bar and 25 ^{o}C. The adsorbent was fully characterized concerning the adsorption equilibrium isotherms of propylene and propane, pore size distribution, experimental mono- and multicomponent breakthrough curves and mercury porosimetry. Also, techniques such as thermogravimetric analysis, Fourier transform infrared spectroscopy (FTIR) and scanning electron microscopy (SEM) were also performed.

4.3. Experimental

4.3.1. CMS preparation

Precursor materials

The precursor material, GLE_prec (cellulosic material), mean particle size of 58 μm, was supplied by Air Products and Chemicals, Inc. Carbon dioxide (99.9 % pure) and helium (99.999 % pure) were supplied by Linde. Propane and propylene were from Praxair (99.5 % pure).

Pyrolysis reaction

The carbonization step was carried in an alumina tube (954 cm^3 of volume) inside a tubular horizontal furnace (Termolab TH). For guaranteeing the temperature homogeneity along the tube, three thermocouples were placed into the furnace (Figure 4.1). Samples were carbonized under N_2 atmosphere with a flow rate of 170 mL·min^{-1}, a heating rate of 0.5 ^{o}C·min^{-1} and an end carbonization temperature of 800 ^{o}C with 120 minutes of soaking time – GLE800. After the carbonization process, samples were cooled naturally until to room temperature and then removed from the furnace.

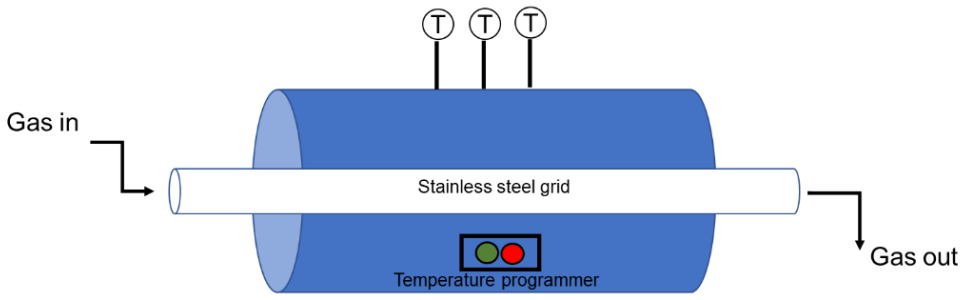

Figure 4.1. Scheme of the carbonization set up

4.3.2. Thermogravimetric analysis

Thermogravimetry analysis was performed in a Netzsch STA 449 F3 Jupiter thermogravimetric balance; a 11.1 mg of sample was used. The yield of fixed carbon was obtained from proximate analysis, where the protocol used is described elsewhere [42] and generally comprises the following steps:

- Temperature rise from room temperature up to 110 ºC at 25 ºC·min^{-1} under 30 mL·min^{-1} in nitrogen atmosphere; in this step all humidity should be released.
- Temperature rise from 110 ºC up to 950 ºC with a 9 min dwell under nitrogen atmosphere with the same flow as mentioned above; in this step it is expected a weight loss attributed to the release of volatile matter.
- The last step includes an 11 min dwell at 950 ºC under oxygen atmosphere where carbon is burned leaving only ashes if this is the case.

4.3.3. Scanning electron microscopy (SEM)

SEM analyses were performed in a Phenom XL Scanning Electron Microscope. The Phenom XL was equipped with two detector systems, one with a fully integrated EDS system for elemental analysis and another that corresponds to a Secondary Electron Detector (SED) that enables surface sensitive imaging. Before the analysis the samples were previously coated with Au/Pd using a Leica EM ACE2000 Sputter Coater equipment.

4.3.4. Particle size distribution

Particle size measurements were performed in a Counter LS 230 equipped with a Mie light scattering Polarization Intensity Differential Scattering (PIDS) and using samples previously dispersed in distilled water.

4.3.5. Mercury porosimetry

Mercury porosimetry analysis was performed in a Quantachrome PoreMaster 60 porosimeter. The equipment allows the measurement of pore size in the range of 3.5 nm to 200 μm. The sample was mechanically outgassed for removing any other species physically adsorbed on samples surface. Mercury pressure increased from 0.139 MPa to 412.8 MPa for entering in smaller pores.

4.3.6. Fourier transform infrared spectroscopy (FTIR)

The infrared spectra were recorded using a VERTEX 70 FTIR spectrometer (BRUKER) in transmittance mode with a high sensitivity DLaTGS detector at room temperature. Samples were measured in transmission mode, using pellets of potassium bromide (KBr) containing a sample mass fraction of 1 %. The spectra were recorded from 4000 cm^{-1} to 400 cm^{-1} with a resolution of 4 cm^{-1}.

4.3.7. Pore size distribution

Pore size distribution of the CMS adsorbent was determined based on adsorption equilibrium isotherms of carbon dioxide at 0 ºC. The methodology used, developed by Do *et al*. [43,44], consists on a structure-based model that describes the adsorption equilibria in heterogeneous carbons. This model requires molecular properties of the adsorbate and adsorbent, and the structural heterogeneity is accounted for with the distribution of micropore size [43]. The equations needed for obtaining the pore size distribution are described elsewhere [45].

Dubinin-Astakhov (DA) equation was used for obtaining the micropore volume (Eq. 4.1) [46]:

$$\frac{W}{W_0} = \exp\left[-\left(\frac{RT\ln(P_0/P)}{E_0}\right)^n\right] \tag{4.1}$$

where W is the micropore volume, P is the pressure, W_0 is the total micropore volume, E_0 is the characteristic energy of adsorption, P_0 is the vapor pressure of the free liquid, R is the gas constant, T is the absolute temperature and where n is an adjustable

parameter. Dubinin-Radushkevich (DR) equation appears as a particular case of DA equation when n = 2.

4.3.8. Adsorption capacity and gas uptake experiments

The adsorption equilibrium isotherms and uptake curves were obtained using the volumetric method. This method consists on determining the steady state pressure of the gas (adsorbate) after contacting with the adsorbent; knowing the pressure decrease and assuming ideal gas behaviour, the adsorbed gas concentration can be calculated [47,48]. Briefly, the volumetric setup, described elsewhere [48], consists of two tanks connected by an on/off valve; the first tank contains the probing gas and has a pressure sensor, while the second tank contains the adsorbent, which was previously evacuated. For measuring pressures until 2 bar a 2 bar Drück pressure sensor was used (reading error of 0.1 % of full scale) and for higher pressure values a 7 bar Drück was used (reading error of 0.1 % of full scale). For guaranteeing isothermal conditions, a thermostatic bath (Huber, K12-cc-NR) was employed. The evacuation of the tanks was obtained using an Alcatel 1004A rotary vacuum pump. Prior to adsorption experiments, samples were regenerated at 70 ^{o}C for 4 h under vacuum (< 0.002 bar).

Literature reports several models for fitting the adsorption isotherms data, although, the most used are Langmuir and Toth. Langmuir equation (Eq. 4.2) displays a simple mathematical formulation thermodynamically consistent. Toth equation (Eq. 4.3) is a semi-empirical model that is also thermodynamically consistent. However, Toth equation has one more parameter than Langmuir appearing as an alternative for overcoming fitting problems from the last one [49]. Toth equation is semi-empirical and takes into account the heterogeneity of the system. SIPS (Eq. 4.4) has also three parameters to account for the surface heterogeneities but is not applicable for low pressures since it does not converge to the Henry law [45,49]. The isosteric heat of adsorption (-ΔH) for a pure component can be determined by applying the Van't Hoff equation (Eq. 4.5) to Langmuir equation [49]. In this work, an enthalpic parameter was obtained by fitting the Toth model to experimental adsorption equilibrium values [3,49].

$$q = q_s \frac{bP}{1+bP} \tag{4.2}$$

$$q = q_s \frac{bP}{\left(1+\left(bP\right)^t\right)^{1/t}} \tag{4.3}$$

$$q = q_s \frac{\left(bP\right)^{1/n}}{1+\left(bP\right)^{1/n}} \tag{4.4}$$

$$b = b_\infty \exp\left(\frac{-\Delta H}{RT}\right) \tag{4.5}$$

where q represents the adsorbed solute concentration at pressure P, q_s is the adsorbed saturation capacity, b is the adsorption affinity constant, b_∞ is the pre-exponential factor of the affinity constant, and t and n are parameters used to characterize the heterogeneity of the system. Generally, t is less than the unity; for t = 1, Toth equation reduces to Langmuir equation [49].

The adsorbed concentration ratio (E_q) at 25 ºC was calculated according to the following equation:

$$E_q = \frac{q_{iC_3H_6}}{q_{iC_3H_8}} \tag{4.6}$$

where q_i is the adsorbed capacity from Toth equation at pressure i.

The inverse of the apparent diffusion time constant ($D \cdot r^{-2}$) is obtained fitting to the uptake curve an appropriate model. The model used was the so-called non-isothermal model for constant-volume and variable-pressure conditions [50]; the fractional uptake by this model is:

$$F = 1 - \sum_{n=1}^{\infty} \frac{9\left(1+\alpha^*\right)\left[\frac{Y_n}{-q_n^2}\right]^2 \exp\left(-q_n^2\tau\right)}{\frac{1}{\beta_n^*} + \frac{3}{2}\frac{\beta}{\beta_n^*}\left[q_n \cot q_n\left(\frac{Y_n}{q_n^2}\right)+1\right] + \frac{3}{2}\frac{\alpha^* B_n}{q_n^4 \beta_n^*}} \tag{4.7}$$

Where $B_n = Y_n\left[(q_n^2 - \alpha)\, q_n \cot q_n - 2\alpha\right] + q_n^2(q_n^2 - \alpha)$, $Y_n = q_n \cot q_n - 1$ and $\alpha^* = KV$. Considering that $V = V_s / V_g$, and, V_s and V_g being the volume of the sorbent particles and the volume of the gaseous phase, respectively.

4.3.9. Breakthrough Experiments

Breakthrough experiments were performed in an in-house built experimental setup described elsewhere [47], now equipped with a smaller volume column. The setup was placed inside a thermostatic chamber for guarantying isothermal conditions [47]. The gas is fed to the adsorption column through one or two thermal mass flow controllers (Bronkhorst High-tech, El Flow F-200CV-FAC-11V, 0–10 $mL_N \cdot min^{-1}$ and F-201C-FAC-21-V, 0–100 $mL_N \cdot min^{-1}$) and the operating pressure is controlled using a back-pressure regulator (Equilibar EB1LF2). A pressure transducer was placed at the inlet of the column and a thermocouple was inserted at column's half-height. The composition of the column's exiting stream was analysed by a mass spectrometer Pfeifer GSD 301 O2.

The adsorption bed characteristics and experimental conditions are indicated in Table 4.1.

Table 4.1. Breakthrough setup characteristics and experimental conditions.

	Mono/Multicomponent
Parameters	
Bed length	10.81 cm
Bed diameter	1.05 cm
Column volume	9.36 cm^3
Temperature	30 °C
C_3H_6 composition (balanced in He)	6 %
C_3H_8 composition (balanced in He)	6 %
Mixture (C_3H_6/C_3H_8/He)	3 % / 3 % / 94 %
Adsorption	
Flowrate	0.05 $L_N \cdot min^{-1}$
Pressure	1.2 bar
Desorption	
Flowrate	0.05 $L_N \cdot min^{-1}$
Pressure	1.2 bar

4.4. Results and discussion

4.4.1. Thermogravimetry analysis

Thermogravimetric analysis (TGA) was performed for assessing the thermal decomposition kinetics and stability of the precursor material [46]. The proximate analysis [42] of GLE_prec is displayed in Figure 4.2.

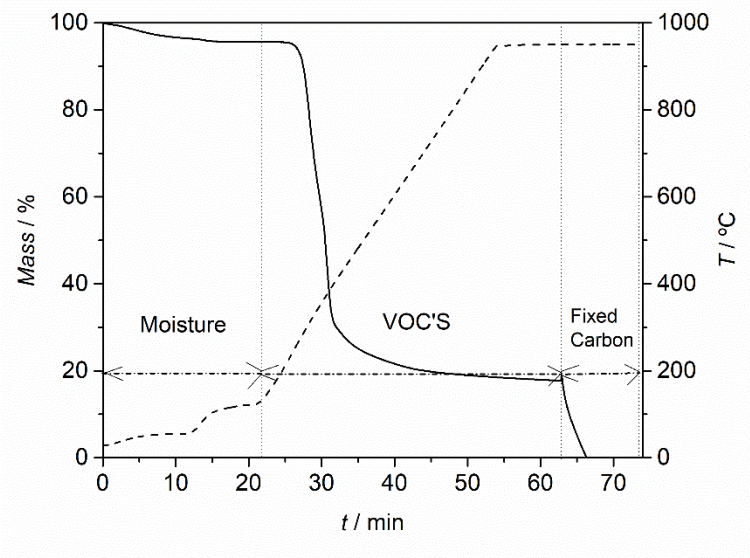

Figure 4.2. Proximate analysis of GLE_prec by thermogravimetric method. The removed species at different intervals are identified.

Table 4.2 shows the proximate analysis weight results for GLE_prec.

Table 4.2. Proximate analysis results by thermogravimetry of GLE_prec.

	GLE_prec
Humidity / %	4.5
Volatile matter / %	77.8
Fixed carbon / %	17.7
Ashes / %	0

The carbon structure of each CMS material depends mostly on the heat treatment employed [45,51]. Generally, higher end temperatures produce higher stability of the carbon structure and, also, as higher is the carbon yield more stable the materials are [45,51]. From Figure 4.2 and Table 4.2 it can be observed that GLE800 CMS adsorbent present a carbon yield of *ca.* 18 %; literature reports, for similar precursor materials, carbon yields of 18 % - 20 % [52–54].

4.4.2. Scanning electron microscopy (SEM)

Figure 4.3 shows SEM images of GLE800 CMS sample and of the respective precursor.

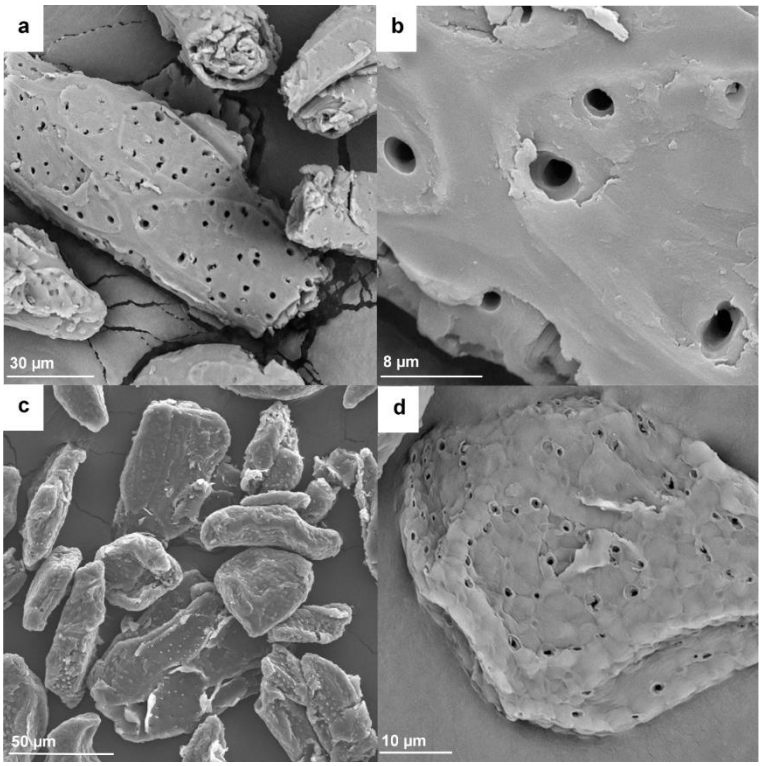

Figure 4.3. Surface SEM photographs with (a) 2000× (b) 9000× magnification for GLE800 precursor and (c) 1500× (d) 5000× magnification for the resultant CMS material.

Figure 4.3c) and Figure 4.3d) shows the presence of stomas, pores present on vegetal material and responsible for the transport of gases in and out of the intercellular spaces, *i.e.*, responsible for the cells respiration [55].

4.4.3. Mercury porosimetry

Figure 4.4 and Table 4.3 show the macropore size distribution of GLE800 CMS adsorbent and the physical properties obtained by mercury porosimetry as well as the skeleton density, obtained by helium picnometry using the volumetric method; in Table 4.3, ρ_{app}, ε_{total} and $\varepsilon_{< 3.5\ nm}$ represent the apparent density, total porosity and porosity for pores smaller than 3.5 nm, respectively.

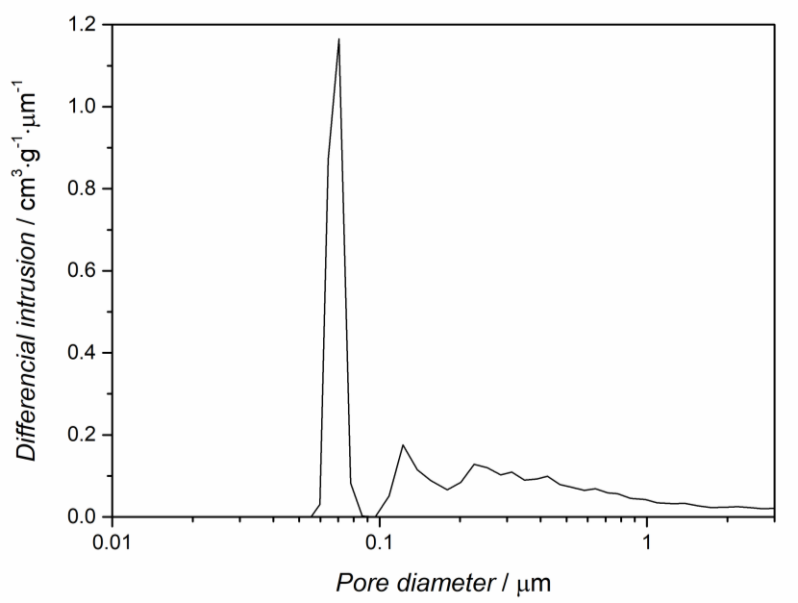

Figure 4.4. Macroporosity of GLE800 obtained from mercury porosimetry.

Table 4.3. Mercury porosimetry results for GLE800 CMS sample.

	GLE800
ρ_{He} / g·cm^{-3}	1.87
ρ_{app} / g·cm^{-3}	0.98
ε_{total} / %	47.49
$\varepsilon_{<3.5\ nm}$ / %	24.89

4.4.4. FTIR analysis

Figure 4.5 shows the FTIR spectra of the GLE_prec precursor and the resultant CMS material, which is the GLE800 sample.

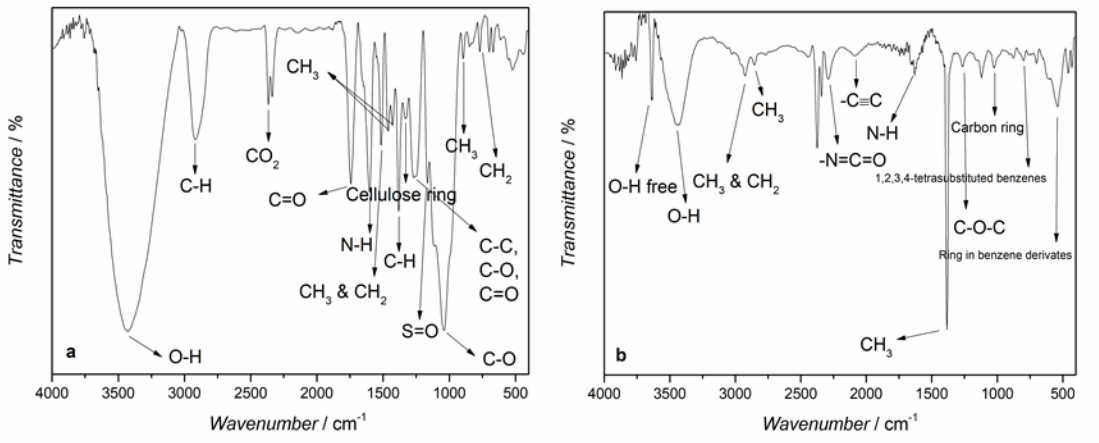

Figure 4.5. FTIR spectrum of GLE800 sample: a) precursor and b) adsorbent.

GLE_prec FTIR spectrum (Figure 4.5a)) shows the presence of a band at 3429 cm^{-1} attributed to O-H stretch vibrations of water molecules adsorbed on sample surface. At 2914 cm^{-1} is registered a C-H (alkenes) stretch vibration band and at 2366 cm^{-1} and 2336 cm^{-1} is observed the presence of twin bands ascribed to CO_2 present in the equipment beam. A stretching vibration band situated at 1740 cm^{-1} is attributed to C=O and at 1604 cm^{-1} is observed a band related to the presence of N-H primary amines. At 1520 cm^{-1} is observed a band ascribed to CH_3 and CH_2 sp^3 groups and at 1379 cm^{-1} a rocking vibration band appeared and is derived from C-H groups (alkanes or to methyl and phenolic alcohols). At 1330 cm^{-1} is observed a band ascribed to the vibration of the cellulose ring. A stretching vibration band attributed to C-C, C-O and C=O groups is situated at 1250 cm^{-1} and at 1167 cm^{-1} is present a S=O stretch vibration band. A C-O stretching vibration band ascribed to alkoxy groups appeared at 1035 $cm^{-1}$and a band attributed to CH_3 group was detected at 895 cm^{-1}. Finally, at 771 cm^{-1} appeared a band attributed to CH_2 groups [56–60].

The FTIR spectrum of GLE800 CMS (Fig. 4.5b)) shows the presence of a O-H free stretch vibration band at 3639 cm^{-1} present in alcohols and phenols and a O-H stretch vibration band attributed to adsorbed water molecules at 3437 cm^{-1}. The bands situated at 2925 cm^{-1} and 2856 cm^{-1} show a C-H antisymmetric and symmetric stretching vibrations attributed to -CH_3 and CH_2 in aliphatic compounds, respectively, and, the bands situated at 2372 cm^{-1} and 2340 cm^{-1} are related to CO_2 present in the beam. At 2297 cm^{-1} is observed a -N=C=O antisymmetric vibration band related to the presence of isocyanates and at 2083 cm^{-1} is registered a -C≡C stretch vibration band attributed to monosubstituted alkynes. A N-H deformation band related to primary amides is observed at 1653 cm^{-1}; at 1385 cm^{-1} a CH_3 symmetric deformation band present in aliphatic compounds is shown and at 1267 cm^{-1} a C-O-C antisymmetric stretch vibration band attributed to esters and lactones is observed. At 1024 cm^{-1} appears a ring breathing mode band attributed to carbon ring in cyclic compounds; at 806 cm^{-1} is registered a band of C-H out-of-plane ring deformations related to 1,2,3,4-tetrasubstituted benzenes; and at 547 cm^{-1} is observed an in-plane and out-plane ring deformation band attributed to the ring of benzene derivates [56–60].

Figure 4.5b) shows that carbonization process induced several changes in samples surface chemistry. Namely, some new functional groups such as C-O-C, -C≡C, O-H free, -N=C=O were formed and others such as C-O, C=O and C-H were removed. The intensity of O-H groups, ascribed to physisorbed water, decreases as expected after carbonization. Also, after carbonization, carbon ring groups replace the cellulose ring groups.

4.4.5. Pore size characterization

The CO_2 adsorption equilibrium isotherm at 0 ºC of GLE800 sample is plotted in Figure 4.6, where it can be observed a type I adsorption isotherm. The shape of the adsorption isotherm indicates that this sample has a significant fraction of micropores [45,61].

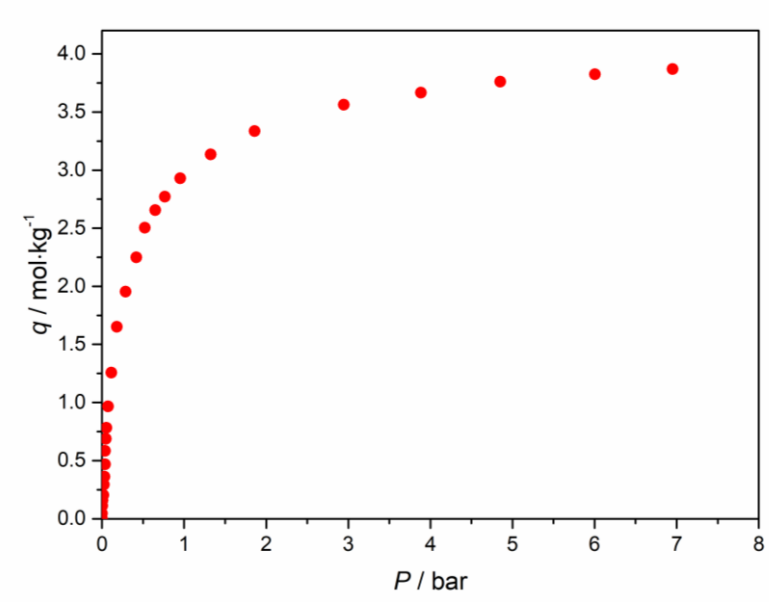

Figure 4.6. CO_2 adsorption equilibrium isotherm at 0 ºC for GLE800.

The micropore size distribution of GLE800 CMS sample was determined using a method developed by Do *et al.* [43,44,62]; the mathematical analysis used for deriving the micropore size distribution of the carbon sample is described elsewhere [63]. Figure 4.7 shows the micropore size distribution of GLE800 CMS sample, where ultramicropores (0.5 nm–0.7 nm range) and larger micropores (0.7 nm-1 nm range) are present. The distribution is similar to the micropore size distribution of other CMS adsorbents [64–66].

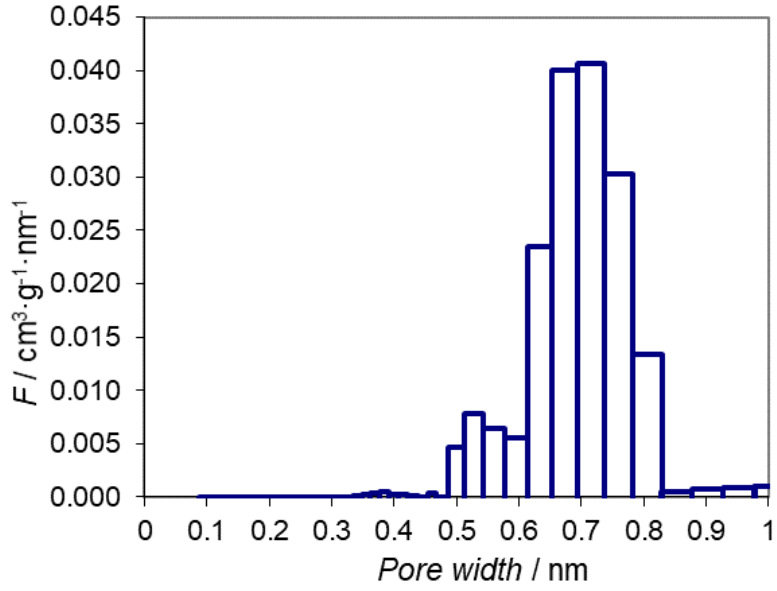

Figure 4.7. Micropore size distribution for GLE800 CMS adsorbent.

The DA plot of the experimental results is plotted in Figure 4.8; the fitting parameters are given in Table 4.4. The empiric correlation developed by Stoeckli is normally used to estimate the mean pore width. However, as DR equation (n = 2) is not applied for this study, Stoeckli equation cannot be also used. Considering this, the mean pore width was obtained by a weighted average [46].

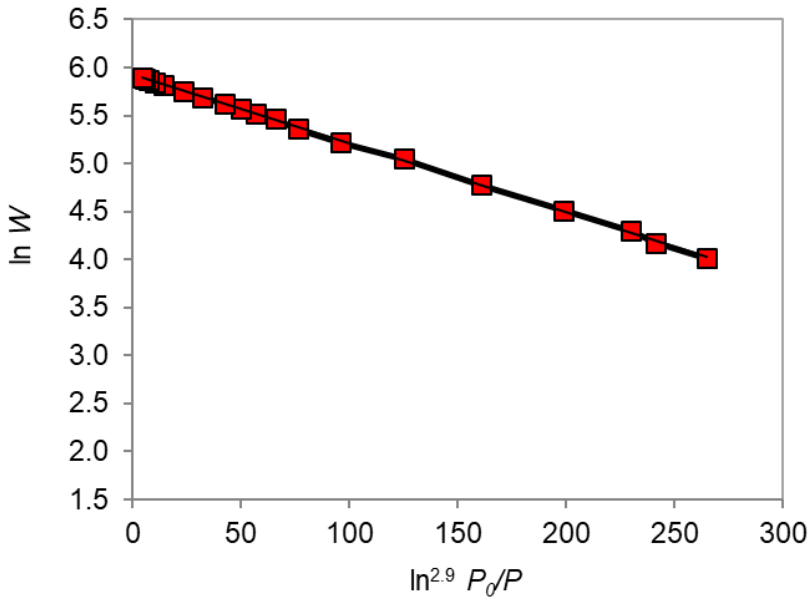

Figure 4.8. CO_2 characteristic curve of GLE800 at 0 ºC – dots correspond to experimental values and solid line to DA fitting.

Table 4.4. Obtained structural parameters by DA equation fitting for GLE800 CMS sample.

Parameter	GLE800
n	2.9
W_0 / $cm^3 \cdot kg^{-1}$	153.02
E_0 / $kJ \cdot mol^{-1}$	16.10
l / nm	0.68

From Table 4.4, the GLE800 micropore volume is *ca.* 153 $cm^3 \cdot kg^{-1}$, which is in agreement with values reported for similar cellulosic carbon materials [67–69]. Also, GLE800 mean pore width is in the range of typical carbon molecular sieve materials [61,70,71]. Not less important, the obtained characteristic energy for GLE800 is situated in an expectable range of 14-20 $kJ \cdot mol^{-1}$ [64,72,73]. The characteristic energy is an important parameter since it gives information about the intensity of the process of adsorption [45].

4.4.6. Adsorption capacity and kinetics

The GLE800 adsorption equilibrium isotherms for propylene and propane were determined at 25 ºC, 35 ºC and 45 ºC.

Adsorption equilibrium isotherms for propylene at 25 ºC, 35 ºC and 45 ºC and for propane at 25 ºC on GLE800 are plotted in Figure 4.9. The obtained experimental adsorption equilibrium isotherms were fitted using the Toth isotherm and the obtained model parameters are shown in Table 4.5.

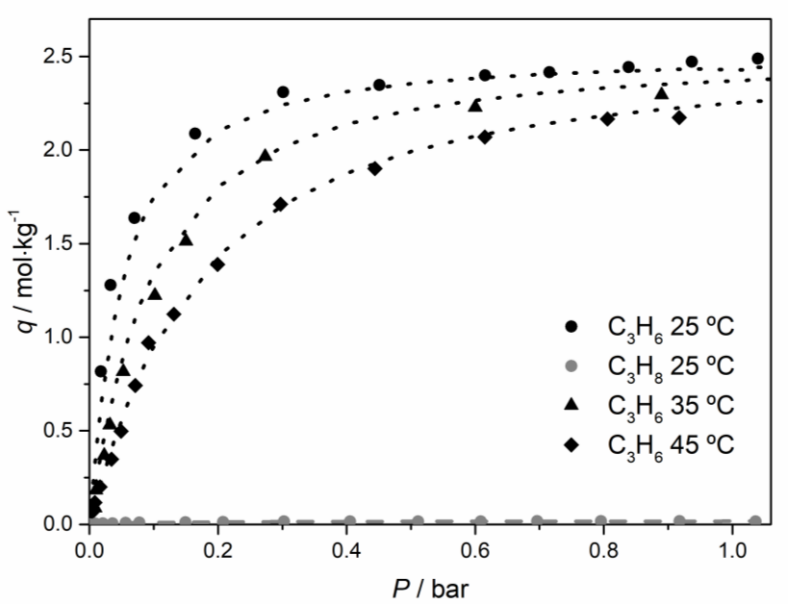

Figure 4.9. Propylene adsorption equilibrium isotherms on GLE800 sample at 25 ºC, 35 ºC and 45 ºC. Propane adsorption equilibrium isotherm at 25 ºC is also plotted. The dashed lines correspond to Toth isotherm fitting.

Table 4.5. Toth equation parameters for C_3H_6 and C_3H_8 on GLE800.

	q_s / mol·kg^{-1}	b^{∞} / bar^{-1}	b / bar^{-1}	t	-ΔH / kJ·mol^{-1}
C_3H_6	2.51	1.4×10^{-7}	-	1.20	46.1
C_3H_8	0.02	n.d.[1]	9.90	0.99	n.d.

[1]not determined

From Figure 4.9 it can be observed that propylene adsorption capacity is remarkably higher than propane for this type of material. The equilibrium adsorption of propylene and propane at 25 ºC and *ca.* 1 bar are 2.489 mol·kg^{-1} and 0.017 mol·kg^{-1}, respectively.

Figure 4.10 shows the adsorbed concentration ratio of propylene over propane at 25 ºC. As it can be observed, the adsorbed concentration ratio decreases from *ca*. 200 at 0.1 bar until *ca.* 140 at 1 bar, which are very high values. This decrease was assigned to adsorption saturation of propylene while propane adsorption concentration still increases with the pressure.

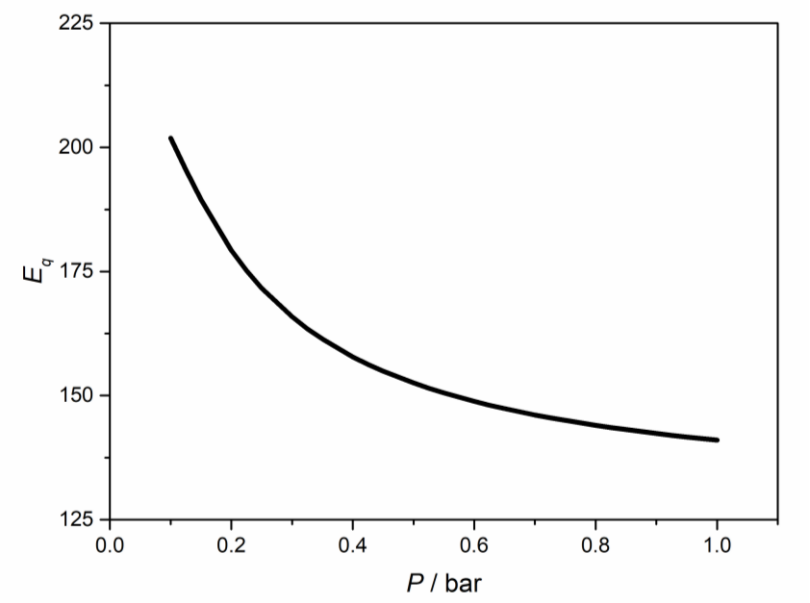

Figure 4.10. Adsorbed concentration ratio of C_3H_6 / C_3H_8 at 25 ºC. Curve was obtained dividing the Toth equation for each component.

Uptake experiments were performed for obtaining the adsorption rate as a function of the temperature and pressure of propylene. Table 4.6 shows the inverse of the apparent diffusion time constant for propylene at *ca.* 1 bar and 25 ºC. The adsorption kinetic of propane was not possible to obtain since it hardly adsorbs on GLE800.

Table 4.6. GLE800 adsorption kinetic parameters for C_3H_6.

Sample	P / bar	T / ºC	$D \cdot r^{-2}$ / s^{-1}
GLE800	1	25	4.43×10^{-4}

Since GLE800 displays a high adsorption capacity to propylene and very low for propane, there is then a synergetic effect between the kinetic and adsorption equilibrium selectivities to propylene.

Table 4.7 summarizes some of the most propylene selective adsorbents. This work displays one of the highest adsorbed concentration ratio and a high propylene adsorption capacity.

Table 4.7. Propylene selective adsorbents.

	Material	Adsorbed concentration ratio	Amount adsorbed (mol·kg^{-1})		VPSA unit integration	Ref.
Zeolites	13X	1.3 at 1 bar 30 ºC	C_3H_6	C_3H_8	*Pur*=98 %; *Rec*=19 % *Prod*=0.785 mol·kg^{-1}·h^{-1}	[16,17]
			2.6	2.0		
	4A	> 9.5 at 1 bar 30 ºC	1.9	< 0.2	*Pur*=97 %; *Rec*=26 % *Prod*=1.03 mol·kg^{-1}·h^{-1}	[16,18]
	Li-exch. 13X	1.3 at 1 bar 50 ºC	2.5	2.0	-	[21]
	13X	1.1 at 1 bar 50 ºC	3.47	3.08	*Pur*=99.54 % *Rec*=85 % *Prod*=1.46 mol·kg^{-1}·h^{-1}	[3]
	$AlPO_4$-14	12 at 1 bar 120 ºC	0.7	0.06	*Pur*=99.38 % *Rec*=52.59 % *Prod*=0.91 mol·kg^{-1}·h^{-1}	[22]
MOFs	CuBTC	1.3 at 1 bar 50 ºC	7.9	6.3	-	[30]
	Co-MOF-74	45 (IAST 1:1 mix.) at 1 bar 25 ºC	7.3	5	-	[31]
	KAUST-7	Inf. at 1 bar 25 ºC	1.4	Excluded	-	[9]
	NJU-Bai8	43.2 at 0.2 bar 25 ºC	2.7	0.06	-	[35]
AC / CMS	Takeda 4A	1.5 at 1 bar 100 ºC	1.2	0.8	*Pur*=83 %; *Rec*=84 %	[27]
	Dowex™ 50wX8 H_2 CMS	2.3 at 1 bar 90 ºC	2.03	0.88	-	[6]
	CMS-18	1.9 at 4.5 bar 35 ºC	3.11	1.59	-	[28]
	GLE800	140 at 1 bar 25 ºC	2.49	0.017	-	This work

4.4.7. Mono/multicomponent breakthrough experiments

A set of adsorption/desorption breakthrough experiments were carried out using a packed column with 5.56 g of fresh adsorbent, initially conditioned with helium to a given temperature and pressure. At instant t = 0 s, the feed composition was changed according to Table 4.1 and the experiment was allowed to run until equilibrium was reached; at the end of the adsorption breakthrough experiment, the column was fed again with helium and the desorption breakthrough curve was recorded.

Monocomponet breakthroughs for propylene and propane are presented in Figure 4.11 and confirm the large propylene / propane adsorbed concentration ratio. Since adsorption is exothermal, a sharp temperature increase is observed in the temperature history (Figure 4.12) [74]. Afterwards, temperature decreases until the original selected value. By contrast, propane temperature profile shows no noticeable changes indicating that the adsorption of this component is very small.

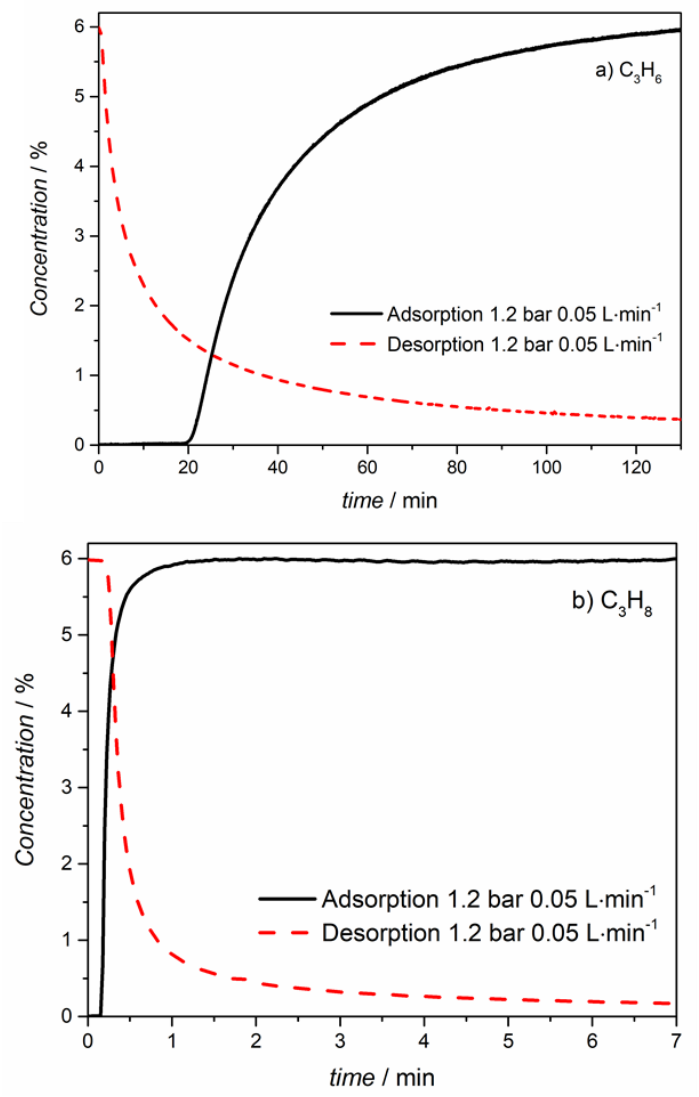

Figure 4.11. Experimental monocomponent adsorption and desorption breakthroughs of a) C_3H_6 and b) C_3H_8. Solid lines correspond to adsorption data and dashed lines to the desorption data.

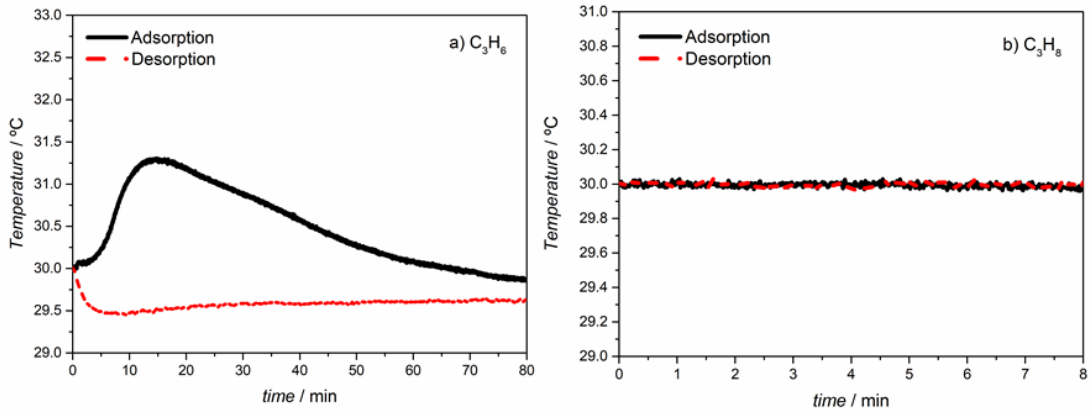

Figure 4.12. Experimental temperature profiles for monocomponent breakthroughs for a) C_3H_6 and b) C_3H_8. The feed flowrate was 0.05 $L_N min^{-1}$; 1.2 bar and 30 ºC. Solid lines represent adsorption, dashed lines the desorption.

Figure 4.13 shows the multicomponent breakthrough for a feed flowrate of 0.05 $L_N \cdot min^{-1}$ (composition: 3 % of propane and 3 % of propylene balanced with helium), 1.2 bar and 30 ºC, as well as the respective temperature profiles.

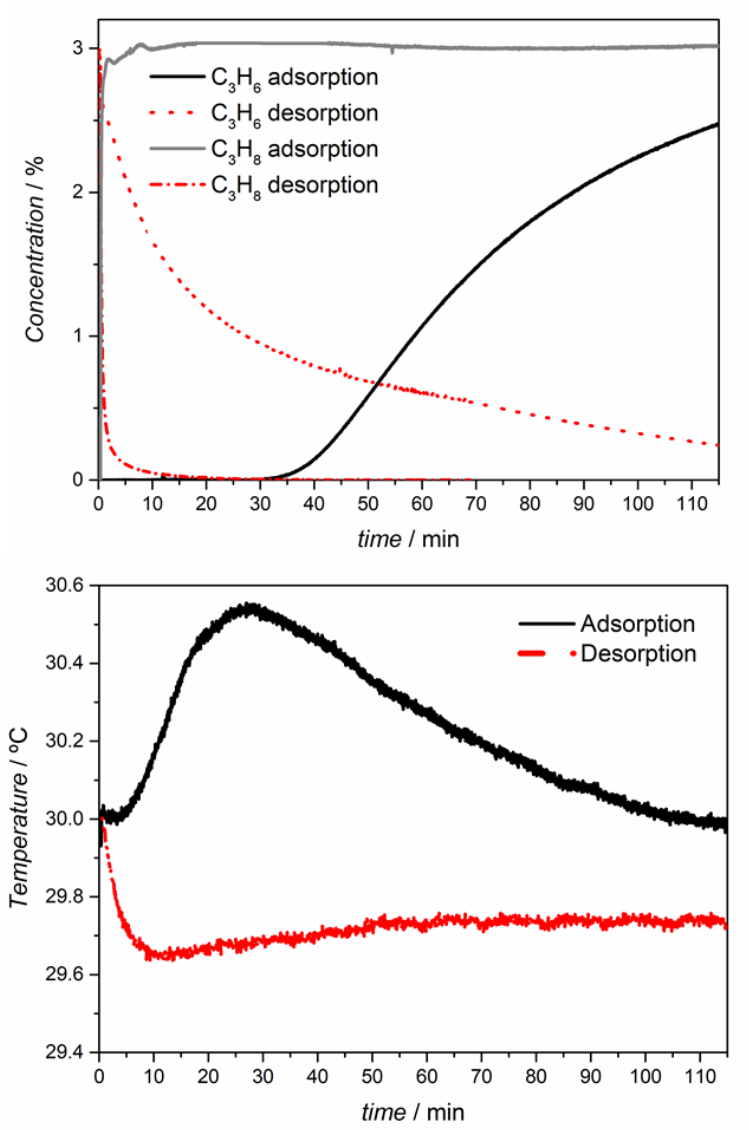

Figure 4.13. Multicomponent breakthrough for a feed flowrate of 0.05 $L_N \cdot min^{-1}$ (composition: 3 % of propane and 3 % of propylene balanced with helium), 1.2 bar and 30 ºC, as well as the respective temperature profiles.

As expected, propane is the first component to break followed by propylene. The obtained results indicate once again that GLE800 adsorption is strongly selective towards the olefin component. Also, temperature history profile just changed when propylene adsorption occurs.

4.5. Conclusions

The present work describes the preparation of a carbon molecular sieve adsorbent, GLE800, highly selective towards propylene. The CMS material was prepared from a single carbonization step at 800 ^{o}C and 120 minutes of soaking time of a low-cost cellulosic material under nitrogen atmosphere. GLE800 adsorbent displays a well-developed microporous structure with a high porosity. The micropore size distribution of this material ranges from 0.5 – 1 nm.

GLE800 showed a propylene / propane adsorbed concentration ratio of *ca.* 140 at 1 bar and 25 ^{o}C. Mono- and multicomponent breakthrough experiments confirm the great propylene selectivity of the prepared adsorbent. This carbon molecular sieve adsorbent is relatively cheap but displays a very high separation performance for propylene / propane mixtures making it potentially attractive for accomplishing this separation using a PSA-based process.

4.6. Acknowledgments

This work was financially supported by: project UID/EQU/00511/2019 - Laboratory for Process Engineering, Environment, Biotechnology and Energy – LEPABE funded by national funds through FCT/MCTES (PIDDAC); Project “LEPABE-2-ECO-INNOVATION” – NORTE-01-0145-FEDER-000005, funded by North Portugal Regional Operational Programme (NORTE 2020), under PORTUGAL 2020 Partnership Agreement, through the European Regional Development Fund (ERDF).

F.R. is grateful to NORTE-08-5369-FSE-000028 supported by North Portugal Regional Operational Programme (NORTE 2020), under the Portugal 2020 Partnership Agreement and the European Social Fund (ESF), for his PhD fellow.

The authors are thankful to Air Products and Chemicals, Inc. for generously providing the precursor material.

4.7. References

[1] M. Kanezashi, S. Miyauchi, S. Hayakawa, H. Nagasawa, T. Yoshioka, T. Tsuru, Propylene/propane permeation properties of metal-doped organosilica membranes with controlled network sizes and adsorptive properties, J. Japan Pet. Inst. 59 (2016) 140–148. doi:10.1627/jpi.59.140.

[2] Y. Wang, S.B. Peh, D. Zhao, Alternatives to cryogenic distillation: advanced porous materials in adsorptive light olefin/paraffin separations, Nano Micro Small. 15 (2019) 1–38. doi:10.1002/smll.201900058.

[3] M.C. Campo, A.M. Ribeiro, A. Ferreira, J.C. Santos, C. Lutz, J.M. Loureiro, A.E. Rodrigues, New 13X zeolite for propylene/propane separation by vacuum swing adsorption, Sep. Purif. Technol. 103 (2013) 60–70. doi:10.1016/j.seppur.2012.10.009.

[4] C.A. Grande, Advances in pressure swing adsorption for gas separation, ISRN Chem. Eng. 2012 (2012) 1–13. doi:10.5402/2012/982934.

[5] C.A. Grande, Propane/propylene separation by adsorption processes, University of Porto, 2004.

[6] J. Liu, Y. Liu, D.K. Talay, E. Calverley, M. Brayden, M. Martinez, A new carbon molecular sieve for propylene/propane separations, Carbon N. Y. 85 (2015) 201–211. doi:10.1016/j.carbon.2014.12.089.

[7] J. Liu, M. Brayden, E. Calverley, S.R. Lakso, Y. Liu, M.V. Martinez, Novel carbon molecular sieve and pellet compositions useful for C_2-C_3 alkane/alkene separations, WO2014/160624A1, 2014.

[8] A. Chauvel, G. Lefebvre, Petrochemical Processes, Éditions-T, Paris, 1989.

[9] A. Cadiau, K. Adil, P.M. Bhatt, Y. Belmabkhout, M. Eddaoudi, A metal-organic framework – based splitter for separating propylene from propane, Science (80-.). 353 (2016) 137–140. doi:10.1126/science.aaf6323.

[10] I. Amghizar, L.A. Vandewalle, K.M. Van Geem, G.B. Marin, New trends in olefin production, Engineering. 3 (2017) 171–178. doi:10.1016/J.ENG.2017.02.006.

[11] N. Cougard, A. Baudot, V. Coupard, Process for separating propane and propylene using a distillation column and a membrane separation column, US8475567B2, 2013.

[12] E. Andres-Garcia, L. Oar-Arteta, J. Gascon, F. Kapteijn, ZIF-67 as silver-bullet in adsorptive propane/propylene separation, Chem. Eng. J. 360 (2019) 10–14. doi:10.1016/j.cej.2018.11.118.

[13] J. Van Den Bergh, C. Gücüyener, E.A. Pidko, E.J.M. Hensen, J. Gascon, F. Kapteijn, Understanding the anomalous alkane selectivity of ZIF-7 in the separation of light alkane/alkene mixtures, Chem. Eur. J. 17 (2011) 8832–8840. doi:10.1002/chem.201100958.

[14] C. Serre, A. Vimont, P. Llewellyn, J.-S. Chang, P. Horcajada, G. Ferey, M. Daturi, Y.-K. Hwang, Reducible porous crystalline hybrid solid for the separation of mixtures of molecules having different degrees and/or a different number of unsaturations, WO 2010/000975 A1, 2010.

[15] C. Gücüyener, J. van den Bergh, J. Gascon, F. Kapteijn, Ethane/ethene separation turned on its head: selective ethane adsorption on the metal-organic framework ZIF-7 through a gate-opening mechanism, J. Am. Chem. Soc. 132 (2010) 17704–17706. doi:10.1021/ja1089765.

[16] F.A. Da Silva, A.E. Rodrigues, Adsorption equilibria and kinetics for propylene and propane over 13X and 4A zeolite pellets, Ind. Eng. Chem. Res. 38 (1999) 2051–2057. doi:10.1021/ie980640z.

[17] F.A. Da Silva, A.E. Rodrigues, Propylene/propane separation by vacuum swing adsorption using 13X zeolite, AlChE J. 47 (2001) 341–357. doi:10.1002/aic.690470212.

[18] F.A. Da Silva, A.E. Rodrigues, Vacuum swing adsorption for propylene/propane separation with 4A zeolite, Ind. Eng. Chem. Res. 40 (2001) 5758–5774. doi:10.1021/ie0008732.

[19] S. Divekar, A. Nanoti, S. Dasgupta, R. Chauhan, P. Gupta, M.O. Garg, S.P. Singh, I.M. Mishra, Adsorption equilibria of propylene and propane on zeolites and

prediction of their binary adsorption with the ideal adsorbed solution theory, J. Chem. Eng. Data. 61 (2016) 2629–2637. doi:10.1021/acs.jced.6b00294.

[20] C.A. Grande, A.E. Rodrigues, Adsorption kinetics of propane and propylene in zeolite 4A, Chem. Eng. Res. Des. 82 (2004) 1604–1612. doi:10.1205/cerd.82.12.1604.58029.

[21] C.A. Grande, J. Gascon, F. Kapteijn, A.E. Rodrigues, Propane/propylene separation with Li-exchanged zeolite 13X, Chem. Eng. J. 160 (2010) 207–214. doi:10.1016/j.cej.2010.03.044.

[22] J. Padin, S.U. Rege, R.T. Yang, L.S. Cheng, Molecular sieve sorbents for kinetic separation of propane/propylene, Chem. Eng. Sci. 55 (2000) 4525–4535. doi:10.1016/S0009-2509(00)00099-3.

[23] M.-G. Olivier, J. Bougard, R. Jadot, Adsorption of propane, propylene and propadiene on activated carbon, Appl. Therm. Eng. 16 (1996) 383–387. doi:10.1016/1359-4311(95)00019-4.

[24] M. Mofarahi, M. Sadrameli, J. Towfighi, Characterization of activated carbon by propane and propylene adsorption, J. Chem. Eng. Data. 48 (2003) 1256–1261. doi:10.1021/je0340553.

[25] H. Järvelin, J.R. Fair, Adsorptive separation of propylene-propane mixtures, Ind. Eng. Chem. Res. 32 (1993) 2201–2207. doi:0888-5885/93/2632-2201.

[26] K. Chihara, M. Suzuki, K. Kawazoe, Adsorption rate on molecular sieving carbon by chromatography, AlChE J. 24 (1978) 237–246. doi:10.1002/aic.690240212.

[27] C.A. Grande, S. Cavenati, F.A. Da Silva, A.E. Rodrigues, Carbon molecular sieves for hydrocarbon separations by adsorption, Ind. Eng. Chem. Res. 44 (2005) 7218–7227. doi:10.1021/ie050376r.

[28] J. Liu, E.M. Calverley, M.H. Mcadon, J.M. Goss, Y. Liu, K.C. Andrews, T.D. Wolford, D.E. Beyer, C.S. Han, D.A. Anaya, R.P. Golombeski, C.F. Broomall, S. Sprague, H. Clements, K.F. Mabe, New carbon molecular sieves for propylene/propane separation with high working capacity and separation factor, Carbon N. Y. 123

(2017) 273–282. doi:10.1016/j.carbon.2017.07.068.

[29] J.W. Yoon, I.T. Jang, K. Lee, Y.K. Hwang, J. Chang, Adsorptive separation of propylene and propane on a porous metal-organic framework, copper trimesate, Bull. Korean Chem. Soc. 31 (2010) 220–223. doi:10.5012/bkcs.2010.31.01.220.

[30] N. Lamia, M. Jorge, M.A. Granato, F.A. Almeida Paz, H. Chevreau, A.E. Rodrigues, Adsorption of propane, propylene and isobutane on a metal-organic framework: molecular simulation and experiment, Chem. Eng. Sci. 64 (2009) 3246–3259. doi:10.1016/j.ces.2009.04.010.

[31] Y.S. Bae, C.Y. Lee, K.C. Kim, O.K. Farha, P. Nickias, J.T. Hupp, S.T. Nguyen, R.Q. Snurr, High propene/propane selectivity in isostructural metal-organic frameworks with high densities of open metal sites, Angew. Chemie - Int. Ed. 51 (2012) 1857–1860. doi:10.1002/anie.201107534.

[32] K. Li, D.H. Olson, J. Seidel, T.J. Emge, H. Gong, H. Zeng, J. Li, Zeolitic imidazolate frameworks for kinetic separation of propane and propene, J. Am. Chem. Soc. 131 (2009) 10368–10369. doi:10.1021/ja9039983.

[33] C.Y. Lee, Y. Bae, N.C. Jeong, O.K. Farha, A.A. Sarjeant, C.L. Stern, P. Nickias, R.Q. Snurr, J.T. Hupp, S.T. Nguyen, Kinetic separation of propene and propane in metal-organic frameworks: controlling diffusion rates in plate-shaped crystals via tuning of pore apertures and crystallite aspect ratios, J. Am. Chem. Soc. 153 (2011) 5228–5231. doi:10.1021/ja200553m.

[34] J.W. Yoon, Y.K. Seo, Y.K. Hwang, J.S. Chang, H. Leclerc, S. Wuttke, P. Bazin, A. Vimont, M. Daturi, E. Bloch, P.L. Llewellyn, C. Serre, P. Horcajada, J.M. Grenèche, A.E. Rodrigues, G. Férey, Controlled reducibility of a metal-organic framework with coordinatively unsaturated sites for preferential gas sorption, Angew. Chemie - Int. Ed. 49 (2010) 5949–5952. doi:10.1002/anie.201001230.

[35] X. Wang, R. Krishna, L. Li, B. Wang, T. He, Y. Zhang, J.-R. Li, J. Li, Guest-dependent pressure induced gate-opening effect enables effective separation of propene and propane in a flexible MOF, Chem. Eng. J. 346 (2018) 489–496. doi:10.1016/j.cej.2018.03.163.

[36] X. Ma, J. Lin, X. Wei, J. Kniep, Ultrathin carbon molecular sieve membrane for propylene/propane separation, AlChE J. 62 (2016) 491–499. doi:10.1002/aic.15005.

[37] X. Ma, B.K. Lin, X. Wei, J. Kniep, Y.S. Lin, Gamma-alumina supported carbon molecular sieve membrane for propylene/propane eparation, Ind. Eng. Chem. Res. 52 (2013) 4297–4305. doi:10.1021/ie303188c.

[38] R.J. Swaidan, X. Ma, I. Pinnau, Spirobisindane-based polyimide as efficient precursor of thermally-rearranged and carbon molecular sieve membranes for enhanced propylene/propane separation, J. Memb. Sci. 520 (2016) 983–989. doi:10.1016/j.memsci.2016.08.057.

[39] K.M. Steel, W.J. Koros, An investigation of the effects of pyrolysis parameters on gas separation properties of carbon materials, Carbon N. Y. 43 (2005) 1843–1856. doi:10.1016/j.carbon.2005.02.028.

[40] M. Teixeira, M. Campo, D.A. Tanaka, M.A. Tanco, C. Magen, A. Mendes, Carbon – Al_2O_3 – Ag composite molecular sieve membranes for gas separation, Chem. Eng. Res. Des. 90 (2012) 2338–2345. doi:10.1016/j.cherd.2012.05.016.

[41] M. Teixeira, S.C. Rodrigues, M. Campo, D.A.P. Tanaka, M.A.L. Tanco, L.M. Madeira, J.M. Sousa, A. Mendes, Boehmite-phenolic resin carbon molecular sieve membranes — permeation and adsorption studies, Chem. Eng. Res. Des. (2014) 1–13. doi:10.1016/j.cherd.2013.12.028.

[42] M. Ottaway, Use of thermogravimetry for proximate analysis of coals and cokes, Fuel. 61 (1982) 713–716. doi:10.1016/0016-2361(82)90244-7.

[43] C. Nguyen, D.D. Do, Adsorption of supercritical gases in porous media: determination of micropore size distribution, J. Phys. Chem. B. 103 (1999) 6900–6908. doi:10.1021/jp9906536.

[44] C. Nguyen, D.D. Do, K. Haraya, K. Wang, The structural characterization of carbon molecular sieve membrane (CMSM) via gas adsorption, J. Memb. Sci. 220 (2003) 177–182. doi:10.1016/S0376-7388(03)00219-9.

[45] M.M.C.C. Santos, Carbon molecular sieve membranes for gas separation: study, preparation and characterization, University of Porto, 2009.

[46] S.C. Rodrigues, R. Whitley, A. Mendes, Preparation and characterization of carbon molecular sieve membranes based on resorcinol–formaldehyde resin, J. Memb. Sci. 459 (2014) 207–216. doi:10.1016/j.memsci.2014.02.013.

[47] D. Ferreira, R. Magalhães, P. Taveira, A. Mendes, Effective adsorption equilibrium isotherms and breakthroughs of water vapor and carbon dioxide on different adsorbents, Ind. Eng. Chem. Res. 50 (2011) 10201–10210. doi:10.1021/ie2005302.

[48] J.C. Santos, F.D. Magalhães, A. Mendes, Contamination of zeolites used in oxygen production by PSA: effects of water and carbon dioxide, Ind. Eng. Chem. Res. 47 (2008) 6197–6203. doi:10.1021/ie800024c.

[49] D.D. Do, Adsorption analysis: equilibria and kinetics, Queensland, 1998. doi:10.1142/p111.

[50] M. Kočiřík, P. Struve, M. Bülow, Analytical solution of simultaneous mass and heat transfer in zeolite crystals under constant-volume/variable-pressure conditions, J. Chem. Soc. Faraday Trans. 1. 80 (1984) 2167–2174. doi:10.1039/F19848002167.

[51] H. Marsh, F. Rodríguez-Reinoso, Activated carbon, 1st ed., Elsevier Ltd, Oxford, 2006.

[52] W. Li, J. Peng, L. Zhang, K. Yang, H. Xia, S. Zhang, S. Guo, Preparation of activated carbon from coconut shell chars in pilot-scale microwave heating equipment at 60 kW, Waste Manag. 29 (2009) 756–760. doi:10.1016/j.wasman.2008.03.004.

[53] S. Ouyang, S. Xu, N. Song, S. Jiao, Coconut shell-based carbon adsorbents for ventilation air methane enrichment, Fuel. 113 (2013) 420–425. doi:10.1016/j.fuel.2013.06.004.

[54] K. Promdee, J. Chanvidhwatanakit, S. Satitkune, C. Boonmee, T. Kawichai, S. Jarernprasert, T. Vitidsant, Characterization of carbon materials and differences

from activated carbon particle (ACP) and coal briquettes product (CBP) derived from coconut shell via rotary kiln, Renew. Sustain. Energy Rev. 75 (2017) 1175–1186. doi:10.1016/j.rser.2016.11.099.

[55] M. Toral, A. Manríquez, R. Navarro-Cerrillo, D. Tersi, P. Naulin, Características de los estomas, densidad e índice estomático en secuoya (Sequoia sempervirens) y su variación en diferentes plantaciones de Chile, Bosque (Valdivia). 31 (2010) 157–164. doi:10.4067/S0717-92002010000200009.

[56] R.M. Silverstein, G.C. Bassler, T.C. Morrill, Spectrometric identification of organic compounds, in: Wiley, New York, 1981.

[57] H.F. Shurvell, Spectra-structure correlations in the mid- and far-infrared, Handb. Vib. Spectrosc. (2006). doi:10.1002/0470027320.s4101.

[58] A. Sartape, A. Mandhare, P. Salvi, D. Pawar, P. Raut, M. Anuse, S. Kolekar, Removal of Bi (III) with adsorption technique using coconut shell activated carbon, Chinese J. Chem. Eng. 20 (2012) 768–775. doi:10.1016/S1004-9541(11)60247-4.

[59] R. Boopathy, S. Karthikeyan, A.B. Mandal, G. Sekaran, Adsorption of ammonium ion by coconut shell-activated carbon from aqueous solution: kinetic, isotherm, and thermodynamic studies, Environ. Sci. Pollut. Res. 20 (2013) 533–542. doi:10.1007/s11356-012-0911-3.

[60] C. Rolence, R.L. Machunda, K.N. Njau, Water hardness removal by coconut shell activated carbon, Int. J. Sci. Technol. Soc. 2 (2014) 97–102. doi:10.11648/j.ijsts.20140205.11.

[61] D. Cazorla-Amorós, J. Alcañiz-Monge, M.A. de la Casa-Lillo, A. Linares-Solano, CO_2 as an adsorptive to characterize carbon molecular sieves and activated carbons, Langmuir. 14 (1998) 4589–4596. doi:10.1021/la980198p.

[62] S.W. Rutherford, C. Nguyen, J.E. Coons, D.D. Do, Characterization of carbon molecular sieves using methane and carbon dioxide as adsorptive probes, Langmuir. 19 (2003) 8335–8342. doi:10.1021/la034472d.

[63] M.C. Campo, F.D. Magalhães, A. Mendes, Comparative study between a CMS

membrane and a CMS adsorbent: part I-morphology, adsorption equilibrium and kinetics, J. Memb. Sci. 346 (2010) 15–25. doi:10.1016/j.memsci.2009.08.045.

[64] M.L. Pinto, A.S. Mestre, A.P. Carvalho, J. Pires, Comparison of methods to obtain micropore size distributions of carbonaceous materials from CO_2 adsorption based on the Dubinin - Radushkevich isotherm, Ind. Eng. Chem. Res. 49 (2010) 4726–4730. doi:10.1021/ie100080r.

[65] A. Ahmadpour, A. Okhovat, M.J.D. Mahboub, Pore size distribution analysis of activated carbons prepared from coconut shell using methane adsorption data, J. Phys. Chem. Solids. 74 (2013) 886–891. doi:10.1016/j.jpcs.2013.01.036.

[66] A. Okhovat, A. Ahmadpour, F. Ahmadpour, Z.K. Yadegar, Pore size distribution analysis of coal-based activated carbons: investigating the effects of activating agent and chemical ratio, ISRN Chem. Eng. 2012 (2012) 1–10. doi:10.5402/2012/352574.

[67] Z. Hu, E.F. Vansant, Carbon molecular sieves produced from walnut shell, Carbon N. Y. 33 (1995) 561–567. doi:10.1016/0008-6223(94)00141-L.

[68] D. Adinata, W.M.A. Wan Daud, M.K. Aroua, Production of carbon molecular sieves from palm shell based activated carbon by pore sizes modification with benzene for methane selective separation, Fuel Process. Technol. 88 (2007) 599–605. doi:10.1016/j.fuproc.2007.01.009.

[69] W.M.A.W. Daud, W.S.W. Ali, Comparison on pore development of activated carbon produced from palm shell and coconut shell, Bioresour. Technol. 93 (2004) 63–69. doi:10.1016/j.biortech.2003.09.015.

[70] S.C. Rodrigues, M. Andrade, J. Moffat, F.D. Magalhães, A. Mendes, Preparation of carbon molecular sieve membranes from an optimized ionic liquid-regenerated cellulose precursor, J. Memb. Sci. 572 (2019) 390–400. doi:10.1016/j.memsci.2018.11.027.

[71] N. Querejeta, M.G. Plaza, F. Rubiera, C. Pevida, Water vapor adsorption on biomass based carbons under post-combustion CO2 capture conditions: effect of post-treatment, Materials (Basel). 9 (2016) 1–19. doi:10.3390/ma9050359.

[72] Y.H. Hu, E. Ruckenstein, Applicability of Dubinin – Astakhov equation to CO_2 adsorption on single-walled carbon nanotubes, Chem. Phys. Lett. 425 (2006) 306–310. doi:10.1016/j.cplett.2006.05.059.

[73] M.M.A. Freitas, J.L. Figueiredo, Preparation of carbon molecular sieves for gas separations by modification of the pore sizes of activated carbons, Fuel. 80 (2001) 1–6. doi:10.1016/S0016-2361(00)00066-1.

[74] F. Relvas, R.D. Whitley, C. Silva, A. Mendes, Single-stage pressure swing adsorption for producing fuel cell grade hydrogen, Ind. Eng. Chem. Res. 57 (2018) 5106–5118. doi:10.1021/acs.iecr.7b05410.

Chapter V

Chapter 5 - Propane selective carbon adsorbents from phenolic resin precursor[1]

Graphical abstract

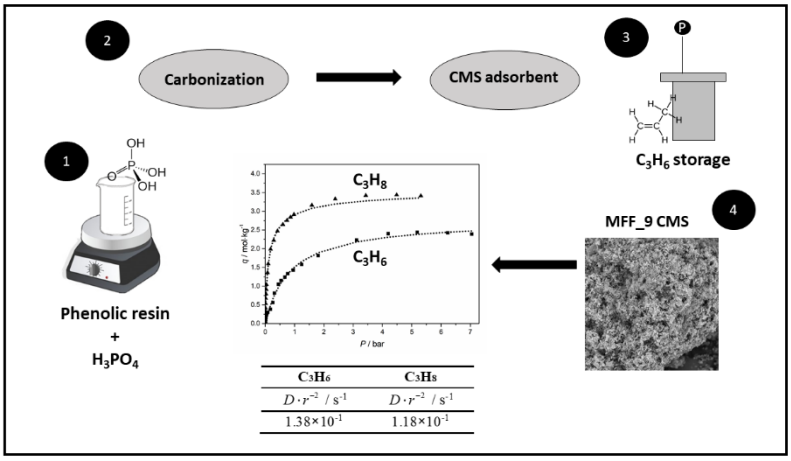

5.1. Abstract

Novel propane selective carbon molecular sieve adsorbents were prepared from a phenolic resin precursor pre-treated with phosphoric acid, carbonized and post-treated with propylene. All the preparation conditions were carefully investigated concerning their role on the separation performance. Samples were characterized concerning adsorption isotherms and uptake curves while the best performed sample was also characterized by scanning electron microscopy, thermogravimetric analysis and Fourier transform infrared spectroscopy. It was concluded that the pre-treatment with phosphoric acid was critical for the obtained unprecedented equilibrium-based propane / propylene separation performance – adsorbed concentration ratio of 2 at *ca.* 1 bar and 25 ºC (sample MFF_9); this sample was carbonized at 1100 ºC end temperature and post-treated with propylene during 12 days at 2 bar. The reported results open the door for the investigation of new materials selective to propane, which can be used for removing efficiently this contaminant from a propylene stream.

[1]M. Andrade, A. Mendes, Propane selective carbon adsorbents from phenolic resin precursor, submitted, (2019).

5.2. Introduction

Olefins are the building blocks for a large number of commodities [1,2]. Their separation/purification remains, however, a great challenge. Olefins such as ethylene and propylene are often mixed with its homologues paraffins ethane and propane, respectively, which have close boiling points [2]. One of the most important uses of ethylene and propylene are the production of their corresponding polymers; the required purity for this application is > 99.5 %, which is quite demanding [3,4]. Since distillation is still the election process for these separations, the corresponding distillation columns need to be very long rendering these separations very energy demanding [5,6]. Literature discloses other separation/purification processes, such as i) adsorption processes: temperature swing adsorption (TSA) [7] or pressure swing adsorption (PSA) [2,8,9]; ii) membrane processes: permeation [10–12] and pervaporation [13]; iii) reaction processes: catalytic pyrolysis processes (CPP) [14], by-product upgrading (C4-9) [15] and propane oxidative dehydrogenation [16]; and iv) hybrid processes: distillation with adsorption [17], membrane [18] and reaction processes [19], however, only few are commercial [20]. The processes that have been receiving more attention are adsorption- [21] and membrane-based [22]. Especially, adsorption-based processes have reached promising recoveries for the required purities [2,8].

Rege *et al.* [21] studied the performance of an equilibrium separation adsorbent, $AgNO_3$ / SiO_3, and a kinetic separation adsorbent, zeolite 4A. By comparing the performance of both adsorbent materials, the authors found that $AgNO_3$ / SiO_3 adsorbent was best performing material for the given separation obtaining a propylene purity of 99 % purity with a recovery of 44 %. Padin *et al.* [23] simulated the performance of an $AlPO_4$-14 adsorbent using a four-steps PSA cycle with a gas feed of 50 % C_3H_6 / 50 % C_3H_8. The results showed a propylene purity of 99 % and a recovery of 53 %. Grande *et al.* [2] used a zeolite 4A adsorbent in a two-stage VPSA unit obtaining a propylene purity of 99.6 % and a recovery of 95.9 %. Despite the very satisfactory results, the energy demand of the overall separation was somewhat higher than the one for distillation process. Furthermore, Campo *et al.* [8] used a modified 13X zeolite in a five-step VPSA and a feed mixture of 75 % C_3H_6 / 25 % C_3H_8. The obtained results showed

a propylene purity of 99.54 % and a recovery of 85 %, which are very interesting results. Despite reported results are suitable for purity, *ca.* 99.0 %-99.5 %, the recovery is still relatively low, *ca.* 50.0-85.0 %, (this with lower operation costs then distillation) [2]. This happens since increasing purity values higher than 99.5 % deals with a recovery decrease, and, moreover, when a VPSA is used, low evacuation pressures are required causing a high energy consumption [2,24].

The adsorbents used in these separations are adsorption selective to the olefins, which is the majority component. This makes the PSA units large, energy demanding and displaying humble recoveries. The ideal would be to have an adsorbent selective, either or both equilibrium or kinetics, to the minority component, the paraffin. However, there were described just a handful of such adsorbents. Herdes *et al.* [25] were among the first to report an paraffin equilibrium selective absorbent. These authors described an aluminium methylphosphonate polymorph alpha (AlMepO-α) selective towards paraffins over olefins. This material has a chemical composition of $Al_2(PO_3CH_3)_3$ and was firstly reported by Maeda *et al.* [26], since then, it was widely studied by another researchers [27–29]. Reported studies found small differences in the adsorbent structure and a strong effect of adsorbent-adsorbate interactions during adsorption process, which possible allowed the unexpected behaviour [30–32]. Additionally, metal organic frameworks (MOFs) such as ZIF-7, $Fe_2(O_2)$(dobdc) and MIL-100 have been investigated for preferable paraffins selectivity over olefins i) ethane / ethylene [5], ii) propane / propylene [33,34] and iii) isobutane / isobutene [34] separations. Gücüyener, *et al.* [5] reported a MOF, ZIF-7, paraffin selective towards ethane / ethylene mixtures. Namely, the authors reported an adsorbed concentration ratio of *ca.* 7 favourable to ethane over ethene with an ethane adsorption capacity of 1.8 $mol \cdot kg^{-1}$, at 0.3 bar 25 ^oC [5]. Very recently, Andres-Garcia *et al.* [35] reported a ZIF-67 MOF that exhibited an adsorbed concentration ratio favourable to propane over propylene of 3.7 with a propane adsorption capacity of 2.24 $mol \cdot kg^{-1}$, at *ca.* 0.2 bar and 25 ^oC.

The discovery of new materials selective towards paraffins over olefins may have to consider changing the adsorbents structure, such as functional surface groups and/or pore structure [32]. Finding the key factors for having the unprecedent separation would allow the development and optimization of materials with the desired characteristics for the given gas separation. Some authors are developing different conceptions for

explaining this separation such as thermodynamic control, *i.e.*, control of specific adsorbate-adsorbent interactions [36]. Studies revealed that whereas polar cation-containing zeolites, such as 13X, show preferable olefins adsorption [2,37], nonpolar cation-free zeolites display higher affinity to paraffins [32,38,39]. These studies were predicted through molecular dynamics calculations by using mixed gas isotherms. For example, Keil *et al*. [40] predicted an ethane adsorbed capacity selectivity of 2 from an equimolar mixture of ethane / ethene with an ethane adsorption capacity of 2.5 $mol \cdot kg^{-1}$ on carbon nanotubes, at 1 bar and 27 ^{o}C. On the other hand, on zeolite silicalite-1 was predicted only a slightly higher ethane adsorption over ethylene [41].

This work reports the preparation of propane selective carbon molecular sieve adsorbents prepared from a phenolic resin precursor. The samples were pre-treated with phosphoric acid and post-treated with propylene; propylene treatment stabilizes the adsorbent against chemisorption of ambient oxygen [42–44]. Adsorbents were characterized concerning adsorption equilibrium isotherms of propane and propylene, pore size distribution and mercury porosimetry; the surface morphology and chemistry were analysed by scanning electron microscopy (SEM), Fourier transform infrared spectroscopy (FTIR) and by thermogravimetric analysis. The best performing material displayed a propane / propylene adsorbed concentration ratio of 2 at *ca.* 1 bar.

5.3. Experimental

5.3.1. CMS preparation

Precursor materials

Phenolic resin MFF-AP supplied by Air Products and Chemicals Inc., mean particle size of *ca*. 1.5 µm, was used as precursor. Carbon dioxide (99.9 % pure) and helium (99.999 % pure) were supplied by Linde. Propane and propylene were provided from Praxair (99.5 % pure).

Pre-treatments

MFF-AP precursor was mixed overnight with 25 wt. % phosphoric acid solution at room temperature; the acid:precursor mass ratio was *ca.* 3. After mixed, the samples were carbonized.

Carbonization

The carbonization step was carried in an alumina tube (one of 954 cm^3 volume for temperatures among 950-1100 ^oC and other of 5049 cm^3 volume for temperatures between 1200-1300 ^oC; with 4.7 cm and 7.1 cm of inner diameter, respectively) inside a tubular horizontal Termolab TH furnace. For guaranteeing the temperature homogeneity along the tube, three separated thermocouples were placed into the furnace. Samples were carbonized under N_2 atmosphere with a 100 $mL \cdot min^{-1}$ (small volume tube) and 300 $mL \cdot min^{-1}$ (large volume tube) flow rate and a 3 $^oC \cdot min^{-1}$ heating rate. End temperatures from 950 ^oC up to 1300 ^oC with 60 minutes of soaking time were employed [45]. After the carbonization, the carbon adsorbents were cooled naturally until room temperature and then removed from the furnace.

Post-treatments

After the carbonization was completed, the carbon adsorbents were stored in 2 bar of propylene for 1 to 12 days.

5.3.2. Thermogravimetric analysis

Thermogravimetric analysis was performed in a Netzsch STA 449 F3 Jupiter thermogravimetric balance; a sample of 11.1 mg was employed. A proximate analysis was performed for obtaining the fraction of fixed carbon. The protocol used is described elsewhere [46] and generally comprises the following steps:

- From room temperature to 110 ^oC at 25 $^oC \cdot min^{-1}$ under 30 $mL \cdot min^{-1}$ of nitrogen; in this step all humidity should be released.
- From 110 ^oC up to 950 ^oC with a 9 min dwell under nitrogen stream; in this step it is expected a mass loss attributed to the release of volatile matter.
- The last step includes a 11 min dwell at 950 ^oC, under oxygen atmosphere, where carbon was burned leaving ashes.

5.3.3. Scanning electron microscopy (SEM)

SEM analyses were performed in a Phenom XL scanning electron microscope. The Phenom XL was equipped with two detector systems, one with a fully integrated EDS

system for elemental analysis and another that corresponds to a Secondary Electron Detector (SED) that enables surface sensitive imaging.

5.3.4. Mercury porosimetry

Mercury porosimetry analysis was performed in a Micromeritics Autopore IV 9500 porosimeter. Samples were mechanically outgassed while under 2.06×10^{-3} MPa prior to mercury intrusion for removing all physically adsorbed species. Mercury pressure increased from 2.06×10^{-3} MPa to 2.068×10^{2} MPa for entering in smaller pores, down to *ca*. 6 nm.

5.3.5. Particle size distribution

Particle size measurements were performed using a Counter LS 230 using Mie light scattering Polarization Intensity Differential Scattering (PIDS) technology. Samples were previously dispersed in distilled water.

5.3.6. Fourier transform infrared spectroscopy (FTIR)

The infrared spectra were recorded using a VERTEX 70 FTIR spectrometer (BRUKER) in transmittance mode with a high sensitivity DLaTGS detector at room temperature. Samples were analysed in transmission mode, using pellets of potassium bromide (KBr) with 1 % (w/w) of the compound. The spectra were recorded from 4000 cm^{-1} to 400 cm^{-1} with a resolution of 4 cm^{-1}.

5.3.7. Micropores characterization

Micropore size distribution of the CMS adsorbents was determined based on adsorption equilibrium isotherms of carbon dioxide at 0 ºC as described elsewhere [47–49]. This method could not be applied to phosphoric acid treated samples due to the change of the CMS inner surface chemistry.

For characterizing the adsorbent microporosity the Dubinin-Astakhov (DA) equation is normally used (Eq. 5.1) [50,51]:

$$\frac{W}{W_0} = \exp\left[-\left(\frac{RT\ln(P_0/P)}{E_0}\right)^n\right] \tag{5.1}$$

where W is the micropore volume, P is the pressure, W_0 is the total micropore volume, E_0 is the characteristic energy for adsorption, P_0 is the vapor pressure of the free liquid, R is the gas constant, T is the absolute temperature and n is a fitting parameter; for n = 2 this equation renders the Dubinin–Raduschkevisch (DR) equation.

5.3.8. Small-angle X-ray scattering

SAXS measurements were carried out at the University of Sheffield using a Xeuss 2.0 instrument (Xenocs, Grenoble France), this particular SAXS system is equipped with a liquid gallium X-ray source (MetalJet Excillum, Sweden). The X-ray beam (9.24 keV) size was 600 µm vertically and 400 µm horizontally, with a distance of 305 mm between sample position and the detector (Pilatus3R 1M 2D, Dectris, Switzerland). The samples were mounted on a sample holder and three measurements were taken from different regions of the sample, spaced by roughly ~ 1 mm. Each sample was also measured in transmission and scaled to the transmission through air and a suitable air background was also collected. The data operation tool in Sasview 4.2 was used to scale the SAXS data and subtract the air background.

5.3.9. Specific surface area

Multipoint Brunauer-Emmett-Teller (BET) specific surface area measurements were performed in a Quantachrome Autosorb AS-1 instrument at -196 ºC. Prior to the analysis samples were outgassed at 80 ºC for 30 minutes, then at 120 ºC for 30 minutes and finally at 300 ºC for 3 hours.

5.3.10. Adsorption equilibrium isotherms and gas uptake experiments

The adsorption equilibrium isotherms and uptake curves for C_3H_6, C_3H_8 and CO_2 were obtained by using the volumetric method as described elsewhere [52,53]. For measuring pressures until 2 bar a 2 bar Drück pressure sensor was used (reading error of 0.1 % of full scale) and for higher pressure values it was employed a 7 bar Drück (reading error of 0.1 % of full scale). The samples and tanks were evacuated at 70 ºC for 4 h to pressures < 0.002 bar using an Alcatel 1004A vacuum pump.

Langmuir (Eq. 5.2) and Toth (Eq. 5.3) adsorption isotherm equations are thermodynamically consistent; Toth has one more parameter to account for the surface

heterogeneities [51]. SIPS (Eq. 5.4) has also three parameters to account for the surface heterogeneities but is not applicable for low pressures since it does not converges to the Henry's law [49,51].

$$q = q_s \frac{bP}{1+bP} \tag{5.2}$$

$$q = q_s \frac{bP}{\left(1+(bP)^t\right)^{1/t}} \tag{5.3}$$

$$q = q_s \frac{(bP)^{1/n}}{1+(bP)^{1/n}} \tag{5.4}$$

where q is the adsorbed solute concentration at pressure P, q_s is the adsorbed saturation capacity, b is the adsorption affinity constant and t and n are parameters used to characterize the heterogeneity of the system. Generally, t is less than the unity; for t = 1, Toth equation converges to Langmuir equation [51].

The adsorption kinetics was calculated using a non-isothermal model for constant-volume and variable-pressure conditions (Eq. 5.5) [54]:

$$F = 1 - \sum_{n=1}^{\infty} \frac{9\left(1+\alpha^*\right)\left[\frac{Y_n}{-q_n^2}\right]^2 \exp\left(-q_n^2\tau\right)}{\frac{1}{\beta_n^*} + \frac{3}{2}\frac{\beta}{\beta_n^*}\left[q_n \cot q_n\left(\frac{Y_n}{q_n^2}\right)+1\right] + \frac{3}{2}\frac{\alpha^* B_n}{q_n^4 \beta_n^*}} \tag{5.5}$$

where $B_n = Y_n\left[(q_n^2 - \alpha)\, q_n \cot q_n - 2\alpha\right] + q_n^2(q_n^2 - \alpha)$, $Y_n = q_n \cot q_n - 1$ and $\alpha^* = KV$. Considering that $V = V_s / V_g$, and V_S correspond to the volume of the sorbent particles and V_g to the volume of the gaseous phase, respectively. This equation was fitted to the experimental uptake curves for obtaining the inverse of the apparent diffusion time constant ($D \cdot r^{-2}$).

5.4. Results and discussion

Several CMS samples were prepared under different conditions – Table 5.1 – and characterized for optimization of the adsorbent performance; the phosphoric acid pre-treatment, the carbonization end temperature and the post-treatment with propylene were changed.

Table 5.1. Adsorbents preparation conditions description.

Sample	Pre-treatment	Carbonization end temp.	Post-treatment
MFF_1	Without	1100 ºC for 1 h	Without
MFF_2	25 wt.% of H_3PO_4 overnight	1100 ºC for 1 h	Without
MFF_3	Without	1100 ºC for 1 h	Propylene for 1 day
MFF_4	Without	1100 ºC for 1 h	Propylene for 7 days
MFF_5	Without	1100 ºC for 1 h	Propylene for 12 days
MFF_6	12.5 wt.% of H_3PO_4 overnight	1100 ºC for 1 h	Propylene for 12 days
MFF_7	25 wt.% of H_3PO_4 overnight	950 ºC for 1 h	Propylene for 12 days
MFF_8	25 wt.% of H_3PO_4 overnight	1100 ºC for 1 h	Propylene for 6 days
MFF_9	25 wt.% of H_3PO_4 overnight	1100 ºC for 1 h	Propylene for 12 days
MFF_9/1200	25 wt.% of H_3PO_4 overnight	1200 ºC for 1 h	Propylene for 12 days
MFF_9/1300	25 wt.% of H_3PO_4 overnight	1300 ºC for 1 h	Propylene for 12 days

5.4.1. CMS adsorption capacity and kinetics

Table 5.2 shows the obtained propane and propylene adsorbed concentration and $D{\cdot}r^{-2}$ at *ca.* 1 bar and 25 ºC for all samples.

Table 5.2. Adsorption capacity and kinetics for both C_3H_8 and C_3H_6 and at *ca.* 1 bar and 25 ºC.

Sample	Gas species					
	C_3H_8		C_3H_6		C_3H_8 selectivity	
	q / mol·kg^{-1}	$D{\cdot}r^{-2}$ / s^{-1}	q / mol·kg^{-1}	$D{\cdot}r^{-2}$ / s^{-1}	Equil.*	Kinet.*
MFF_1	0.4	1.95×10^{-3}	1.6	1.23×10^{-3}	< 1	1.6
MFF_2	3.0	1.94×10^{-3}	2.5	2.53×10^{-3}	1.2	≈1
MFF_3	0.2	1.22×10^{-2}	1.8	3.29×10^{-4}	< 1	37.1
MFF_4	0.3	4.02×10^{-2}	1.6	7.27×10^{-3}	< 1	55.3
MFF_5	0.9	1.99×10^{-3}	1.8	3.28×10^{-2}	< 1	< 1
MFF_6	2.0	3.88×10^{-2}	2.3	2.36×10^{-2}	< 1	1.6
MFF_7	2.4	4.97×10^{-2}	2.9	4.51×10^{-2}	< 1	1.1
MFF_8	2.7	3.12×10^{-2}	2.5	1.47×10^{-3}	1.1	21.2
MFF_9	2.9	1.18×10^{-1}	1.4	1.38×10^{-1}	2.1	≈1
MFF_9/1200	3.7	1.85×10^{-1}	3.5	3.92×10^{-2}	1.1	4.7
MFF_9/1300	3.8	2.36×10^{-2}	3.3	4.17×10^{-2}	1.2	< 1

From Table 5.2 it can be observed that the sample without any pre- or post-treatment – MFF_1 (control) – is selective towards propylene. The propane adsorption selective samples are MFF_2, MFF_8, MFF_9 and MFF_9/1200; MFF_9 sample displays the highest adsorbed concentration ratio of *ca.* 2 at 1 bar. Among these samples MFF_8 and MFF_9/1200 display kinetic selectivity to propane, where sample MFF_8 displays the highest kinetic selectivity of 21.

Samples MFF_2 and MFF_9 display the highest equilibrium selectivity and are produced under similar carbonization conditions and pre-treatment; however, sample MFF_9 was also submitted to 12 days of propylene atmosphere treatment. It seems that carbonization conditions and pre-treatment are more relevant than the post-treatment for the adsorption selectivity. MFF_9 displays the highest equilibrium selectivity but also very high adsorption kinetics making it ideal for equilibrium-based PSA gas separation.

5.4.2. Thermogravimetry analysis

Proximate analysis [46] of precursor MFF-AP was obtained - Figure 5.1.

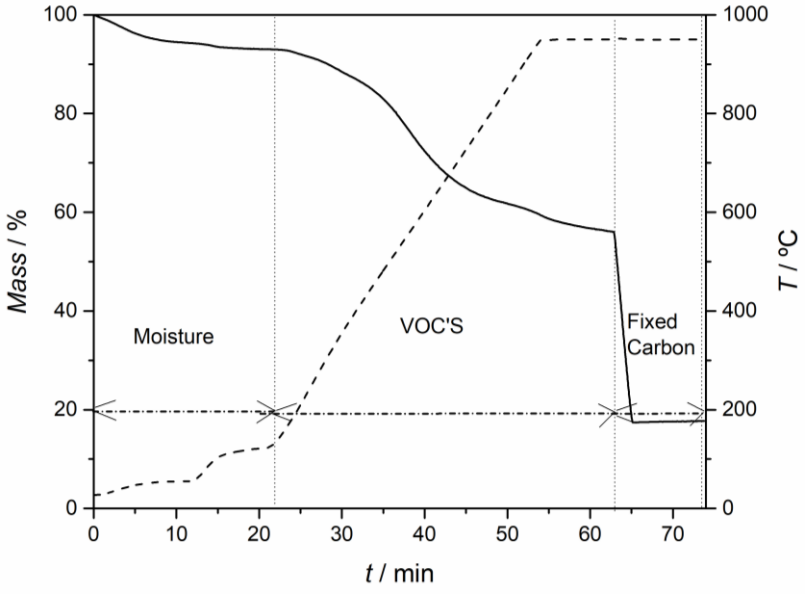

Figure 5.1 Proximate analysis of MFF-AP precursor by thermogravimetric method. The removed species at different intervals are identified.

Table 5.3 shows the obtained TGA weight results for MFF-AP precursor.

Table 5.3. Proximate analysis results by thermogravimetry of MFF-AP precursor.

	MFF.AP precursor
Humidity / %	7
Volatile matter / %	34.2
Fixed carbon / %	41.2
Ashes / %	18.0

Proximate analysis shows that the obtained fixed carbon value is within the values for similar materials 40 % - 60 % [55–57]. The fixed carbon is related to the mechanical resistance of the carbonized adsorbent and values above 40 % are envisioned [49].

5.4.3. Scanning electron microscopy

Figure 5.2 shows SEM micrographs of MFF-AP precursor material as well as CMS MFF_9.

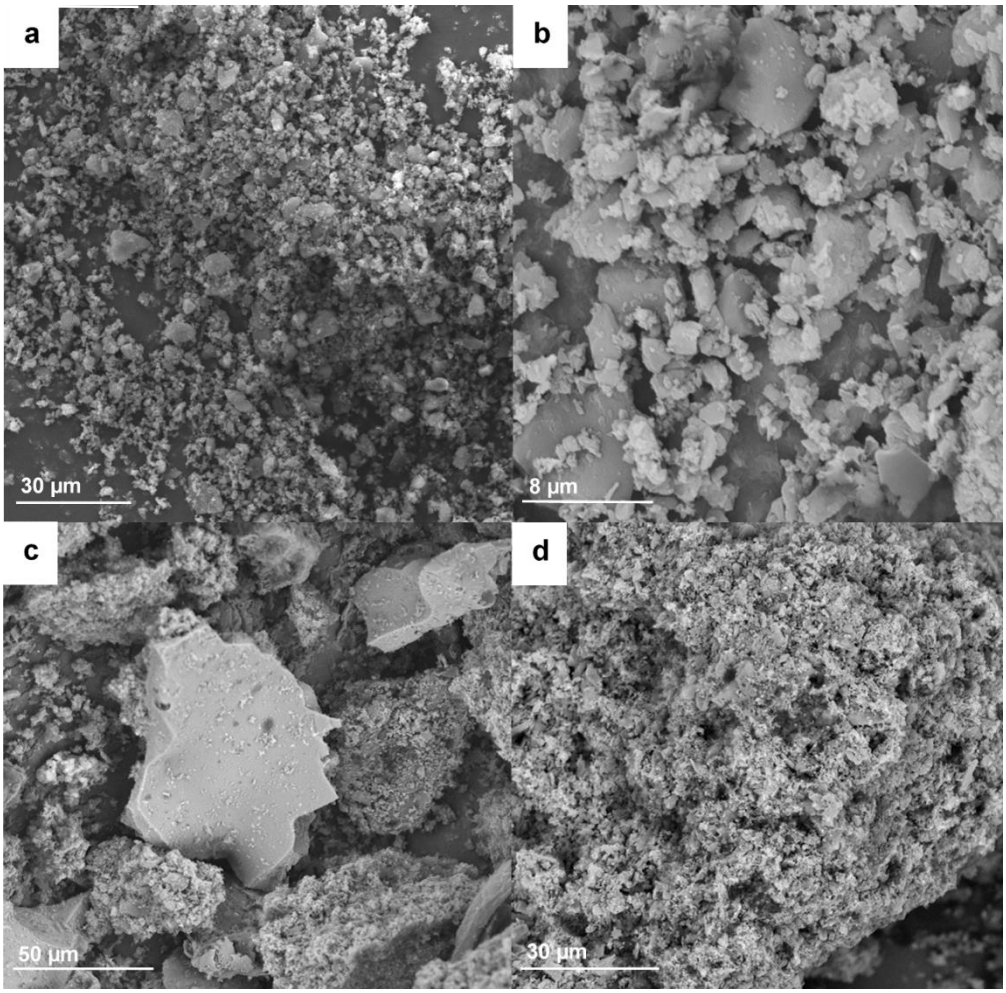

Figure 5.2. SEM micrographs with a) 2000× b) 10000× of magnification for MFF-AP precursor material and c) 1500× d) 2500× of magnification for the MFF_9 CMS adsorbent.

From Figure 5.2a) and Figure 5.2b) it can be observed that MFF-AP precursor material is a very fine powder showing some particle agglomeration. Figure 5.2c) and Figure 5.2d) show that the resultant CMS adsorbent exhibits larger agglomerated particles. The particle size distribution of sample MFF_9 is shown in Figure 5.3; particles range from 0.38 μm to 4 μm.

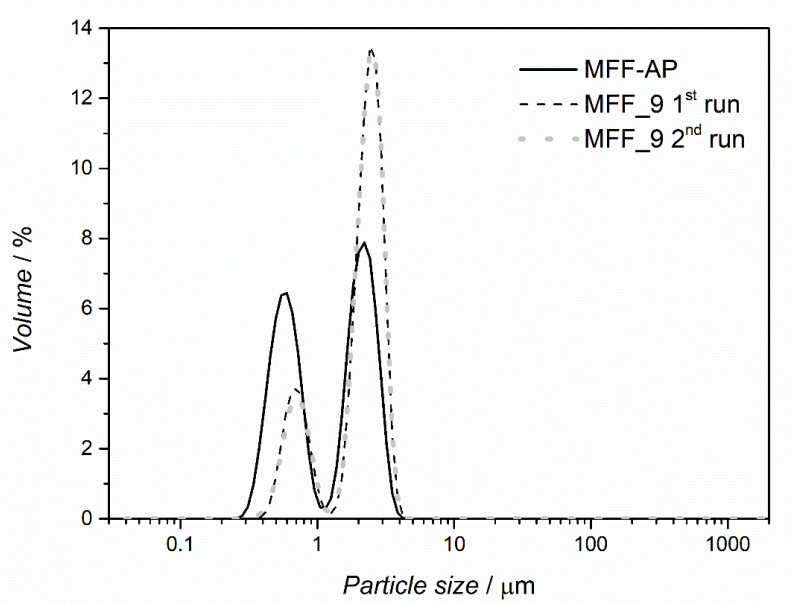

Figure 5.3. Particle size distribution of precursor MFF-AP and of the derived CMS adsorbent MFF_9.

5.4.4. Mercury porosimetry

Table 5.4 summarizes the morphology characteristics of MFF_9 adsorbent, including skeleton density, ρ_{He}, obtained by helium pycnometry.

Table 5.4. Mercury porosimetry results for MFF_9 adsorbent.

	MFF_9
ρ_{He} / g·cm^{-3}	2.43
Total pore area / m^2·g^{-1}	25.33
Median pore diameter (volume) / μm	0.86
Median pore diameter (area) / μm	0.04
ε_{total} / %	66.28

5.4.5. FTIR analysis

Figures 5.4 and 5.5 show the FTIR spectra of precursor MFF-AP and samples MFF_2 (pre-treated with phosphoric acid and without post-treatment), MFF_5 (without pre-treatment and post-treated for 12 days with propylene) and MFF_9 (best performing, pre-treated with phosphoric acid and post-treated for 12 days with propylene). Band assignments of Figures 5.4 and 5.5 are summarized in Table 5.5.

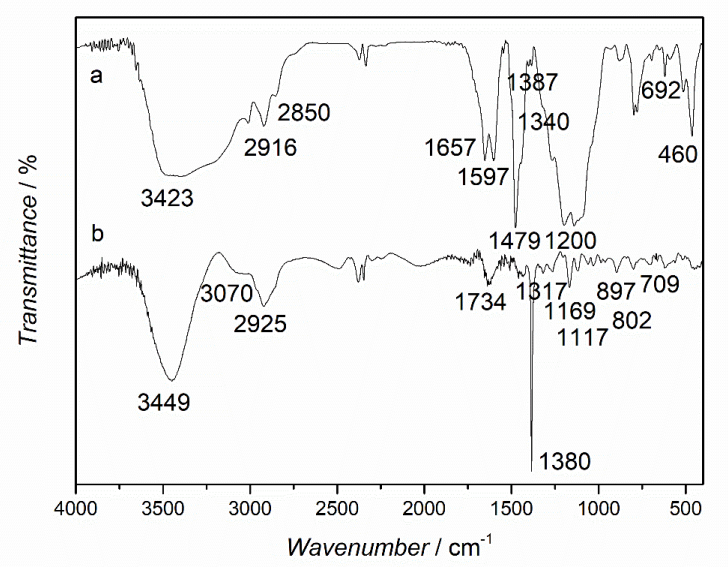

Figure 5.4. FTIR spectrum: a) precursor (sample MFF-AP) and; b) sample MFF_2, pre-treated with phosphoric acid and without post-treatment.

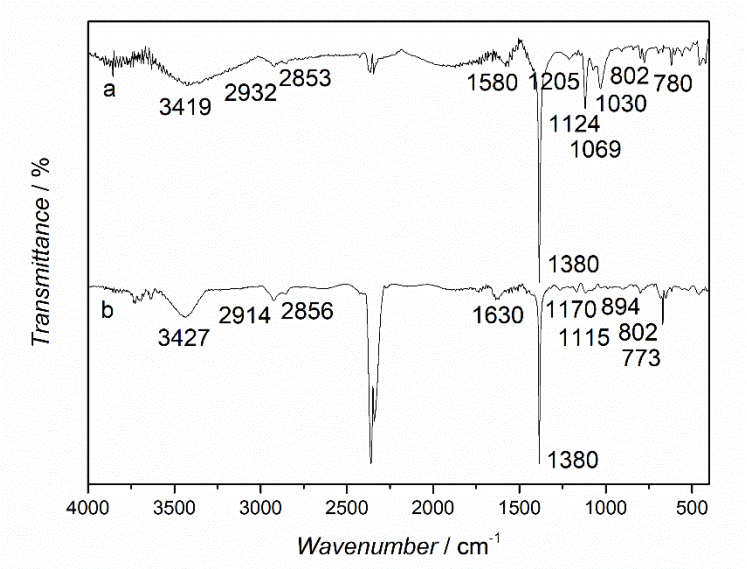

Figure 5.5. FTIR spectrum: a) sample MFF_5, without pre-treatment and post-treated for 12 days with propylene and; b) sample MFF_9, pre-treated with phosphoric acid and post-treated with propylene for 12 days.

Figures 5.4 and 5.5 indicate that pre- and post-treatments, as well as carbonization end temperature, cause several changes in the surface chemistry of the samples. Namely, after carbonization most functional groups are removed, which is expectable since several heteroatoms are released during this stage. However, in all samples O-H stretching vibrations ascribed to alcohols and phenols at 3400-3200 cm^{-1} and C-H stretching vibrations assigned to aliphatic compounds at 2950-2800 cm^{-1}, are present [58,59]. The bands located between 2364-2343 cm^{-1} are attributed to CO_2 present in the ambient air. Also, the O-H functional group intensity increases for sample MFF_2 pre-treated with phosphoric acid and decreases when post-treated with propylene, samples MFF_5 and MFF_9. These results indicate that phosphoric acid should hydrolyze the surface of the carbon samples, as suggested by Myglovets *et al.* [60]. Not less important, in all CMS adsorbents a strong band at 1380 cm^{-1} assigned to a C-H stretching vibration is observed [61]. Since the precursor material has a phenolic nature, this functional group could result from phenolic surface groups derived from the precursor material. Also, the sample pre-treated with phosphoric acid and not exposed to propylene, sample MFF_2, shows the presence of a C=O stretching vibration band at 1734 cm^{-1} [59]. Since samples treated with propylene do not present this functional group, propylene should act as a cleaning agent of this oxygenated functional group, as reported before [42,43]. Spectra of Figures 5.4b) and 5.5b) – samples pre-treated with phosphoric acid – indicate the presence of phosphor surface-functional groups, these samples exhibit a P=O stretching vibration band at 1170-1169 cm^{-1} [62–64]. However, the sample not exposed to propylene, MFF_2, displays a P-O-C stretching mode band at 1317 cm^{-1} assigned to P-O-C groups in phosphate-carbon complexes [63]. Since sample MFF_9, among the four samples, is the one displaying the highest propane selectivity, this feature could be assigned to the deletion of P-O-C, benzene rings and C=O functional groups and the presence of C=C and P=O groups in the adsorbent inner surface.

Table 5.5. FTIR spectra bands and assignments.

Wavenumber / cm^{-1}	Functional group	Assignment
3449, 3427, 3423, 3419	O-H	O-H stretching assigned to alcohols and phenols
3070	=C-H	=C-H stretching in aromatic structures
2932, 2925, 2916, 2914	$-CH_3$ and $-CH_2-$	Aliphatic C-H stretching vibration
2856, 2853, 2850	$-CH_2-$	C-H out-of-plane stretching vibration in alkanes
1734	C=O	C=O stretching vibration in ketones, aldehydes, lactones or carboxyl groups
1657, 1597	C=O and NH_2	Two bands; C=O stretching and NH_2 deformation vibrations
1630	C=C	C=C stretching vibration in alkenes
1580	Benzene ring	Benzene ring stretching vibration in aromatic compounds
1479	$-CH_2$	Scissor vibration of CH_2
1387, 1380	C-H	Stretch vibration of C-H
1340	O-H	Phenolic O-H in-plane deformation
1317	P-O-C	Stretching mode of P-O-C groups on phosphate-carbon complexes
1205, 1200, 1124,1117, 1115	C-O-C	C-O-C antisymmetric stretching vibration
1170, 1169	P=O	P=O stretching vibration in phosphorous oxyacids and phosphates
1069	C-C	C-C stretching vibration
1030	Carbon ring	Carbon ring in cyclic compounds; ring breath mode
897, 894, 802, 780, 773	C-H	Out-of-plane deformation mode of C-H substituted in different benzene rings
692	C-H	C-H out-of-plane deformation of mono-substituted benzenes
460	C-O-C	C-O-C bend vibration in ethers

5.4.6. Surface area and pore volume

Figure 5.6 plots the carbon dioxide and sulfur hexafluoride adsorption equilibrium isotherms at 25 ºC on sample MFF_9.

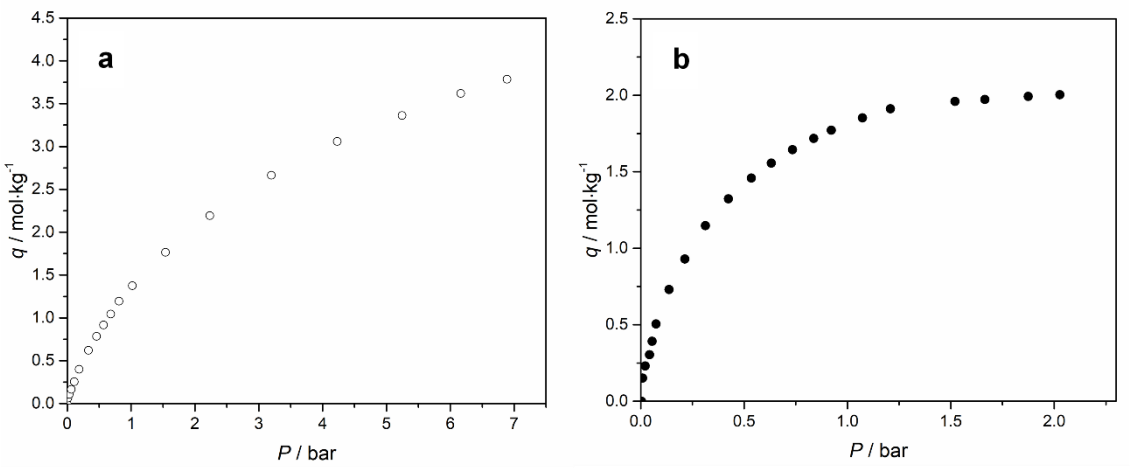

Figure 5.6. Adsorption equilibrium isotherms at 25 ºC on MFF_9 a) CO_2 and b) SF_6.

Figure 5.6 indicates that MFF_9 CMS adsorbent displays a wide micropore size distribution since carbon dioxide (kinetic diameter of 0.33 nm [65]) and sulfur hexafluoride (kinetic diameter of 0.55 nm [66]) are highly adsorbed. Furthermore, the amount adsorbed of carbon dioxide is clearly higher than sulfur hexafluoride, which reaches the saturation at *ca.* 1.1 bar; carbon dioxide isotherm reaches the saturation above 7 bar. These results indicate a limited volume of pores lager than the size of sulfur hexafluoride.

Figure 5.7 shows the CO_2 adsorption isotherm at 0 ºC and the respective Dubinin-Astakhov linearization for MFF_9 CMS adsorbent. The DA fitting parameters are given in Table 5.6.

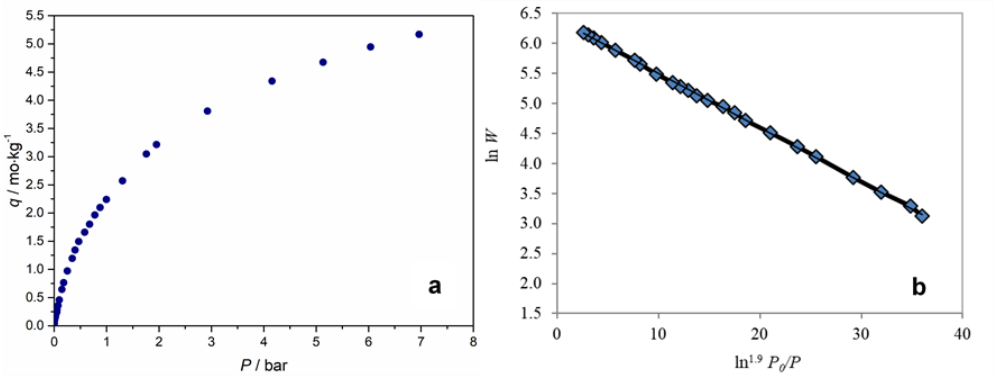

Figure 5.7. CO_2 adsorption isotherm at 0 ºC (a) and respective linearization employing Dubinin-Astakhov equation (b) for MFF_9 adsorbent (scatter corresponds to experimental data and solid line to DA fitting).

Table 5.6. Structural parameters for MFF_9 CMS sample.

Parameter	MFF_9
n	1.9
W_0 / $cm^3 \cdot kg^{-1}$	347.27
E_0 / $kJ \cdot mol^{-1}$	9.45
S / $m^2 \cdot g^{-1}$	834.83

The obtained specific surface area and micropore volume for MFF_9 adsorbent is in the range of other values reported in literature [67–71].

5.4.7. SAXS analysis

Small angle X-ray scattering (SAXS) was implemented for analysing the shape and size of pores in MFF_9 CMS adsorbent [72]. The obtained results are placed in Figure 5.8. The SAXS data was fitted with the Guinier-Porod model [73] in the Q range from 0.1 $Å^{-1}$ to 1.0 $Å^{-1}$. This model is empirical and can be used to determine the size and dimensionality of the nano-pores including asymmetric nano-pores with different shapes as spheres, rods, platelets and shapes intermediate between spheres and rods and between rods and platelets.

The Guinier-Porod model is shown in the following equations:

$$I(Q) = \frac{G}{Q_s} \exp\left[\frac{-Q^2 R_g^{\,2}}{3-s}\right] \text{for } Q \le Q_1 \tag{5.6}$$

$$I(Q) = \frac{D}{Q_m} \text{ for } Q \ge Q_1 \tag{5.7}$$

where Q is the scattering variable, $I(Q)$ is the scattered intensity, R_g is the radius of gyration and G and D are the Guinier and Porod scale factors, respectively. For globular pores (such as perfect spheres) s = 0, for rod shape (2D symmetry) structures s = 1 and for platelet shaped structures (1D symmetry) s = 2. The Guinier-Porod experimental data fitting (shown as red dots in Figure 5.8b), produced an s = 0.977 and R_g = 6.01 Å values. The value of s shows that the pores have approximately rod-shaped geometries. Considering that the radius-of-gyration of a randomly oriented cylinder of radius R is

given by R_g = R / √2, then a value of R ~ 8.5 Å is obtained, *i.e.*, the rods have an average diameter of 1.7 nm.

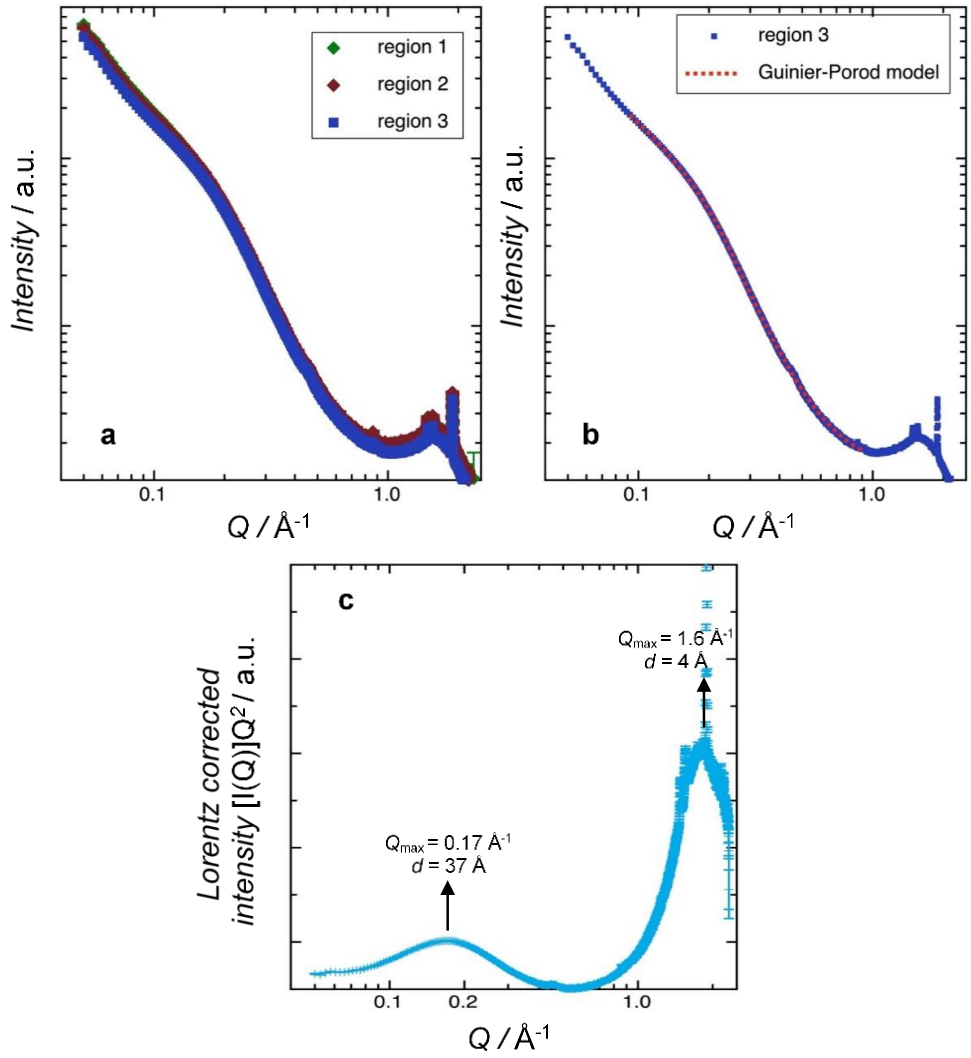

Figure 5.8. SAXS data for MFF_9 for a) three spatially separated regions; b) data fitted to the Guinier-Porod model and c) Lorentz corrected SAXS data with a distribution of nanoscale structures centred around Q values of *ca.* 0.17 Å^{-1} and 1.6 Å^{-1} (a.u. = arbitrary units).

The intensity function $I(Q)$ is related to the scattering vector amplitude, and, Q comes from the subtraction of the buffer from the sample [74].

$$Q = \frac{4\pi \sin\theta}{\lambda} \tag{5.8}$$

Bragg's law (Eq. 5.9) can be applied for determining d which is the lattice interplanar spacing of the crystal [72] :

$$n\lambda = 2d\sin\theta \tag{5.9}$$

$$d = \frac{2\pi}{Q} \tag{5.10}$$

where θ is the X-ray incident angle (Bragg angle), n is an "integer", λ is the wavelength of the characteristic X-ray. By applying Eq. 5.10, the sample pore size distribution was determined for each $Q_{\max}$ values. Then, Figure 5.8c) shows that the MFF_9 adsorbent displays smaller pores in the range of 0.4 nm and larger pores in the range of 3.7 nm.

5.4.8. Adsorption equilibrium and kinetics

The adsorption equilibrium isotherms of propane and propylene at 25 ºC on sample MFF_9 are plotted in Figure 5.9.

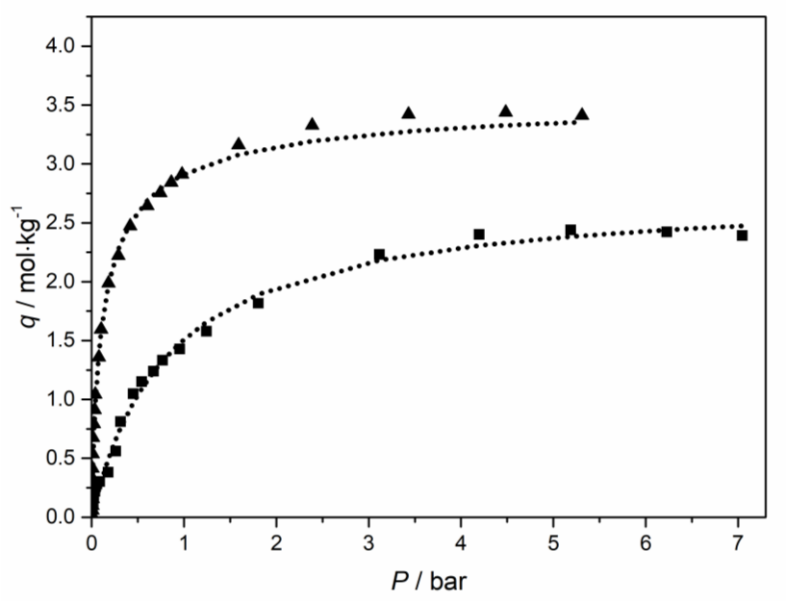

Figure 5.9. Propane (▲) and propylene (■) experimental isotherms on MFF_9 at 25 ºC. The dotted lines are the Toth equation fitting.

MFF_9 displays a higher adsorption capacity for propane compared with propylene; the adsorbed concentration ratio is *ca.* 2 at 1 bar. Normally, an activated carbon, as well as most of the adsorbents, are selective to propylene, which makes this adsorbent very special. This adsorbent is especially suited for the propylene purification, which implies the removal of small concentrations of propane. Table 5.7 shows the fitting parameters of the Toth equation for propane and propylene on MFF_9.

Table 5.7. Toth equation parameters of C_3H_6 and C_3H_8 on MFF_9 adsorbent.

	Toth equation		
	q_s / mol·kg^{-1}	b / bar^{-1}	t
C_3H_6	2.889	1.298	0.887
C_3H_8	3.594	13.934	0.700

Figure 5.10 shows the experimental uptake curves and the respective fitting model for propane and propylene at *ca.* 1 bar and 25 ºC. The adsorption kinetics for both propane and propylene is very fast and similar. Adsorbent MFF_9 is then suitable only for adsorption equilibrium separation processes.

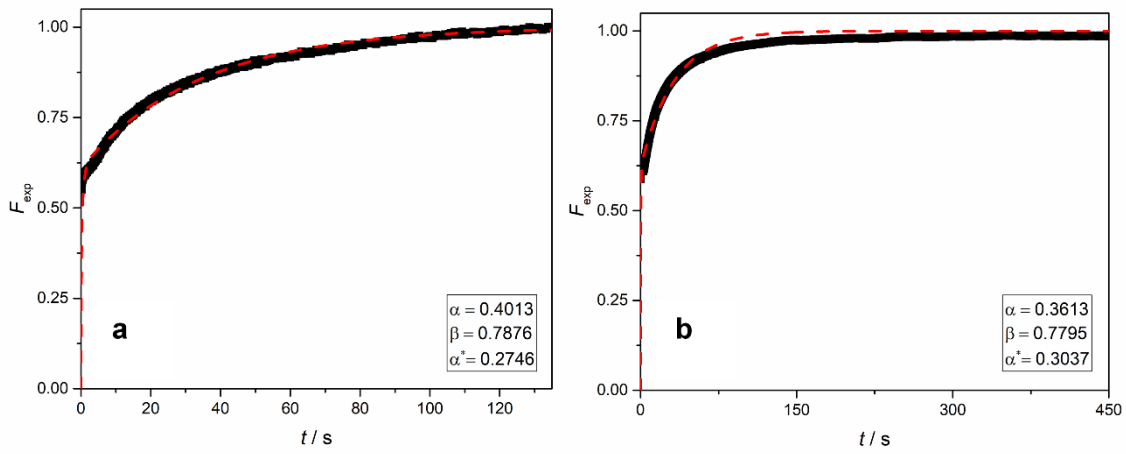

Figure 5.10. Experimental uptake curves (black symbols) and fitting model (red dashed lines) for: a) propane and b) propylene. The fitting parameters are also given.

5.5. Conclusions

Carbon molecular sieve adsorbents with kinetic and equilibrium selectivity to propane over propylene, were successfully prepared from a phenolic resin precursor. The phenolic resin precursor was pre-treated with phosphoric acid, followed by carbonization and propylene post-treatment. Eleven samples were prepared changing the end temperature (950 ºC – 1300 ºC), pre-treatment (phosphoric acid concentration – 0 wt.% to 25 wt.%) and post-treatment (time of contact with propylene 0 to 12 days). The best performing samples, samples MFF_8 and MFF_9, were pre-treated with phosphoric acid at 25 wt.%, carbonized at 1100 ºC and post-treated with propylene for 6 and 12 days, respectively. MFF_8 exhibited a kinetic selectivity of propane over propylene of *ca.* 21 and MFF_9 displayed an equilibrium selectivity of *ca.* 2, at 1 bar and 25 ºC. MFF_9 sample was fully characterized to investigate the reasons for this unprecedented equilibrium-based separation performance. The FTIR spectra showed that both pre- and post-treatments cause several changes in surface chemistry of the samples. Moreover, the results obtained from volumetric method indicated that phosphoric acid may play a key role in the inverse equilibrium-based selectivity, since all samples pre-treated with phosphoric acid display a significant increase in the propane adsorption. On the other hand, the post-treatment with propylene, though relevant, has a smaller role for the equilibrium-based selectivity to propane.

5.6. Acknowledgments

This work was financially supported by: project UID/EQU/00511/2019 - Laboratory for Process Engineering, Environment, Biotechnology and Energy – LEPABE funded by national funds through FCT/MCTES (PIDDAC); Project “LEPABE-2-ECO-INNOVATION” – NORTE-01-0145-FEDER-000005, funded by North Portugal Regional Operational Programme (NORTE 2020), under PORTUGAL 2020 Partnership Agreement, through the European Regional Development Fund (ERDF).

The authors are thankful to Andrew Parnell from University of Sheffield for kindly perform the SAXS analysis.

The authors are thankful to Air Products and Chemicals, Inc. for generously providing the precursor material.

5.7. References

[1] R.B. Eldridge, Olefin/paraffin separation technology: a review, Ind. Eng. Chem. Res. 32 (1993) 2208–2212. doi:10.1021/ie00022a002.

[2] C.A. Grande, F. Poplow, A.E. Rodrigues, Vacuum pressure swing adsorption to produce polymer-grade propylene, Sep. Sci. Technol. 45 (2010) 1252–1259. doi:10.1080/01496391003652767.

[3] P.F. Bryan, Removal of propylene from fuel-grade propane, Sep. Purif. Rev. 33 (2004) 157–182. doi:10.1081/SPM-200042095.

[4] A.M. Aitani, Propylene production, in: T.& Francis (Ed.), Encycl. Chem. Process., New York, 2006: pp. 2461–2466. doi:10.1081/E-ECHP-120037901.

[5] C. Gücüyener, J. van den Bergh, J. Gascon, F. Kapteijn, Ethane/ethene separation turned on its head: selective ethane adsorption on the metal-organic framework ZIF-7 through a gate-opening mechanism, J. Am. Chem. Soc. 132 (2010) 17704–17706. doi:10.1021/ja1089765.

[6] W. Zhu, F. Kapteijn, J.A. Moulijn, Shape selectivity in the adsorption of propane/propene on the all-silica DD3R, Chem. Commun. (1999) 2453–2454. doi:10.1039/A906465F.

[7] S.C. Reys, V. V. Krishnan, G.J. DeMartin, J.H. Sinfelt, K.G. Strohmaier, J.G. Santiesteban, Separation of propylene from hydrocarbon mixtures, USOO6730142B2, 2004.

[8] M.C. Campo, A.M. Ribeiro, A. Ferreira, J.C. Santos, C. Lutz, J.M. Loureiro, A.E. Rodrigues, New 13X zeolite for propylene/propane separation by vacuum swing adsorption, Sep. Purif. Technol. 103 (2013) 60–70. doi:10.1016/j.seppur.2012.10.009.

[9] M. Mofarahi, M. Sadrameli, J. Towfighi, Four-bed vacuum pressure swing adsorption process for propylene/propane separation, Ind. Eng. Chem. Res. 44 (2005) 1557–1564. doi:10.1021/ie034016k.

[10] J.-W. Chang, T.R. Marrero, H.K. Yasuda, Continuous process for

propylene/propane separation by use of silver nitrate carrier and zirconia porous membrane, J. Memb. Sci. 205 (2002) 91–102. doi:10.1016/S0376-7388(02)00066-2.

[11] I.G. Giannakopoulos, V. Nikolakis, Recovery of hydrocarbons from mixtures containing C_3H_6, C_3H_8 and N_2 using NaX membranes, J. Memb. Sci. 305 (2007) 332–337. doi:10.1016/j.memsci.2007.08.023.

[12] X. Ma, S. Williams, X. Wei, J. Kniep, Y.S. Lin, Propylene/propane mixture separation characteristics and stability of carbon molecular sieve membranes, Ind. Eng. Chem. Res. 54 (2015) 9824–9831. doi:10.1021/acs.iecr.5b02721.

[13] N. Schmeling, R. Konietzny, D. Sieffert, P. Rölling, C. Staudt, Functionalized copolyimide membranes for the separation of gaseous and liquid mixtures, Beilstein J. Org. Chem. 6 (2010) 789–800. doi:10.3762/bjoc.6.86.

[14] Z. Genquan, X. Chaogang, Research and commercial application of CPP technology for producing light olefins from heavy oil, China Pet. Process. Petrochemical Technol. 15 (2013) 7–12.

[15] T. Ren, M. Patel, K. Blok, Olefins from conventional and heavy feedstocks: energy use in steam cracking and alternative processes, Energy. 31 (2006) 425–451. doi:10.1016/j.energy.2005.04.001.

[16] K. Fukudome, T. Suzuki, Highly selective oxidative dehydrogenation of propane to propylene over VO_x – SiO_2 catalysts, Catal. Surv. from Asia. 19 (2015) 172–187. doi:10.1007/s10563-015-9192-4.

[17] T.K. Ghosh, H.-D. Lin, A. Hines, Hybrid adsorption-distillation process for separating propane and propylene, Ind. Eng. Chem. Res. 32 (1993) 2390–2399. doi:10.1021/ie00022a024.

[18] J. Park, K. Kim, J. Shin, K. Tak, Y. Park, Performance study of multistage membrane and hybrid distillation processes for propylene/propane separation, Can. J. Chem. Eng. 95 (2017) 2390–2397. doi:10.1002/cjce.22914.

[19] V. Sakhre, Reactive distillation: modeling, simulation, and optimization, in: V.

Steffen (Ed.), Distill. - Model. Simul. Optim., 2019. doi:10.5772/intechopen.85433.

[20] T. Ren, M. Patel, K. Blok, Energy efficiency and innovative emerging technologies for olefin production, 2004.

[21] S.U. Rege, J. Padin, R.T. Yang, Olefin/paraffin separations by adsorption: π-complexation vs. kinetic separation, AlChE J. 44 (1998) 799–809. doi:10.1002/aic.690440405.

[22] R.W. Baker, Future directions of membrane gas separation technology, Ind. Eng. Chem. Res. 41 (2002) 1393–1411. doi:10.1021/ie0108088.

[23] J. Padin, S.U. Rege, R.T. Yang, L.S. Cheng, Molecular sieve sorbents for kinetic separation of propane/propylene, Chem. Eng. Sci. 55 (2000) 4525–4535. doi:10.1016/S0009-2509(00)00099-3.

[24] C.A. Grande, A.E. Rodrigues, Adsorption of binary mixtures of propane−propylene in carbon molecular sieve 4A, Ind. Eng. Chem. Res. 43 (2004) 8057–8065. doi:10.1021/ie049327p.

[25] C. Herdes, A. Valente, Z. Lin, J. Rocha, J.A.P. Coutinho, F. Medina, L.F. Vega, Selective adsorption of volatile organic compounds in micropore aluminum methylphosphonate-α: a combined molecular simulation - experimental approach, Langmuir. 23 (2007) 7299–7305. doi:10.1021/la063518a.

[26] K. Maeda, J. Akimoto, Y. Kiyozumi, F. Mizukami, Structure of aluminium methylphosphonate, AlMepO-β, with unidimensional channels formed from ladder-like organic-inorganic polymer chains, J. Chem. Soc. (1995) 1033–1034. doi:10.1039/C39950001033.

[27] M. Edgar, V.J. Carter, D.P. Tunstall, P. Grewal, V. Favre-Nicolin, P.A. Cox, P.A. Wright, Structure solution of a novel aluminium methylphosphonate using a new simulated annealing program and powder X-ray diffraction data, R. Soc. Chem. (2002) 808–809. doi:10.1039/b200318j.

[28] S.P. Brown, S.E. Ashbrook, S. Wimperis, Al multiple-quantum magic angle spinning

NMR study of the thermal transformation between the microporous aluminum methylphosphonates AlMePO-β and AlMePO-α, J. Phys. Chem. B. 103 (1999) 812–817. doi:10.1021/jp9824858.

[29] N. Li, S. Xiang, Hydrothermal synthesis and crystal structure of two novel aluminophosphites containing infinite Al – O – Al chains, J. Mater. Chem. 12 (2002) 1397–1400. doi:10.1039/b200507g.

[30] K. Maeda, Metal phosphonate open-framework materials, Microporous Mesoporous Mater. 73 (2004) 47–55. doi:10.1016/j.micromeso.2003.10.018.

[31] K. Maeda, Y. Kiyozumi, F. Mizukami, Characterization and gas adsorption properties of aluminum methylphosphonates with organically lined unidimensional channels, J. Phys. Chem. 101 (1997) 4402–4412. doi:10.1021/jp962112b.

[32] M.C. Kroon, L.F. Vega, Selective paraffin removal from ethane/ethylene mixtures by adsorption into aluminum methylphosphonate- α: a molecular simulation study, Langmuir. 25 (2009) 2148–2152. doi:10.1021/la803042z.

[33] C. Serre, A. Vimont, P. Llewellyn, J.-S. Chang, P. Horcajada, G. Ferey, M. Daturi, Y.-K. Hwang, Reducible porous crystalline hybrid solid for the separation of mixtures of molecules having different degrees and/or a different number of unsaturations, WO 2010/000975 A1, 2010.

[34] J. Van Den Bergh, C. Gücüyener, E.A. Pidko, E.J.M. Hensen, J. Gascon, F. Kapteijn, Understanding the anomalous alkane selectivity of ZIF-7 in the separation of light alkane/alkene mixtures, Chem. Eur. J. 17 (2011) 8832–8840. doi:10.1002/chem.201100958.

[35] E. Andres-Garcia, L. Oar-Arteta, J. Gascon, F. Kapteijn, ZIF-67 as silver-bullet in adsorptive propane/propylene separation, Chem. Eng. J. 360 (2019) 10–14. doi:10.1016/j.cej.2018.11.118.

[36] U. Böhme, B. Barth, C. Paula, A. Kuhnt, W. Schwieger, A. Mundstock, J. Caro, M. Hartmann, Ethene/ethane and propene/propane separation via the olefin and paraffin selective metal − organic framework adsorbents CPO-27 and ZIF-8,

Langmuir. 29 (2013) 8592–8600. doi:10.1021/la401471g.

[37] F.A. Da Silva, A.E. Rodrigues, Propylene/propane separation by vacuum swing adsorption using 13X zeolite, AlChE J. 47 (2001) 341–357. doi:10.1002/aic.690470212.

[38] D.H. Olson, M.A. Camblor, L.A. Villaescusa, G.H. Kuehl, Light hydrocarbon sorption properties of pure silica Si-CHA and ITQ-3 and high silica ZSM-58, Microporous Mesoporous Mater. 67 (2004) 27–33. doi:10.1016/j.micromeso.2003.09.025.

[39] D.D. Do, H.D. Do, Cooperative and competitive adsorption of ethylene, ethane, nitrogen and argon on graphitized carbon black and in slit pores, Adsorption. 11 (2005) 35–50. doi:10.1007/s10450-005-1091-y.

[40] F.J. Keil, Molecular simulation of adsorption in zeolites and carbon nanotubes, in: Springer (Ed.), Adsorpt. Phase Behav. Nanochannels Nanotub., 2010: pp. 9–40. doi:10.1007/978-90-481-2481-7.

[41] S. Jakobtorweihen, N. Hansen, F.J. Keil, Molecular simulation of alkene adsorption in zeolites, Mol. Phys. 103 (2005) 471–489. doi:10.1080/00268970512331316021.

[42] C.W. Jones, W.J. Koros, Carbon molecular sieve gas separation membranes-II. Regeneration following organic exposure, Carbon N. Y. 32 (1994) 1427–1432. doi:10.1016/0008-6223(94)90136-8.

[43] S.C. Rodrigues, M. Andrade, J. Moffat, F.D. Magalhães, A. Mendes, Carbon membranes with extremely high separation factors and stability, Energy Technol. 7 (2019). doi:10.1002/ente.201801089.

[44] I. Menendez, A.B. Fuertes, Aging of carbon membranes under different environments, Carbon N. Y. 39 (2001) 733–740. doi:10.1016/S0008-6223(00)00188-3.

[45] T. Budinova, E. Ekinci, F. Yardim, A. Grimm, E. Björnbom, V. Minkova, M. Goranova, Characterization and application of activated carbon produced by H_3PO_4 and water vapor activation, Fuel Process. Technol. 87 (2006) 899–905.

doi:10.1016/j.fuproc.2006.06.005.

[46] M. Ottaway, Use of thermogravimetry for proximate analysis of coals and cokes, Fuel. 61 (1982) 713–716. doi:10.1016/0016-2361(82)90244-7.

[47] C. Nguyen, D.D. Do, K. Haraya, K. Wang, The structural characterization of carbon molecular sieve membrane (CMSM) via gas adsorption, J. Memb. Sci. 220 (2003) 177–182. doi:10.1016/S0376-7388(03)00219-9.

[48] C. Nguyen, D.D. Do, Adsorption of supercritical gases in porous media: determination of micropore size distribution, J. Phys. Chem. B. 103 (1999) 6900–6908. doi:10.1021/jp9906536.

[49] M.M.C.C. Santos, Carbon molecular sieve membranes for gas separation: study, preparation and characterization, University of Porto, 2009.

[50] S.C. Rodrigues, R. Whitley, A. Mendes, Preparation and characterization of carbon molecular sieve membranes based on resorcinol–formaldehyde resin, J. Memb. Sci. 459 (2014) 207–216. doi:10.1016/j.memsci.2014.02.013.

[51] D.D. Do, Adsorption analysis: equilibria and kinetics, Queensland, 1998. doi:10.1142/p111.

[52] D. Ferreira, R. Magalhães, P. Taveira, A. Mendes, Effective adsorption equilibrium isotherms and breakthroughs of water vapor and carbon dioxide on different adsorbents, Ind. Eng. Chem. Res. 50 (2011) 10201–10210. doi:10.1021/ie2005302.

[53] J.C. Santos, F.D. Magalhães, A. Mendes, Contamination of zeolites used in oxygen production by PSA: effects of water and carbon dioxide, Ind. Eng. Chem. Res. 47 (2008) 6197–6203. doi:10.1021/ie800024c.

[54] M. Kočiřík, P. Struve, M. Bülow, Analytical solution of simultaneous mass and heat transfer in zeolite crystals under constant-volume/variable-pressure conditions, J. Chem. Soc. Faraday Trans. 1. 80 (1984) 2167–2174. doi:10.1039/F19848002167.

[55] E. V. Krivokorytov, A.G. Gur'ev, B.I. Polyak, High-carbon binders in refractories

and corrosion-resistant ceramics technology (a review), Glas. Ceram. 55 (1998) 144–147. doi:10.1007/BF02694727.

[56] R. Lum, C.W. Wilkins, M. Robbins, A.M. Lyons, R.P. Jones, Thermal analysis of graphite and carbon-phenolic composites by pyrolysis-mass spectrometry, Carbon N. Y. 21 (1983) 111–116. doi:10.1016/0008-6223(83)90165-3.

[57] P. Xu, X. Jing, High carbon yield thermoset resin based on phenolic resin, hyperbranched polyborate, and paraformaldehyde, Polym. Adv. Technol. 22 (2011) 2592–2595. doi:10.1002/pat.1806.

[58] M.A. Mohamed, J. Jaafar, A.F. Ismail, M.H.D. Othman, M.A. Rahman, Fourier transform infrared (FTIR) spectroscopy, in: Membr. Charact., Elsevier B.V., 2017: pp. 3–29. doi:10.1016/B978-0-444-63776-5.00001-2.

[59] Z. Chen, Y. Chen, H. Liu, Pyrolysis of phenolic resin by TG-MS and FTIR analysis, Adv. Mater. Res. 631–632 (2013) 104–109. doi:10.4028/www.scientific.net/AMR.631-632.104.

[60] M. Myglovets, O.I. Poddubnaya, O. Sevastyanova, M.E. Lindström, B. Gawdzik, M. Sobiesiak, M.M. Tsyba, V.I. Sapsay, D.O. Klymchuk, A.M. Puziy, Preparation of carbon adsorbents from lignosulfonate by phosphoric acid activation for the adsorption of metal ions, Carbon N. Y. 80 (2014) 771–783. doi:10.1016/j.carbon.2014.09.032.

[61] O.A. Ekpete, A.C. Marcus, V. Osi, Preparation and characterization of activated carbon obtained from plantain (Musa paradisiaca) fruit stem, Hindawi J. Chem. 2017 (2017) 1–6. doi:10.1155/2017/8635615.

[62] A.M. Puziy, O.I. Poddubnaya, A. Martínez-Alonso, F. Suárez-García, J.M.D. Tascón, Synthetic carbons activated with phosphoric acid I. Surface chemistry and ion binding properties, Carbon N. Y. 40 (2002) 1493–1505. doi:10.1016/S0008-6223(01)00317-7.

[63] S. Bourbigot, M. Le Bras, R. Delobel, Carbonization mechanisms resulting from intumescence - part II. Association with an ethylene terpolymer and the ammonium polyphosphate-pentaerythritol fire retardant system, Carbon N. Y. 33

(1995) 283–294. doi:10.1016/0008-6223(94)00131-I.

[64] S.M. Yakout, G.S. El-Deen, Characterization of activated carbon prepared by phosphoric acid activation of olive stones, Arab. J. Chem. 9 (2016) S1155–S1162. doi:10.1016/j.arabjc.2011.12.002.

[65] N. Mehio, S. Dai, D. Jiang, Quantum mechanical basis for kinetic diameters of small gaseous molecules, J. Phys. Chem. A. 118 (2014) 1150–1154. doi:10.1021/jp412588f.

[66] T. Hasell, M. Miklitz, A. Stephenson, M.A. Little, S.Y. Chong, R. Clowes, L. Chen, D. Holden, G.A. Tribello, K.E. Jelfs, A.I. Cooper, Porous organic cages for sulfur hexafluoride separation, J. Am. Chem. Soc. 138 (2016) 1653–1659. doi:10.1021/jacs.5b11797.

[67] S.R. Tennison, Phenolic-resin-derived activated carbons, Appl. Catal. A. 173 (1998) 289–311. doi:10.1016/S0926-860X(98)00186-0.

[68] C. Lei, N. Amini, F. Markoulidis, P. Wilson, S. Tennison, C. Lekakou, Activated carbon from phenolic resin with controlled mesoporority for an electric double-layer capacitor (EDLC), J. Materaisl Chem. A. 1 (2013) 6037–6042. doi:10.1039/c3ta01638b.

[69] D. Lee, J.-Y. Jung, M.-S. Park, Y.-S. Lee, Preparation of novolac-type phenol-based activated carbon with a hierarchical pore structure and its electric double-layer capacitor performance, Carbon N. Y. 15 (2014) 192–197. doi:10.5714/CL.2014.15.3.192.

[70] K. Nakagawa, S.R. Mukai, K. Tamura, H. Tamon, Mesoporous activated carbons from phenolic resins, IChemE. 85 (2007) 1331–1337. doi:10.1205/cherd06119.

[71] Y. Li, Z.-H. Huang, F.Y. Kang, B.-H. Li, Preparation of activated carbon microspheres from phenolic resin with metal compounds by sub- and supercritical water activation, New Carbon Mater. 25 (2010) 109–113. doi:10.1016/S1872-5805(09)60019-6.

[72] A.K. Singh, Experimental methodologies for the characterization of nanoparticles,

in: Eng. Nanoparticles, Academic Press, 2016: pp. 125–170. doi:10.1016/B978-0-12-801406-6.00004-2.

[73] B. Hammouda, A new Guinier – Porod model, J. Appl. Crystallogr. 43 (2010) 716–719. doi:10.1107/S0021889810015773.

[74] L. Boldon, F. Laliberte, L. Liu, Review of the fundamental theories behind small angle X-ray scattering, molecular dynamics simulations, and relevant integrated application, Nano Rev. 6:25661 (2015) 1–21. doi:10.3402/nano.v6.25661.

Chapter VI

Chapter 6 – General Conclusions and Future Work

6.1. General Conclusions

The present thesis focused on the development and characterization of carbon molecular sieve adsorbents with high performance for O_2 / N_2 and C_3H_6 / C_3H_8 (vice-versa) gas separations and stable in the presence of aging factors such as oxygen and humidity.

Oxygen and humidity aging-free carbon molecular sieve adsorbents were obtained by using a propylene post-treatment for passivating surface-active sites. The carbon adsorbents preparation included the carbonization of a cellulosic precursor at end temperatures of 1200 ºC under nitrogen atmosphere. After carbonization, the samples were milled to *ca*. 11 µm, post-treated in a propylene atmosphere and characterized by Fourier transform infrared spectroscopy, scanning electron microscopy, thermogravimetric analysis, micropores characterization by Dubinin-Astakhov analysis and gas adsorption. Fourier transform infrared spectroscopy revealed remarkable differences between untreated and propylene-treated samples, which allowed to propose a mechanism of passivation. Briefly, carbonyl and hydroxymethyl groups at the CMS inner surface react with propylene producing C=C-H and R-O-R' and group of $CH=CH_2$ to produce R-O-R', which are less reactive groups, rendering the CMS adsorbent unreactive to oxygen and humidity.

Carbon molecular sieve adsorbents with high separation performance towards O_2 / N_2 gas separation and stable to oxygen were successfully prepared. The CMS samples were prepared from the carbonization of a cellulosic precursor. The best performing sample was carbonized at 1000 ºC end temperature, milled to *ca.* 1.6 µm and propylene post-treated for 4 days. This sample was characterized by techniques such as Fourier transform infrared spectroscopy, scanning electron microscopy, thermogravimetric analysis, adsorption isotherms of CO_2 at 0 ºC for determining the pore size distribution and O_2 / N_2 monocomponent adsorption experiments for obtaining the capacity and kinetics of adsorption.

One of the most important and challenging industrial separations is the propylene / propane mixture, which is currently accomplished by cryogenic distillation. Since these two components have close boiling points, its separation is difficult and

energy demanding. Thus, the development of new and more efficient separation/purification processes is highly needed.

A carbon molecular sieve adsorbent with remarkable propylene gas separation performance was obtained. The CMS material was prepared by a single-step carbonization process from a low-cost cellulosic precursor material at 800 ºC. The prepared CMS displayed a C_3H_6 / C_3H_8 equilibrium selectivity of *ca*. 140 at *ca.* 1 bar and 25 ºC; the amount of propane adsorbed was almost negligible. Mono- and multicomponent breakthrough experiments were performed confirming the unprecedent performance of the developed adsorbent. The sample was fully characterized using additional techniques such as scanning electron microscopy, Fourier transform infrared spectroscopy, thermogravimetric analysis and CO_2 isotherm at 0 ºC (for obtaining the micropore size distribution). The adsorbent material exhibited a well-developed microporous structure with a high porosity; the micropore size distribution of this material ranged from 0.5 – 1 nm. This new CMS adsorbent is relatively cheap, making it potentially attractive for PSA separation of propylene / propane. However, this adsorbent is selective to the majority component – propylene, making the corresponding adsorption-based separation process expensive. Propane selective adsorbents are then quite desirable but a cheap, reliable and suitable for PSA operation adsorbent is still elusive.

This thesis prepared for the first time a propane selective CMS. The adsorbent preparation combined a phosphoric acid pre-treatment of a phenolic resin precursor material, followed by carbonization and propylene post-treatment. The new CMS was optimized by changing the pre- and post-treatment conditions as well as carbonization end temperature. The precursor was immersed in an aqueous solution of phosphoric acid with concentration ranging between 0 wt.% to 25 wt.%, carbonized at an end temperature between 950-1300 ºC, and post-treated in propylene from 0 to 12 days. The best-performing samples, MFF_8 and MFF_9, were pre-treated in a 25 wt.% phosphoric acid solution, followed by carbonization at 1100 ºC and post-treated with propylene for 6 and 12 days, respectively. MFF-9 sample exhibited a propane equilibrium selectivity of *ca.* 2 at 1 bar and 25 ºC. This sample was fully characterized; FTIR analyses revealed that both pre- and post-treatments introduce several changes in the surface chemistry of the samples. Also, the adsorption characterization indicated

that phosphoric acid pre-treatment plays a critical role for obtained equilibrium-based selectivity. On the other hand, propylene post-treatment reveals minor influence in the propane selectivity. This finding boosted the hosting laboratory research in propane selective CMS; these materials are very promising for the cheap and effective propylene purification.

6.2. Future work

Looking forward with all obtained results of the present thesis, it would be important to fully investigate the action of propylene on carbon molecular sieve adsorbents. Namely, it would be of great relevance a more extensive study on *in-situ* surface-functional groups modifications by propylene post-treatment for better understanding its action on the surface chemistry. Also, by understanding this action mechanisms, propylene interaction with CMS can be controlled and carbon materials can be tailored for suiting a given application. Studies regarding the interaction of adsorbate molecules and the adsorbent morphology and surface chemistry (including surface functional groups) should be addressed using techniques such as high-resolution transmission electron microscopy and Fourier transform infrared spectroscopy. High-resolution transmission electron microscopy should provide information about pores morphology and Fourier transform infrared spectroscopy should give important information about the surface chemistry. Combining these two techniques a more complete understanding of samples performance for a given gas separation should be achieved.

Regarding propane selective carbon adsorbents, further optimization studies on samples structure should be accomplished by deeper characterization for understanding the remarkable gas separation performance. Studies including temperature programming desorption, inductively coupled plasma, atomic force microscopy, X-ray photoelectron spectroscopy and inelastic neutron scattering should be performed for both precursor material and derived carbon molecular sieve adsorbents. Further, propane kinetic-selective CMS adsorbents should be fully characterized concerning adsorption studies, breakthrough experiments and detailed surface chemistry and morphology analyses.

Finally, the prepared carbon molecular sieves adsorbents should be optimized and pelletized for addressing commercial proposals for pressure swing adsorption applications. Regarding CMS pelletization, its mechanical and chemical resistance should be ensured as well as its optimum performance.

Appendix A

Appendix A – Experimental set-ups

A.1. Adsorption set-up – volumetric method

The used set-up for measuring the adsorption equilibrium isotherms and uptake curves for oxygen, nitrogen, carbon dioxide, propylene, propane and sulfur hexafluoride is shown on Figure A.1. This set-up, already assembled, was employed for adsorption characterization of carbon molecular sieve materials reported on Chapters II, III, IV and V.

Figure A.1. Volumetric method setup.

A.2. Carbonization set-up

The carbonization process, performed on carbon materials described in Chapters II, III, IV and V, was performed in two ceramic tubes with volumes of 7536 cm^3 (already assembled) and 954 cm^3 (assembled by the author), present on Figure A.2. and Figure A.3., respectively.

Figure A.2. Alumina tube inside a tubular horizontal Termolab TH furnace.

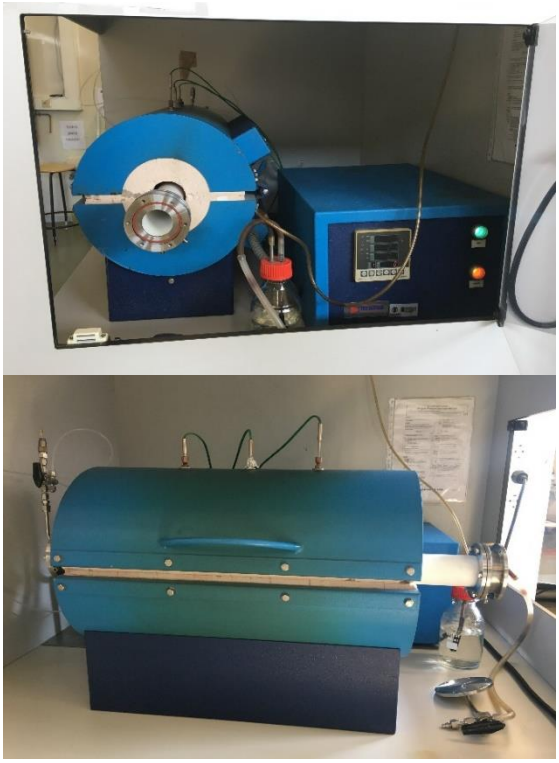

Figure A.3. Ceramic tube inside a tubular horizontal Termolab TH furnace.

A.3. Breakthrough set-up

Breakthrough experiments performed on the carbon molecular sieve adsorbent described in Chapter IV took place in a set-up present on Figure A.4. The small volume column was assembled by the author. The mass spectrometer used for analysing the outlet elements compositions is shown on Figure A.5.

Figure A.4. Breakthrough set-up.

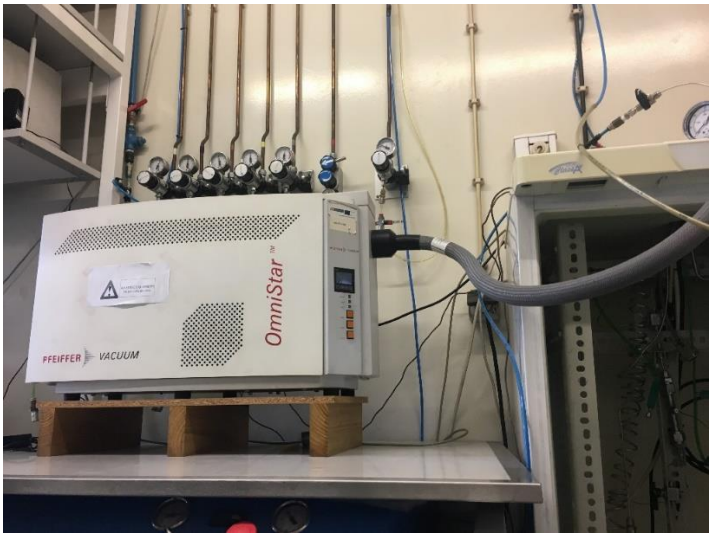

Figure A.5. Mass spectrometer analyser (MS).